



Technische Universität München
Lehrstuhl für Technische Chemie II

Impact of pH on adsorption of H₂ and hydrogenation of phenol on Pt in the aqueous phase

Xi Chen

Vollständiger Abdruck der von der Fakultät für Chemie der Technischen Universität München zur Erlangung des akademischen Grades eines

Doktors der Naturwissenschaften (Dr. rer. nat.)

genehmigten Dissertation.

Vorsitzende(r): Prof. Dr.-Ing. Kai-Olaf Martin Hinrichsen

Prüfer der Dissertation:

1. Prof. Dr. Johannes A. Lercher
2. Prof. Dr. Tom Nilges

Die Dissertation wurde am 30.06.2021 bei der Technischen Universität München eingereicht und durch die Fakultät für Chemie am 04.08.2021 angenommen.

Chance favors only the prepared mind.

— *Louis Pasteur (1822–1895)*

Acknowledgements

Foremost, I would like to express my sincere gratitude to my thesis advisor Prof. Dr. Johannes A. Lercher for providing me not only the opportunity to work in his group but also the excellent research environment in Catalysis Research Center, chair of Technical Chemistry II at department of Chemistry. It is a precious experience for me to conduct such research full of challenges and interests under his guidance and support. Besides knowledge, the treasures that more important I gained are the way of thinking and motivated attitude for encountered difficulties, which are beneficial to both my scientific and personal life in future.

I would also like to express my grateful appreciation to my mentor Dr. Yue Liu for his patient guidance and discussions in every detailed step, which helps me growing in research. I'm fortunate enough to start my research topic and finish my doctoral thesis with his warm support and uncountable assistance, which are highly valuable to my research. Thank a lot for the time and efforts you spent on coaching me.

Next, I would like to thank all the HDO group members, Dr. Hui Shi, Dr. Yuanshuai Liu, Dr. Guoju Yang, Dr. Meng Wang, Dr. Qiang Liu, Dr. Karen Resende, Dr. Eszter Baráth, Niklas Pfriem, Lara Milakovic Christoph Denk for their kind help and suggestions.

Then, I would like to thank our senior scientist and administrative staff in TC II: Prof. Dr. Andreas Jentys, Dr. Erika Ember, Dr. Maricruz Sanchez-Sanchez, Dr. Ricardo Bermejo-Deval, Dr. Rachit Khare, Ulrike Sanwald, Xaver Hecht, Bettina Federmann, Martin Neukamm, Andreas Marx, Stefanie Seibold, Kateryna Kryvko, who all give me help during my stay at TUM. In addition, I give my thanks to other colleagues, Dr. Yu Lou, Dr. Yang Song, Dr. Wanqiu Luo, Dr. Yang Zhang, Dr. Yong Wang, Dr. Wei Zhang, Dr. Kaming Yu, Dr. Jie Zhang, Dr. Mingwu Tan, Ruixue Zhao, Guanhua Cheng, Lingli Ni, Fuli Deng, Lei Tao and Hongwen Chen. It's a good time to be working with all of you.

Furthermore, I would like to thank Martin Baumgaertl, Martina Aigner, Simon Krebs and all the colleagues in TC II for your kind help.

Finally, heartfelt thanks to my family and friends for giving me endless support and unconditional trust, which are the solidest backbone to me.

Symbols and Abbreviations

AAS	Atomic absorption spectroscopy
BAS	Brønsted acid site
C_{phenol}	Phenol concentration
CH	Conventional hydrogenation
DFT	Density functional theory
E_{F}	Fermi level
E_{a}	Activation energy in Arrhenius equation
GC	Gas chromatography
h	Hour
HDO	Hydrodeoxygenation
HBE	Hydrogen binding energy
IR	Infrared
I	Moment of inertia
K	Kelvin
K_{a}	Adsorption equilibrium constant
k_{a}	Adsorption rate constant
$k_{-\text{a}}$	Desorption rate constant
KIE	Kinetic isotope effect
LAS	Lewis acid site
mL	Milliliter
min	Minute
MS	Mass spectrometer
M	Molarity
nm	Nanometer
NMR	Nuclear magnetic resonance
NP(s)	Nanoparticle(s)
P_{H_2}	H_2 partial pressure
PCET	Proton coupled electron transfer
Q_{ads}	Adsorption heat
RDS	Rate-determining step
TOF	Turnover frequency
wt %	Weight percent
W	Work
XRD	X-ray diffraction
ZPE	Zero point energy
α	Cathodic transfer coefficient
θ	Coverage
Φ	Work function
$\Delta H_{\text{a}}^{\circ}$	Enthalpy of adsorption
$\Delta G_{\text{rds}}^{\ddagger}$	Activation Gibbs energy

Abstract

The heat of adsorption of H₂ on Pt at the water-metal interface is smaller than that at the Pt-gas interface. With decreasing pH its enthalpy of adsorption decreases further. The further decline is caused by the higher energy required to reorganize the Helmholtz layer. Hydrogen addition to the oxygen of phenol and concerted proton coupled electron transfer have been determined to be rate determining in hydrogenation of phenol. Higher concentrations of hydronium ions favor the latter.

Kurzzusammenfassung

Die Adsorptionswärme von H₂ an Pt an der Wasser-Metall-Grenzfläche ist kleiner als die an der Pt-Gas-Grenzfläche. Mit sinkendem pH-Wert nimmt seine Adsorptionsenthalpie weiter ab. Der weitere Rückgang wird durch den höheren Energiebedarf zum Umbau der Helmholtz-Schicht verursacht. Es wurde festgestellt, dass die Wasserstoffaddition an den Sauerstoff von Phenol und der konzertierte protonengekoppelte Elektronentransfer bei der Hydrierung von Phenol geschwindigkeitsbestimmend sind. Höhere Konzentrationen an Hydroniumionen begünstigen letzteres.

Table of Contents

Acknowledgements	i
Symbols and Abbreviations	ii
Abstract	iii
Kurzzusammenfassung	iii
Chapter 1	1
Introduction	1
1.1 General background.....	2
1.2 Lignocellulose derived compounds.....	5
1.2.1 Structures and components of lignocellulose	5
1.2.2 Conventional technologies for lignocellulose conversion	6
1.2.3 Bio-oil upgrading.....	8
1.2.4 Depolymerization of lignin.....	9
1.2.5 HDO of lignin-derived phenolic compounds	11
1.3 Hydrogenation of phenol.....	12
1.3.1 Hydrogenation of phenol in the gas phase	13
1.3.2 Hydrogenation of phenol in the liquid phase	14
1.3.3 Electrocatalytic hydrogenation (ECH) of phenol	15
1.4 Scope of this thesis	18
1.5 References	19
Chapter 2	25
Adsorption of H₂ on Pt/CNT in the aqueous phase	25
2.1 Introduction	26
2.2 Experimental and theoretical method.....	27
2.2.1 Preparation of catalyst materials	27
2.2.2 Characterization of catalyst materials	27
2.2.3 Determination of H ₂ adsorption heat in the gas phase	28

2.2.4 Determination of H ₂ adsorption heat in the aqueous phase by kinetic method of reaction of H ₂ (g) with D ₂ O (l)	28
2.3 Results and discussion	29
2.3.1 Physicochemical properties of the catalyst.....	29
2.3.2 Derivation of kinetic method and calculation of adsorption heat of H ₂ in the aqueous phase.....	29
2.3.3 Adsorption heat of H ₂ in the gas phase	32
2.3.4 Influence of water on H ₂ adsorption heat	32
2.3.5 Influence of Pt electronic structure on H ₂ adsorption heat	33
2.4 Conclusions	36
2.5 Appendix	37
2.6 References	43
Chapter 3.....	45
Impact of pH on H₂ adsorption on Pt in the aqueous phase	45
3.1 Introduction	46
3.2 Experimental and theoretical method.....	47
3.2.1 Preparation and characterization of catalyst materials	47
3.2.2 Determination of H ₂ adsorption heat in the aqueous phase Kinetic method-reaction of H ₂ (g) with D ₂ O (l)	47
3.3 Results and discussion.....	47
3.3.1 Thermodynamic and kinetic properties of H ₂ adsorption on Pt under different pH.....	47
3.3.2 Influence of pH dependent electronic structure of surface Pt on Pt-H bond strength.....	50
3.3.3 Influence from water layer	53
3.3.4 Influence of electrical double layer	54
3.4 Conclusions	56
3.5 Appendix	56
3.6 Reference	63

Chapter 4	65
Impact of pH on hydrogenation of phenol on Pt in the aqueous phase	65
4.1 Introduction	66
4.2 Experimental and theoretical method.....	67
4.2.1 Preparation and characterization of catalyst materials	67
4.2.2 Catalytic tests.....	67
4.3 Results and discussions	68
4.3.1 Impact of pH on hydrogenation of phenol over Pt/CNT in the aqueous phase	68
4.3.2 Reaction pathway with pH	69
4.3.3 Adsorption model for H ₂ and phenol.....	71
4.3.4 Impact of pH on adsorption of H ₂ on Pt/CNT in the aqueous phase	74
4.3.5 Impact of pH on adsorption of phenol on Pt in the aqueous phase	74
4.3.6 Conventional hydrogenation	75
4.3.7 Proton coupled electron transfer.....	76
4.4 Conclusions	80
4.5 Appendix	81
4.6 References	96
Chapter 5	98
Summary and conclusions	98
Curriculum Vitae	101
List of publications	102

Chapter 1

Introduction

1.1 General background

The demand for primary energy and the associated production capacity are steadily increasing to maintain the momentum of the sustained economic growth across the world. In principle, primary energy could be classified as non-renewable, a natural resource that is not readily generated as quick as the pace of its consumption (e.g. coal, petroleum, nuclear and natural gas), and renewable, a resource that could be constantly replenished in nature such as solar, wind, tides, waves, geothermal heat and biomass. According to the renewable capacity statistics, the addition of total global renewable energy by 2020 has exceeded 50% in comparison to 2011.^[1] Figure 1.1 shows the share of renewable or non-renewable in TPES historically and predictably. Although the total primary energy supply (TPES) is still dominated by non-renewable, the share of renewable would be projected to rise up to 65 % in 2050, nearly a two-thirds of TPES which is almost a 7-fold increase relative to that in 2017.^[2]

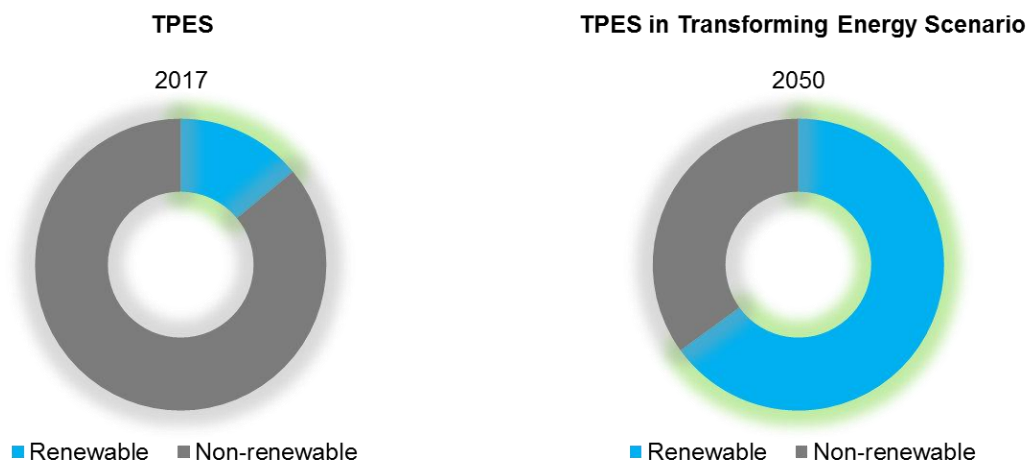


Figure 1.1. Total primary energy supply (TPES), renewable and non-renewable share for the Transforming Energy Scenario, 2017, 2050. Source: International Renewable Energy Agency (Global renewables outlook, Edition 2020).^[2]

In the field of power generation, more than half of all global capacity additions have been accounted for by renewables since 2012. The global newly installed renewable power capacity achieved 167 GW in 2017, with more than 60% of all new electricity capacity was derived from renewables.^[3] Figure 1.2^[3] shows the share of renewables in the power sector. Under the Remap Case, the consumption of electricity in end-use sectors would raise to around 55 000 TWh by

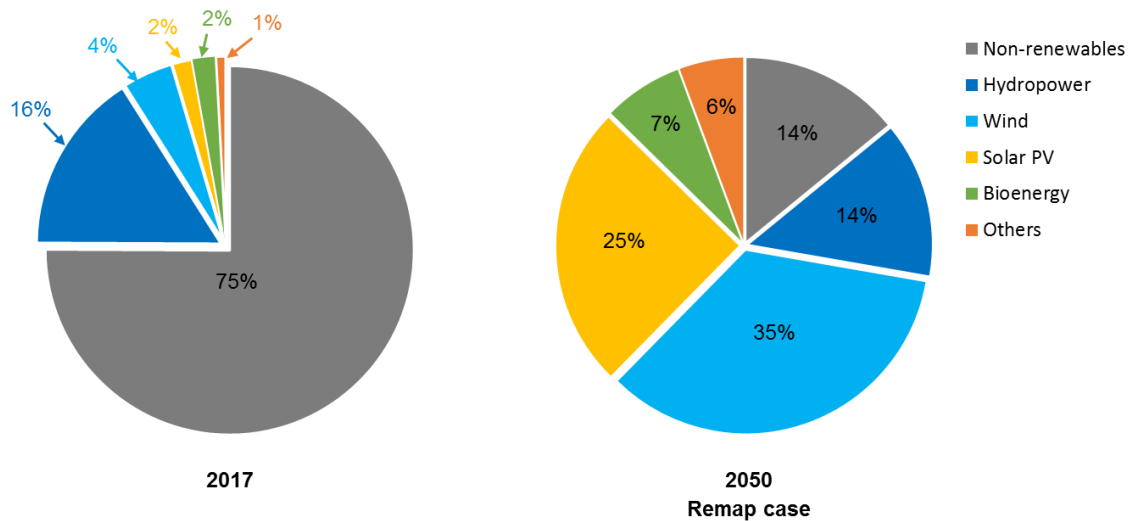


Figure 1.2. The rising importance of renewable energy in the power sector. Source: International Renewable Energy Agency (Global energy transformation: A roadmap to 2050 (2019 edition)).^[3]

2050, over 130% compared to 2016. By 2050, the share of renewable energy in generation would achieve 86%, up from an estimated 62% in 2016. In addition, strong growth is taken placed in geothermal, bioenergy and hydropower as well. In contrast, the non-renewables continuously decrease and would occupy only 14% of the total electricity generation.

In a geographical point of view from 2018 to 2050,^[4] the total addition of renewable power generation capacity is expected to be 14333 GW, among which China accounts for over one third (4993 GW), followed by the United States (2506 GW), India (1795 GW) and the European Union (1154 GW).

Bioenergy, taking up a large share of the renewable energy supply today, has a significant role in the end-use sectors (industry, transport and buildings) and the power sector. The use of bioenergy is mainly divided into two parts: traditional and modern.^[5] Traditional use is the combustion of wood, charcoal, agricultural residues and animal waste. Modern use refers to the technologies for generation of liquid biofuels via plants through conventional or advanced conversion routes, biogas via anaerobic digestion of residue, syngas via gasification of biomass and others. The demand primary modern bioenergy would increase from 30 EJ in 2016 to 125 EJ by 2050 to meet all bioenergy demand. Biofuels is predicted to play significant roles not only in aviation and marine energy supply by 2050, but also in industry for providing thermal energy and fuel for power generation.^[3] Figure 1.3 gives the consumption of renewable energy

along time in The United States. It is clear that the consumption of biomass in 2019 rises as twice as that in 1950.^[6]

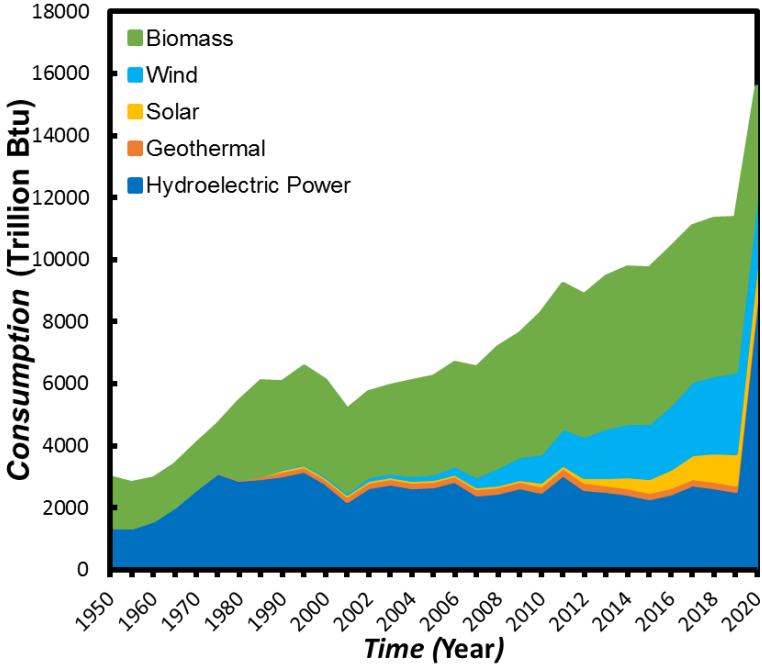


Figure 1.3. Renewable Energy Consumption from 1950 to 2020. Source: The U.S. Energy Information Administration's (The Monthly Energy Review, May 2021).^[6]

International renewable energy agency (IRENA) gave the indicator regarding the contribution of bioenergy to the energy transition.^[2] In historical progress, the use of bioenergy increased by 1% in the share of TPES, which is resulted from the growth of modern use of bioenergy from 4.1% to 5.1% from 2015 to 2018. The liquid biofuel production increased by 5.4% from 2015 to 2017. By 2030, the modern utilization of bioenergy will nearly account for all the use of bioenergy, achieving 8% (PES) and 12% (TES) in the share of TPES, while by 2050, the share will come up to 10% in PES and 23% in TES.

1.2 Lignocellulose derived compounds

1.2.1 Structures and components of lignocellulose

The utilization of biomass energy includes (1) growth of biomass, (2) the conversion of biomass to fuel, and (3) utilization of fuel. The CO₂ formed in the third step would be used for biomass growth in the first step, which closes the loop. During the whole process, the inputs are CO₂, H₂O, light, air and nutrients while the outputs are food and energy.^[7]

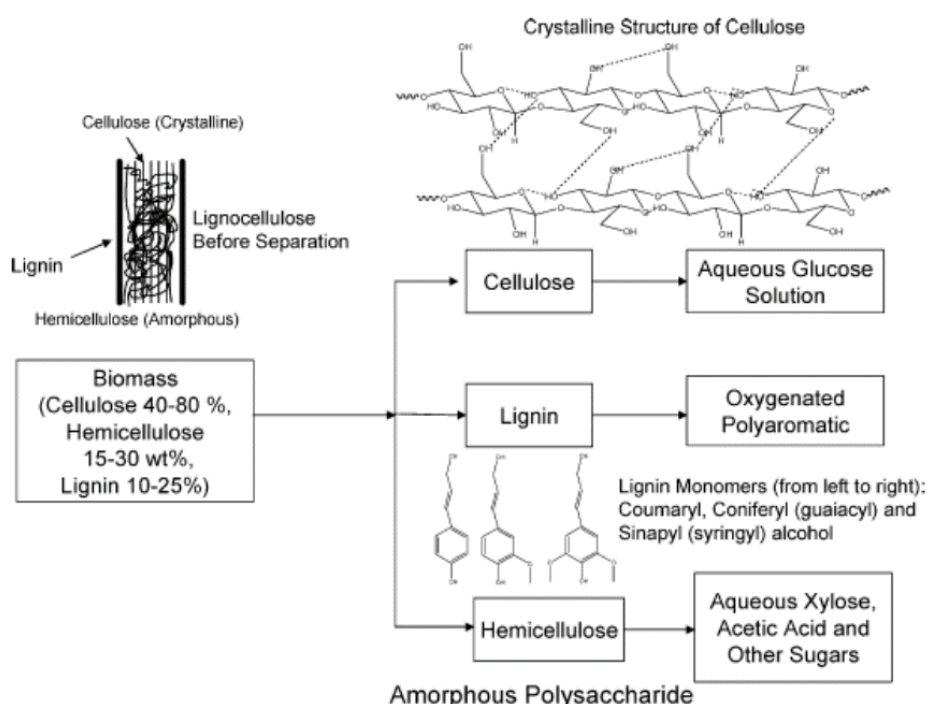


Figure 1.4. Structures of different biomass fractions (lignocellulose, cellulose, lignin and hemicellulose) before and after reactions.^[7] (Adapted with permission from reference 4. Copyright © 2006, American Chemical Society.)

Figure 1.4 shows the structures of different biomass fractions before and after reactions. Among biomass sources, lignocellulose is currently the most inexpensive and abundant source of plant biomass and a sustainable source of the second generation bio-fuel that could be the substitution for fossil fuel. The major compounds of lignocellulose are cellulose (40-80 wt%), hemicellulose (15-30 wt%) and lignin (10-25 wt%). As the basic compound of lignocellulose, cellulose is a crystalline polymer of glucose consisting of a linear polysaccharide with β -1,4 linkages of D-glucopyranose monomers. In contrast to cellulose, hemicellulose is an amorphous polymer containing five different sugars, with xylose unit as the most abundant building block. Lignin

is an irregular aromatic polymer consisting of phenylpropane unit and its structure and reactivity are greatly dependent on the manner in which it is produced. While processes for cellulose and hemicellulose conversion into valuable products are already advanced, adding value to lignin is still a challenge, due to its complex structure and relatively high stability towards a variety of chemical transformations. Even though, lignin is still considered as a promising feedstock for valuable chemicals and fuels due to its aromatic feature.

1.2.2 Conventional technologies for lignocellulose conversion

There are three primary routes to convert lignocellulosic material into liquid fuels,^[7] as shown in Figure 1.5, including gasification for syngas production, pyrolysis or liquefaction for bio-oil production and hydrolysis of biomass for production of sugar monomer units.

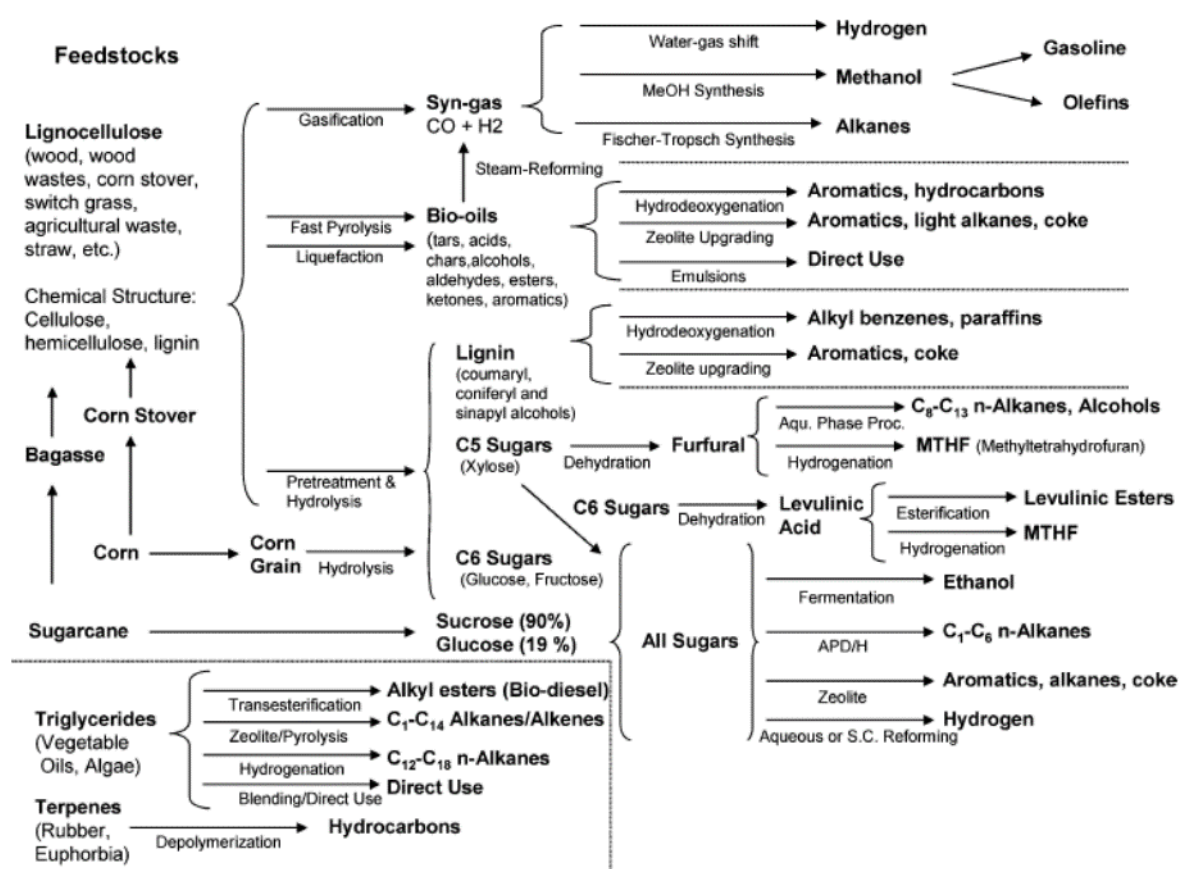


Figure 1.5. Strategies for production of fuels from lignocellulosic biomass.^[7] (Adapted with permission from reference 4. Copyright © 2006, American Chemical Society.)

Syn-gas by Gasification

Gasification is a process for production of syn-gas or producer gas involving CO, H₂, CO₂, CH₄, and N₂ in different proportions by means of reaction of carbonaceous material (biomass, coal, or oil) with air and/or steam.^[8-10]

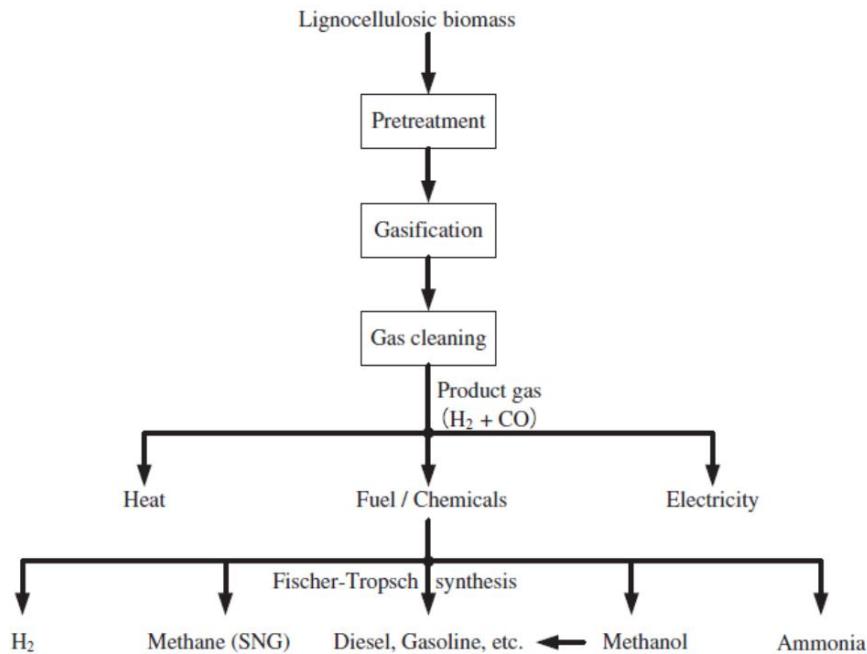


Figure 1.6. The modern routine of lignocellulosic biomass utilization via gasification.^[11] (Adapted with permission from reference 8. Copyright © 2012 Elsevier Ltd.)

As shown in Figure 1.6, gasification of biomass is a conventional technology that was used to power vehicle and generate heat and electricity.^[11, 12] The utilization of syn-gas is to produce fuels and chemicals, including the water gas shift reaction for generation of H₂, Fischer-Tropsch synthesis for diesel fuel, methanol synthesis for methanol and methanol-derived fuels.^[13, 14]

Bio-Oils by Fast Pyrolysis and Liquefaction

Bio-oils could be derived by pyrolysis processes or liquefaction. In pyrolysis process, the gaseous product is produced by heating biomass feedstock in the absence of air before condensation. Slow pyrolysis generates a mass of coke that can be used as a solid fuel, while fast pyrolysis could generate bio-oils in high yields of dry feed.^[15, 16]

In liquefaction of biomass process, a water-insoluble bio-oil could be generated via treatments in conditions at relatively high pressure and low temperature. Biomass liquefaction is aimed to synthesize a premium liquid oil by adjusting the reaction rate and mechanisms, and reaction

conditions, such as pressure, gases, and catalysts.^[17]

Table 1.1 shows the properties of bio-oils derived from wood via fast pyrolysis or liquefaction process, and diesel fuel.^[7] In comparison to diesel fuel, the oils from pyrolysis possess a higher oxygen and moisture content with lower heating value. The bio-oils from liquefaction have a higher energy content than pyrolysis-derived oils due to the lower oxygen content.^[18, 19]

Table 1.1. Typical Properties of Wood Pyrolysis Bio-Oil, Liquefaction Bio-Oil, and Heavy Fuel Oil.^[7] (Adapted with permission from reference 4. Copyright © 2006, American Chemical Society.)

property	pyrolysis oil	liquefaction oil	heavy fuel oil
moisture content, wt %	15–30	5.1	0.1
pH	2.5		
specific gravity	1.2	1.1	0.94
elemental composition, wt %			
carbon	54–58	73	85
hydrogen	5.5–7.0	8	11
oxygen	35–40	16	1.0
nitrogen	0–0.2		0.3
ash	0–0.2		0.1
higher heating value, MJ/kg	16–19	34	40
viscosity (50°C), cP	40–100	15000 (at 61°C)	180
solids, wt %	0.2–1		1
distillation residue, wt %	up to 50		1

Hydrolysis

The conversion of cellulose into sugar polymers could be carried out by hydrolysis reaction, which is more difficult compared to starches hydrolysis due to a crystalline form of cellulose with hydrogen bonding.^[20] Typically, the hydrolysis reaction are catalyzed by acids or enzymes. The hydrolysis reactions catalyzed by acid are reactions of solid biomass with liquid acid, in which mass transfer limitations plays a key role.

Enzymatic hydrolysis is catalyzed by cellulase that has been classified into three major types including, endoglucanases or 1,4-β-D-glucan-4-glucanohydrolases, exoglucanases or 1,4-β-D-glucan glucanohydrolases and β-glucosidases or β-glucoside glucohydrolases.^[21, 22]

1.2.3 Bio-oil upgrading

The most critical problems that limit the applications of bio-oils as a fuel are poor volatility, high viscosity, coking, corrosiveness, and cold flow problems, for which upgrading of bio-oils is necessary before usage as a substitution for diesel and gasoline fuels in engines. Two main

routes are employed for bio-oils upgrading: zeolite upgrading and hydrodeoxygenation (HDO). Upgrading by using zeolite catalysts can reduce oxygen content in the absence of H₂. Several products, such as hydrocarbons, water or oil-soluble organics can be formed from the reactions involving dehydration, cracking, polymerization, deoxygenation, and aromatization. The advantages of this route are no need of H₂ and low cost for operation, whereas the disadvantages are low hydrocarbon yields and high generation yields of coke under reaction conditions, leading to the limitation of the application of zeolite upgrading.

HDO is assumed as the most efficient method and will be discussed in sector 1.2.5 in detail.

1.2.4 Depolymerization of lignin

Depolymerization of lignin is underutilized because of the robustness of C–C and C–O bonds.^[23] Lignin is composed of several types of linkages dependent on the source of plant.^[24] As shown in Figure 1.7, three major monomers of lignin are p-coumaryl alcohol, coniferyl alcohol and sinapyl alcohol,^[25] which are connected typically by several common linkages, including β -O-4, α -O-4, 4-O-5, β - β , β -5 and 5-5.^[26, 27] These linkages could be classified into two major linkages, carbon-carbon bonds and ether bonds (accounting for 56% or more in total linkages).^[28] Compared to carbon-carbon bonds, it is more efficient to cleave the aryl ether C–O bonds.^[29]

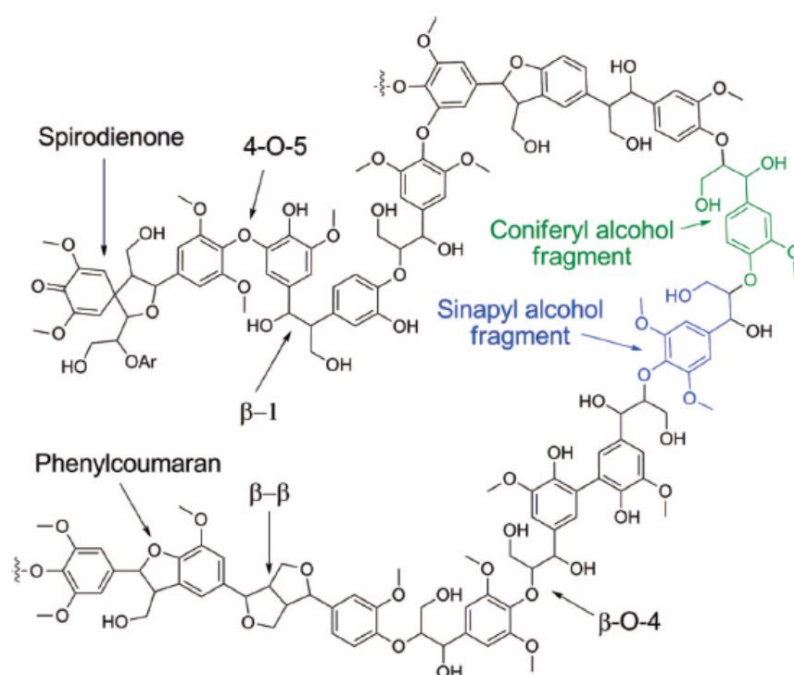


Figure 1.7. Schematic representation of a hardwood lignin structure.^[25] (Adapted with permission from reference 22. Copyright © 2010, American Chemical Society.)

Thus, the cleavage of the C-O bond is critical to the depolymerization of lignin. The main strategies for the conversion of lignin into low-weight molecules involve oxidizing, reducing, neutral treatment (shown in Figure 1.8) and bio-catalysis.^[30] Oxidative treatment usually occurs at lower temperatures ranging from 0 to 250 °C and gives the products containing aromatic alcohols, aldehydes, and acids for fine or platform chemicals.^[31-36] Reductive treatment involves thermal reduction with hydrogen source under relatively harsh reaction conditions typically ranging from 100 to 350 °C, which mainly targets to produce simple bulk aromatic compounds like phenols, benzene and alkane fuels through upgrading with hydrogen.^[16, 37-43] Pyrolysis, as one of lignin conversion in neutral environment, is used to produce bio-oil (typically at 450–700 °C),^[44-48] while catalysis conversion of lignin by acid (typically at 0–200 °C)^[49-53] and base (typically at 100–300 °C) could offer small segments such as monomeric phenols by breaking the C–O or C–C linkages between the building blocks of lignin.^[29, 54, 55] The compounds produced from these depolymerization methods, such as substituted phenols, coniferyl alcohol, sinapyl alcohol, guaiacol, catechol and ethers which contain oxygen groups required for further upgrading.^[48, 56-60]

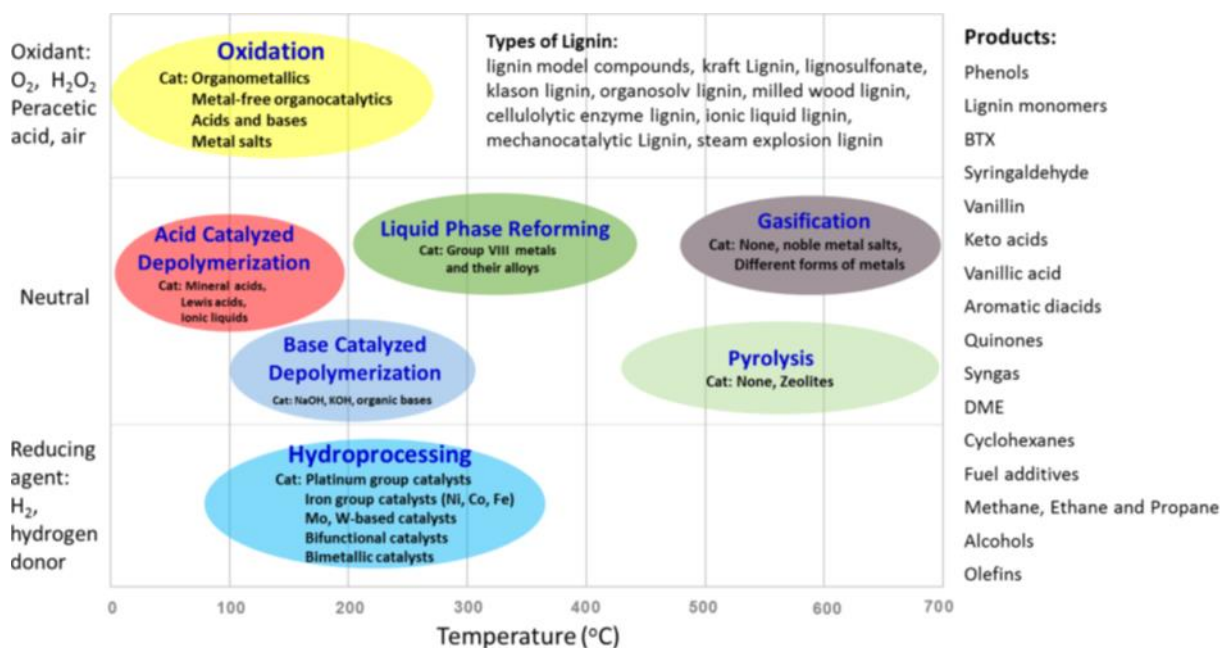


Figure 1.8. Summary of processes for conversion of lignin (Note: the abscissa represents the typical temperature range of the lignin conversion processes).^[30] (Adapted with permission from reference 27. Copyright © 2015, American Chemical Society.)

1.2.5 HDO of lignin-derived phenolic compounds

Bio-oil derived from lignin is taken as a competitive source for second-generation bio-derived energy carriers.^[61] However, the direct application of bio-oil is limited by its poor volatility, high viscosity, as well as its low stability caused by high contents of oxo-functionalized compounds.^[62, 63] A viable route to improve the properties of bio-oil is the removal of oxygenated groups by a catalytic hydrotreatment called hydrodeoxygenation (HDO), which is considered as the most efficient method for bio-oil upgrading.^[64, 65] In the HDO process, the oxygen in the aromatic oxygenates could be removed in the form of water and other small oxygenates in the presence of hydrogen atmosphere and catalyst at a relatively moderate temperature usually ranging from 200 °C to 500 °C.^[66-68]

Sulfided NiMo/Al₂O₃ and CoMo/Al₂O₃ catalysts, typically used for hydrodesulfurization (HDS) and hydrodenitrogenation (HDN) in petroleum refineries, are utilized for hydrodeoxygenation process.^[69-71] Heterogeneous catalytic hydroprocessing for bio-oil upgrading has been focused on with initial work involving tests of model phenolic compounds with CoMo, NiMo, NiW, Ni, Co, Pd, and CuCrO catalysts in batch reactor.^[72] The sulfided CoMo catalyst gave a higher activation with product of 33.8% benzene and 3.6% cyclohexane at 400 °C. Co and Ni were introduced as promoters to donate electrons to the active sites of Molybdenum.^[73-76]

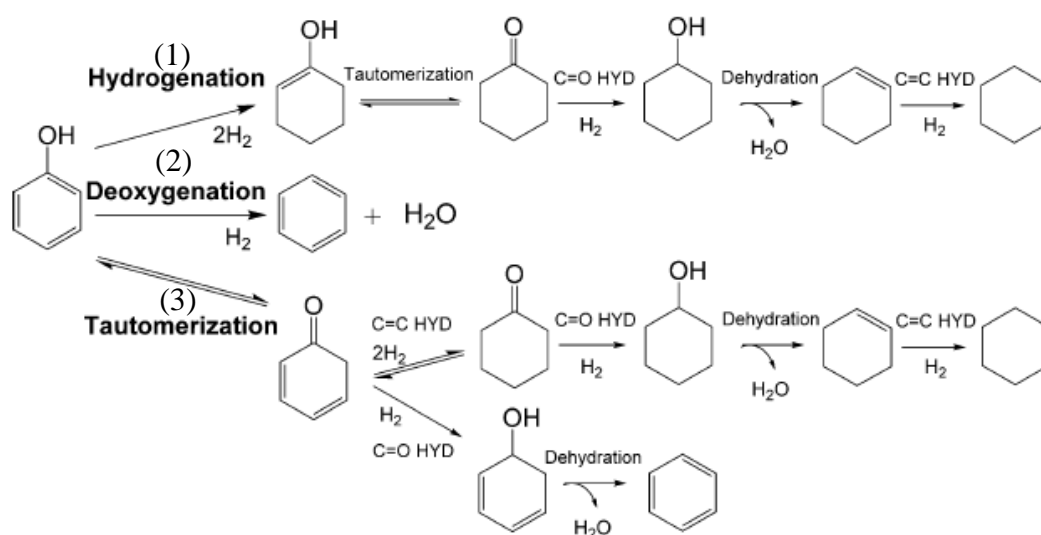


Figure 1-9. Typical pathways of phenol hydrodeoxygenation. (1) Hydrogenation; (2) direct deoxygenation; (3) tautomerization followed by hydrogenation and dehydration.^[77] (Adapted with permission from reference 74. Copyright © 2016 WILEY - VCH Verlag GmbH & Co. KGaA, Weinheim.)

However, the stability of sulfides catalysts is still affected by the deactivation of these sites due to the loss of sulfur species. Stabilization of sulfide sites is usually required co-feeding of H₂S, which will lead to contamination problems.^[78-81] Furthermore, Ni, Pd, Ru, Pt, Rh and Co have been investigated for HDO reaction.^[82-87] HDO of phenol, the simplest phenolic monomer, has been investigated with the most representative reaction pathways given in Figure 1.9.

The hydrogenation route (1) (Figure 1.9) starts from partial hydrogenation of the aromatic ring to form cyclohexanone occurring by tautomerization before further hydrogenation to form cyclohexanol. In the presence of acid sites, the dehydration of cyclohexanol, the rate-determining step for the whole pathway, occurs by C–O bond cleavage, followed by hydrogenation of the generated cyclohexene to cyclohexane. The direct deoxygenation route (2) gives benzene as product which is unfavorable due to the strong C-O bond for cleavage even with less consumption of hydrogen in the process. The tautomerization route (3), starting from the generation of keto intermediate (2,4-cyclohexadienone), could undergo hydrogenation pathways with its partial or total saturation of the ring followed by dehydration reactions.

Our group focused on the alkane products converted from HDO of phenol under acidic conditions. In the presence of noble-metal catalysts (M/C, M stands for Pd, Pt, Ru and Rh) and H₃PO₄ acid, the yield of cyclohexane could achieve 90% in the aqueous. It is proved that metal active sites are responsible for hydrogenation since only hydrogenated pathway proceeded under neutral conditions, with cyclohexanol as the main products over Pd/C (80 °C, 5 MPa H₂). While in 0.5 wt% H₃PO₄ solution at 200 °C, cyclohexene is produced from dehydration of cyclohexanol and further hydrogenated to cyclohexane.^[88] This thesis concentrates on the hydrogenation of phenol, the first step of HDO of phenol in hydrogenation route, in the aqueous phase.

1.3 Hydrogenation of phenol

As the initial product from aryl ethers, e.g. diphenyl ether, and the simplest phenolic compounds of bio-oil, phenol has been widely studied as a model compound for the optimization of bio-oil upgrading and selective synthesis of targeting chemicals (e.g. cyclohexanone).^[89] Hydrogenation of phenol, with cyclohexanone and cyclohexanol as typical products, is strongly dependant on the reaction conditions such as types of metals, supports, reaction media (liquid or gas phase), types of acids and pH of solution.^[90-93]

1.3.1 Hydrogenation of phenol in the gas phase

As early as 1970s, hydrogenation of phenol in the gas phase was carried out on Pt catalysts, leading to a high selectivity of cyclohexanol in products.^[94] Pd catalysts have a better selectivity of cyclohexanone.^[95] Furthermore, the supports play a significant role in the activation and selectivity of phenol hydrogenation. Metal oxides such as MgO and Al₂O₃ are always chosen for the test of reaction in vapor phase. It was found that Pd/MgO has a better performance on cyclohexanone selectivity and stability than Pd/Al₂O₃.^[96] The interpretation is ascribed to the adsorption models of phenol on metal oxides given in Figure 1.10.

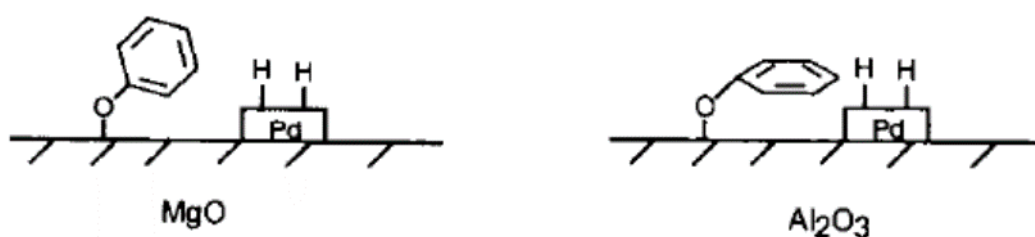


Figure 1.10. The different adsorption model of phenol on MgO with a “co-planar” orientation (a) and on Al₂O₃ with a “non-planar” orientation (b).^[96] (Adapted with permission from reference 93. Copyright © 1994 Published by Elsevier B.V.)

Taylor and Lundlum have reported that phenol molecule anchors to the γ -Al₂O₃ surface through oxygen atom (phenolate form), with a “co-planar” aromatic ring.^[97] Tanabe has suggested the same orientation form of phenol on acidic silica-alumina surface but a “non-planar” form on basic MgO.^[96] It was proposed that a “co-planar” adsorption of phenol favours the hydrogenation of phenol to cyclohexanol, while a “non-planar” adsorption tends to cyclohexanone as the main hydrogenated product. Due to the low mechanic resistance, MgO isn't likely to be chosen as supports for industrial utilization despite its better properties.

Scirè et al. reported that the catalytic properties of Pd-based catalysts in selective hydrogenation of phenol to cyclohexanone is determined by adsorption–desorption equilibrium of reactants and products, which are greatly relied on both the acidity of supports and the electron surrounding Pd active sites.^[98] The state of Pd sites makes the major contribution to the catalytic activity. Furthermore, the deactivation rate of the catalyst is mainly influenced by the strong acid sites. The catalytic performance also affected by the interaction between metal and support.

Too strong or weak interaction is not beneficial to the activities of phenol hydrogenation in vapor phase.

1.3.2 Hydrogenation of phenol in the liquid phase

In comparison to vapor phase, hydrogenation of phenol in the liquid phase attracts more attention due to savings of cost and energy. Yoon has reported that the metal/aqueous interface would favor hydrogenation of phenol to cyclohexanone (see the upper pathway in Figure 1.11) through a cyclohex-3-enone intermediate formed from rapid keto/enol isomerization. The solid/vapor interface facilitates phenol hydrogenation to cyclohexanol via the partially hydrogenated phenol that remains on the metal surface due to the keto/enol equilibrium which is thermodynamically unfavorable and kinetically hindered (lower route in Figure 1.11). The metal work function is lowered by 1 eV in the aqueous phase, leading to a lower adsorption energy of phenol.^[99] In presence of water, the activation barriers of adding surface-bound H atoms to phenol is lowered by 10–20 kJ mol⁻¹, resulted from a small influence of charge for stabilization at the transition state by the solvating water molecules.^[100]

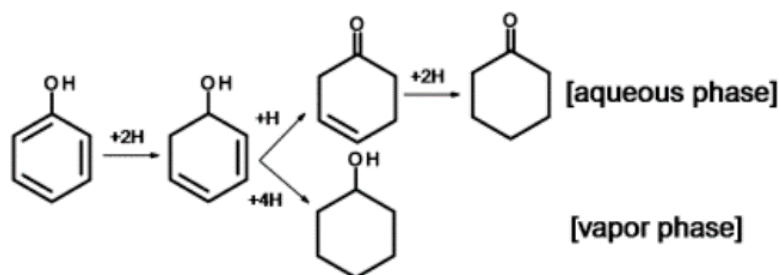


Figure 1.11. Proposed phenol hydrogenation pathways resulting from the study in the liquid phase (upper route) and vapor phase (lower route).^[100] (Adapted with permission from reference 80. Copyright © 2014, American Chemical Society.)

Furthermore, the type of acid would have a great impact on the activation and distribution of products. Liu et al has reported a great enhancement of activity and selectivity of cyclohexanone by Lewis acid at mild conditions.^[101]

In step 1, the aromatic ring of phenol is partially hydrogenated to enol, which is not stable and quickly isomerizes to cyclohexanone before further hydrogenated to cyclohexanol (step 2). In presence of Lewis acid, the supported Pd catalysts have higher activity in step 1, while no activity showing in step 2 under the experimental conditions. It is proposed that the inhibition of cyclohexanone hydrogenation (step 2) is resulted from the Lewis acid. Hydrogenation of

cyclohexanone was conducted over Pd/C and Pd/C-AlCl₃ catalysts. Pd/C-AlCl₃ shows a much lower activity of cyclohexanone hydrogenation compared with Pd/C, which is consistent with the shift of the C=O stretching vibration from 1714 cm⁻¹ to 1624 cm⁻¹ with AlCl₃ due to the coordination of the C=O group to the Lewis acid.

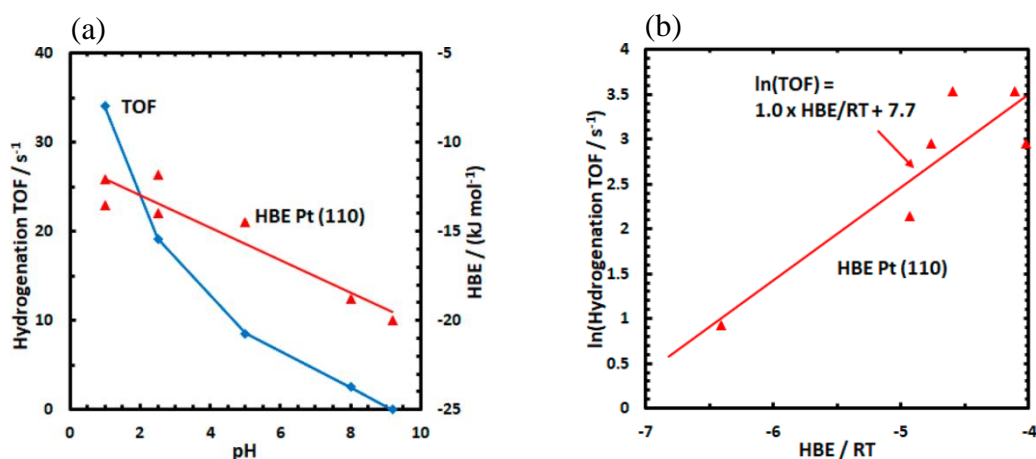


Figure 1.12. Initial TOFs of phenol hydrogenation for 5 wt % Pt/C at 353 K and 20 bar H₂ and HBEs for Pt(110) plotted as a function of pH (a).^[102] Plotting ln(TOF) of phenol hydrogenation versus HBE/RT, where R is the ideal gas constant and T is 353 K (b). (Adapted with permission from reference 99. Copyright © 2019, American Chemical Society.)

Recently, our group has reported that the thermodynamic activity of hydronium ion (homogeneous Brønsted acid) has a strong impact on the rate of phenol hydrogenation in the aqueous phase.^[102] As shown in Figure 1.12, the turnover frequency is increased by 15-fold as pH decreasing from 8 to 1 at 80 °C with 20 bar H₂, that could be ascribed to the weakening of hydrogen binding energy (HBE) on Pt surface with decrease of pH.

By using Brønsted–Evans–Polanyi relation, the activation energy of the rate-determining step decreases with weakening of HBE as pH decreasing, leading to a higher hydrogenation rate of phenol in the aqueous phase.

1.3.3 Electrocatalytic hydrogenation (ECH) of phenol

The electrocatalytic hydrogenation is another pathway to reduce phenol.^[103] The ECH of phenol on different carbon supported catalyst (Pt/C, Rh/C, and Pd/C) was proceeded in order to investigate the impact of electrolyte, pH, current, and catalyst concentration on catalytic activity. In Figure 1.13 the activation energy for ECH was 29 kJ/mol on Pt/C, having the same activation energy with thermocatalytic hydrogenation (TCH) by H₂ on the same catalyst.

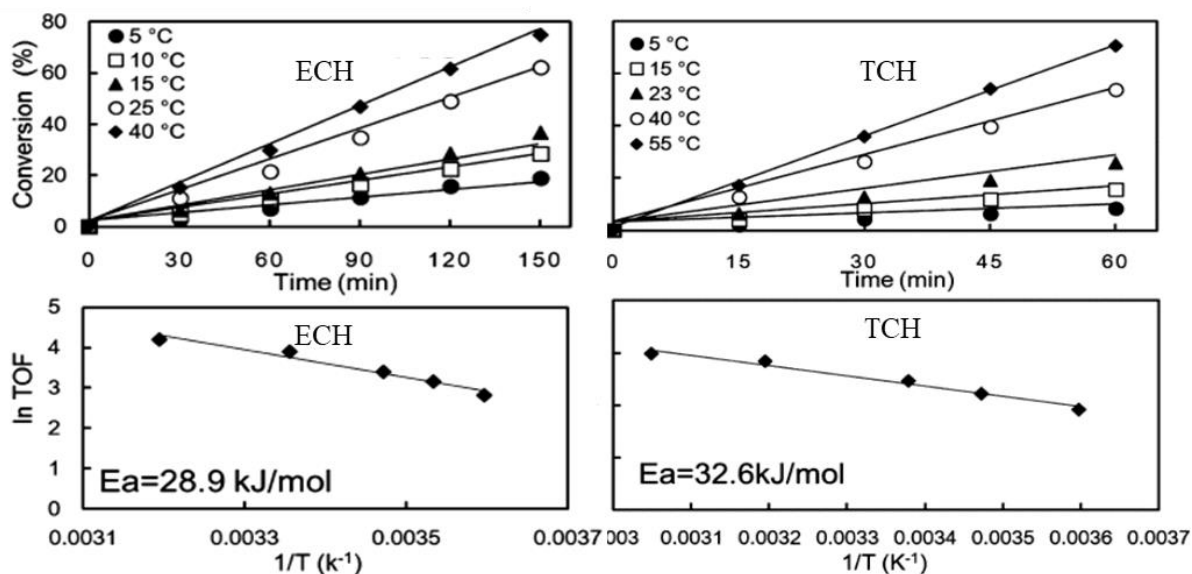


Figure 1.13. Conversion of phenol in ECH and TCH along with time at varying temperatures on Pt/C (upper panels). Arrhenius plots for the ECH and TCH of phenol on Pt/C (lower panels). The reactions in ECH were performed with 50 mg Pt/C in acetic acid at pH 5 (-0.75 V vs Ag/AgCl). The reactions in TCH were performed at atmospheric pressure, 20 mg of Pt/C in acetic acid at pH 5.^[103] (Adapted with permission from reference 100. Copyright © 2015 Elsevier B.V.)

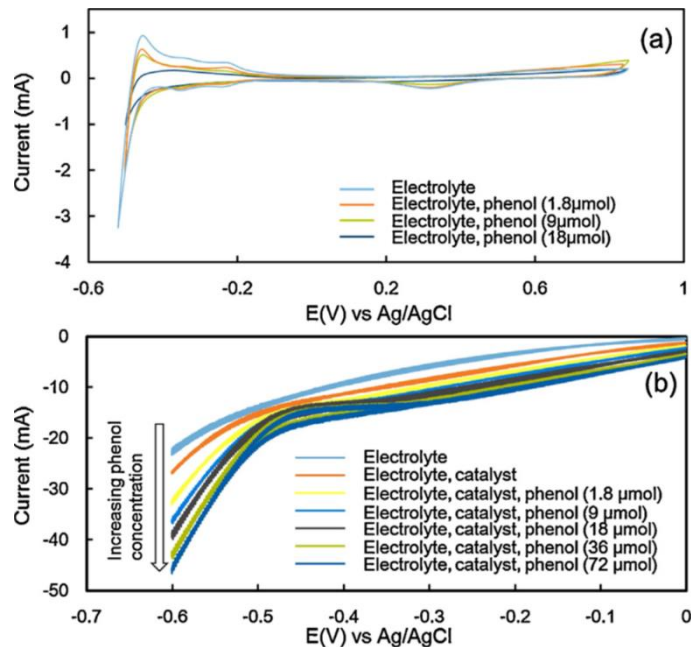


Figure 1.14. Cyclic voltammograms on the Pt cathode at varying concentration of phenol (a). Cyclic voltammograms on the RVC cathode with Pt/C as catalyst, at different concentration of phenol (b). CVs are performed in acetic acid with pH 5, at a scan rate of 20 mV/s.^[103] (Adapted with permission from reference 100. Copyright © 2015 Elsevier B.V.)

Cyclic voltammetry (CV) curves (shown in Figure 1.14) of Pt wire and Pt/C with phenol indicated that phenol molecule is adsorbed and reacted with H sorbed on Pt surface. Thus, the ECH reaction is performed through a Langmuir-Hinshelwood type mechanism, in which the surface adsorbed H atom is generated via proton reduction on the electrode.

In TCH, phenol reacts with surface H atom derived from dissociative adsorption of H₂ on Pt surface. In both ECH and TCH, the reaction products are cyclohexanone and cyclohexanol. Cyclohexene and cyclohexane were not observed.^[103]

1.4 Scope of this thesis

The target of this research is to develop a basic insight into the impact of pH on hydrogenation of phenol in the aqueous phase.

In chapter 2, the adsorption heat of H₂ on Pt in the aqueous phase is obtained by a novel kinetic method and a comparison is made with that in the gas phase. It is found that the lower adsorption heat in water is resulted from the decrease of work function of Pt when it is immersed in the water, which shifts the fermi level of Pt higher and consequently a weaker Pt-H bond in the aqueous phase.

In chapter 3, the impact of pH on adsorption of hydrogen on Pt in the aqueous phase is determined by a novel kinetic method. As pH decreasing from 5.3 to 2, the activation energy of adsorption of H₂ increases, while that of desorption remains constant. As a result, the adsorption heat of H₂ on Pt decreases.

In chapter 4, a mechanistic study of the impact of pH on hydrogenation of phenol is carried out in the aqueous phase. The rate determining step is indicated to be the first H addition step under pH ranging from 5.3 to 2. Besides conventional hydrogenation (CH) pathway, that H₂ firstly dissociatively adsorbed on Pt surface to form adsorbed H atom for hydrogenation, proton coupled electron transfer (PCET) pathway is also involved in the hydrogenation of phenol, in particular under low pH, e.g. pH 2. We propose that the predominant reaction pathway for phenol hydrogenation shifts from CH to PCET with decrease of pH. This is supported by the determined kinetic isotope effect. In addition, the impact of pH on the rates of CH and PCET pathway is also discussed.

The final chapter gives the summary, conclusion and a brief outlook.

1.5 References

- [1] Renewable capacity statistic. 2021, The International Renewable Energy Agency (IRENA). <https://www.irena.org/publications/2021/March/Renewable-Capacity-Statistics-2021>.
- [2] Global Renewables Outlook: Energy transformation 2050. 2020, The International Renewable Energy Agency (IRENA). <https://www.irena.org/publications/2020/Apr/Global-Renewables-Outlook-2020>.
- [3] Global energy transformation: A roadmap to 2050. 2019, The International Renewable Energy Agency (IRENA). <https://www.irena.org/publications/2019/Apr/Global-energy-transformation-A-roadmap-to-2050-2019Edition>.
- [4] D. Gielen, F. Boshell, D. Saygin, M. D. Bazilian, N. Wagner, R. Gorini, *Energy Strategy Reviews* **2019**, 24, 38-50.
- [5] Global energy transformation: The REmap transition pathway. 2019, The International Renewable Energy Agency (IRENA). <https://www.irena.org/publications/2019/Apr/Global-energy-transformation-The-REmap-transition-pathway>.
- [6] The Monthly Energy Review. May 2021, The U.S. Energy Information Administration's (EIA). <https://www.eia.gov/totalenergy/data/monthly/>.
- [7] G. W. Huber, S. Iborra, A. Corma, *Chemical reviews* **2006**, 106, 4044-4098.
- [8] A. V. Bridgwater, **1984**.
- [9] D. Klass, Elsevier: London, **2004**.
- [10] S. P. Babu, *Biomass & bioenergy* **2005**, 29, I-XII.
- [11] K. Zhang, J. Chang, Y. Guan, H. Chen, Y. Yang, J. Jiang, *Renewable Energy* **2013**, 49, 175-184.
- [12] T. A. Milne, R. J. Evans, N. Abatzoglou, **1998**.
- [13] J. R. Rostrup-Nielsen, *Catalysis today* **2002**, 71, 243-247.
- [14] J. R. Rostrup - Nielsen, *Catalysis reviews* **2004**, 46, 247-270.
- [15] A. Bridgwater, G. Peacocke, *Renewable and sustainable energy reviews* **2000**, 4, 1-73.
- [16] D. Mohan, C. U. Pittman Jr, P. H. Steele, *Energy & fuels* **2006**, 20, 848-889.
- [17] J. Moffatt, R. Overend, *Biomass* **1985**, 7, 99-123.
- [18] S. Czernik, A. Bridgwater, *Energy & fuels* **2004**, 18, 590-598.
- [19] D. Elliott, G. Schiefelbein, *Division of Fuel Chemistry* **1989**, 34, 1160.

- [20] C. Wyman, S. Decker, M. Himmel, J. Brady, C. Skopec, L. Viikari 2nd, Marcel Dekker: New York, **2005**.
- [21] L. R. Lynd, P. J. Weimer, W. H. Van Zyl, I. S. Pretorius, *Microbiology and molecular biology reviews* **2002**, *66*, 506-577.
- [22] N. S. Mosier, P. Hall, C. M. Ladisch, M. R. Ladisch, *Recent progress in bioconversion of lignocellulosics* **1999**, 23-40.
- [23] P. J. Deuss, K. Barta, *Coordination Chemistry Reviews* **2016**, *306*, 510-532.
- [24] Z. Strassberger, S. Tanase, G. Rothenberg, *Rsc Advances* **2014**, *4*, 25310-25318.
- [25] J. Zakzeski, P. C. Bruijninx, A. L. Jongerijs, B. M. Weckhuysen, *Chemical reviews* **2010**, *110*, 3552-3599.
- [26] F. S. Chakar, A. J. Ragauskas, *Industrial Crops and Products* **2004**, *20*, 131-141.
- [27] E. Dorrestijn, L. J. Laarhoven, I. W. Arends, P. Mulder, *Journal of Analytical and Applied Pyrolysis* **2000**, *54*, 153-192.
- [28] Y. Pu, D. Zhang, P. M. Singh, A. J. Ragauskas, *Biofuels, Bioproducts and Biorefining: Innovation for a sustainable economy* **2008**, *2*, 58-73.
- [29] Z. Yuan, S. Cheng, M. Leitch, C. C. Xu, *Bioresource technology* **2010**, *101*, 9308-9313.
- [30] C. Li, X. Zhao, A. Wang, G. W. Huber, T. Zhang, *Chemical reviews* **2015**, *115*, 11559-11624.
- [31] K. Stärk, N. Taccardi, A. Bösmann, P. Wasserscheid, *ChemSusChem* **2010**, *3*, 719-723.
- [32] A. Rahimi, A. Ulbrich, J. J. Coon, S. S. Stahl, *Nature* **2014**, *515*, 249-252.
- [33] L. Das, P. Kolar, R. Sharma-Shivappa, J. J. Classen, J. A. Osborne, *Waste and Biomass Valorization* **2017**, *8*, 2673-2680.
- [34] M. D. Scanlon, P. Peljo, M. A. Méndez, E. Smirnov, H. H. Girault, *Chemical science* **2015**, *6*, 2705-2720.
- [35] G. Chatel, R. D. Rogers, *ACS Sustainable Chemistry & Engineering* **2014**, *2*, 322-339.
- [36] R. Behling, S. Valange, G. Chatel, *Green chemistry* **2016**, *18*, 1839-1854.
- [37] H. P. Godard, J. L. McCarthy, H. Hibbert, *Journal of the American Chemical Society* **1941**, *63*, 3061-3066.
- [38] L. M. Cooke, J. L. McCarthy, H. Hibbert, *Journal of the American Chemical Society* **1941**, *63*, 3056-3061.
- [39] E. E. Harris, J. D'Ianni, H. Adkins, *Journal of the American Chemical Society* **1938**, *60*, 1467-1470.

- [40] C. Zhao, J. He, A. A. Lemonidou, X. Li, J. A. Lercher, *Journal of Catalysis* **2011**, *280*, 8-16.
- [41] J. Akhtar, N. A. S. Amin, *Renewable and Sustainable Energy Reviews* **2011**, *15*, 1615-1624.
- [42] S. Xiu, A. Shahbazi, *Renewable and Sustainable Energy Reviews* **2012**, *16*, 4406-4414.
- [43] A. H. Zacher, M. V. Olarte, D. M. Santosa, D. C. Elliott, S. B. Jones, *Green Chemistry* **2014**, *16*, 491-515.
- [44] A. V. Bridgwater, *Biomass and bioenergy* **2012**, *38*, 68-94.
- [45] T. Barth, M. Kleinert, *Chemical Engineering & Technology: Industrial Chemistry - Plant Equipment - Process Engineering - Biotechnology* **2008**, *31*, 773-781.
- [46] M. A. Serio, S. Charpenay, R. Bassilakis, P. R. Solomon, *Biomass and Bioenergy* **1994**, *7*, 107-124.
- [47] Y. Shen, K. Yoshikawa, *Renewable and Sustainable Energy Reviews* **2013**, *21*, 371-392.
- [48] R. J. Evans, T. A. Milne, *Energy & Fuels* **1987**, *1*, 123-137.
- [49] S. Jia, B. J. Cox, X. Guo, Z. C. Zhang, J. G. Ekerdt, *ChemSusChem* **2010**, *3*, 1078-1084.
- [50] L. Chen, J. Dou, Q. Ma, N. Li, R. Wu, H. Bian, D. J. Yelle, T. Vuorinen, S. Fu, X. Pan, *Science advances* **2017**, *3*, e1701735.
- [51] P. J. Deuss, M. Scott, F. Tran, N. J. Westwood, J. G. de Vries, K. Barta, *Journal of the American Chemical Society* **2015**, *137*, 7456-7467.
- [52] C. W. Lahive, P. J. Deuss, C. S. Lancefield, Z. Sun, D. B. Cordes, C. M. Young, F. Tran, A. M. Slawin, J. G. de Vries, P. C. Kamer, *Journal of the American Chemical Society* **2016**, *138*, 8900-8911.
- [53] R. Jastrzebski, S. Constant, C. S. Lancefield, N. J. Westwood, B. M. Weckhuysen, P. C. Bruijninx, *ChemSusChem* **2016**, *9*, 2074.
- [54] R. Thring, *Biomass and Bioenergy* **1994**, *7*, 125-130.
- [55] L. Evans, A. Littlewolf, M. Lopez, J. Miller, Sandia National Laboratories, Albuquerque, NM, and Livermore, CA, **1999**.
- [56] M. Asmadi, H. Kawamoto, S. Saka, *Journal of analytical and applied pyrolysis* **2011**, *92*, 88-98.
- [57] J. Pepper, Y. Lee, *Canadian Journal of Chemistry* **1969**, *47*, 723-727.
- [58] F. P. Petrocelli, M. T. Klein, *Industrial & engineering chemistry product research and development* **1985**, *24*, 635-641.
- [59] E. Laurent, B. Delmon, *Applied Catalysis A: General* **1994**, *109*, 77-96.

- [60] G. De la Puente, A. Gil, J. Pis, P. Grange, *Langmuir* **1999**, *15*, 5800-5806.
- [61] M. Stöcker, *Angewandte Chemie International Edition* **2008**, *47*, 9200-9211.
- [62] M. Saidi, F. Samimi, D. Karimipourfard, T. Nimmanwudipong, B. C. Gates, M. R. Rahimpour, *Energy & Environmental Science* **2014**, *7*, 103-129.
- [63] J. Zhang, J. Sun, Y. Wang, *Green Chemistry* **2020**, *22*, 1072-1098.
- [64] E. Furimsky, *Catalysis reviews science and engineering* **1983**, *25*, 421-458.
- [65] D. D. Laskar, B. Yang, H. Wang, J. Lee, *Biofuels, Bioproducts and Biorefining* **2013**, *7*, 602-626.
- [66] T.-S. Nguyen, D. Laurenti, P. Afanasiev, Z. Konuspayeva, L. Piccolo, *Journal of Catalysis* **2016**, *344*, 136-140.
- [67] C. Zhao, Y. Kou, A. A. Lemonidou, X. Li, J. A. Lercher, *Chemical Communications* **2010**, *46*, 412-414.
- [68] Y. Hong, A. Hensley, J.-S. McEwen, Y. Wang, *Catalysis Letters* **2016**, *146*, 1621-1633.
- [69] M. Badawi, J.-F. Paul, S. Cristol, E. Payen, *Catalysis Communications* **2011**, *12*, 901-905.
- [70] W. Wang, K. Zhang, Z. Qiao, L. Li, P. Liu, Y. Yang, *Industrial & Engineering Chemistry Research* **2014**, *53*, 10301-10309.
- [71] V. O. Gonçalves, S. Brunet, F. Richard, *Catalysis Letters* **2016**, *146*, 1562-1573.
- [72] D. Elliott, Pacific Northwest Lab., Richland, WA (USA), **1983**.
- [73] E. Furimsky, *Applied Catalysis A: General* **2000**, *199*, 147-190.
- [74] H. Weigold, *Fuel* **1982**, *61*, 1021-1026.
- [75] D. Laurenti, P. Afanasiev, C. Geantet, *Applied Catalysis B: Environmental* **2011**, *101*, 239-245.
- [76] N. Van, D. Laurenti, P. Delichere, C. Geantet, *Applied Catalysis B: Environmental* **2011**, *101*, 246-255.
- [77] H. Y. T. Chen, G. Pacchioni, *ChemCatChem* **2016**, *8*, 2492-2499.
- [78] E. Churin, R. Maggi, P. Grange, B. Delmon, in *Research in Thermochemical biomass conversion*, Springer, **1988**, pp. 896-909.
- [79] M. Ferrari, S. Bosmans, R. Maggi, B. Delmon, P. Grange, *Catalysis Today* **2001**, *65*, 257-264.
- [80] M. Ferrari, R. Maggi, B. Delmon, P. Grange, *Journal of Catalysis* **2001**, *198*, 47-55.
- [81] E. Laurent, B. Delmon, *Journal of Catalysis* **1994**, *146*, 281-291.

- [82] F. Yang, D. Liu, Y. Zhao, H. Wang, J. Han, Q. Ge, X. Zhu, *ACS Catalysis* **2018**, *8*, 1672-1682.
- [83] J. A. Hunns, M. Arroyo, A. F. Lee, D. Serrano, K. Wilson, *Catalysis Science & Technology* **2016**, *6*, 2560-2564.
- [84] X. Xue, J. Liu, D. Rao, S. Xu, W. Bing, B. Wang, S. He, M. Wei, *Catalysis Science & Technology* **2017**, *7*, 650-657.
- [85] M. S. Zanuttini, B. O. Dalla Costa, C. A. Querini, M. A. Peralta, *Applied Catalysis A: General* **2014**, *482*, 352-361.
- [86] A. Kumar, A. Kumar, B. Biswas, J. Kumar, S. R. Yenumala, T. Bhaskar, *Renewable Energy* **2020**, *151*, 687-697.
- [87] C. A. Teles, R. C. Rabelo-Neto, J. R. de Lima, L. V. Mattos, D. E. Resasco, F. B. Noronha, *Catalysis Letters* **2016**, *146*, 1848-1857.
- [88] C. Zhao, Y. Kou, A. A. Lemonidou, X. Li, J. A. Lercher, *Angewandte Chemie International Edition* **2009**, *48*, 3987-3990.
- [89] V. M. Roberts, R. T. Knapp, X. Li, J. A. Lercher, *ChemCatChem* **2010**, *2*, 1407-1410.
- [90] N. Mahata, V. Vishwanathan, *Catalysis today* **1999**, *49*, 65-69.
- [91] Y. Wang, J. Zhang, X. Wang, M. Antonietti, H. Li, *Angewandte Chemie International Edition* **2010**, *49*, 3356-3359.
- [92] G. Gao, P. Sun, Y. Li, F. Wang, Z. Zhao, Y. Qin, F. Li, *ACS Catalysis* **2017**, *7*, 4927-4935.
- [93] M. Li, Y. Li, L. Jia, Y. Wang, *Catalysis Communications* **2018**, *103*, 88-91.
- [94] V. Hančič, L. Beranek, *Chemical Engineering Science* **1970**, *25*, 1121-1126.
- [95] G. Li, J. Han, H. Wang, X. Zhu, Q. Ge, *ACS Catalysis* **2015**, *5*, 2009-2016.
- [96] G. Neri, A. Visco, A. Donato, C. Milone, M. Malentacchi, G. Gubitosa, *Applied Catalysis A: General* **1994**, *110*, 49-59.
- [97] D. Taylor, K. Ludlum, *The Journal of Physical Chemistry* **1972**, *76*, 2882-2886.
- [98] S. Scirè, S. Minicò, C. Crisafulli, *Applied Catalysis A: General* **2002**, *235*, 21-31.
- [99] Y. Yoon, R. Rousseau, R. S. Weber, D. Mei, J. A. Lercher, *Journal of the American Chemical Society* **2014**, *136*, 10287-10298.
- [100] Y. Yoon, R. Rousseau, R. S. Weber, D. Mei, J. A. Lercher, *Journal of the American Chemical Society* **2014**, *136*, 10287-10298.
- [101] H. Liu, T. Jiang, B. Han, S. Liang, Y. Zhou, *Science* **2009**, *326*, 1250-1252.

- [102] N. Singh, M.-S. Lee, S. A. Akhade, G. Cheng, D. M. Camaioni, O. Y. Gutiérrez, V.-A. Glezakou, R. Rousseau, J. A. Lercher, C. T. Campbell, *ACS Catalysis* **2018**, *9*, 1120-1128.
- [103] Y. Song, O. Y. Gutiérrez, J. Herranz, J. A. Lercher, *Applied Catalysis B: Environmental* **2016**, *182*, 236-246.

Chapter 2

Adsorption of H₂ on Pt/CNT in the aqueous phase

The adsorption heat of H₂ in the aqueous phase was compared to that in the gas phase by using a kinetic method based on the reaction of D₂O with H₂ on Pt/CNT. In contrast to the gas phase, the adsorption heat of H₂ in the aqueous phase is smaller due to 1) competitive adsorption of H₂ with water on Pt; 2) the change of electronic structure on Pt surface. When immersed into water, the Fermi level of Pt would be in line with that of water at a certain H₂ pressure with a redox couple (hydronium ions and H₂). The Fermi level in the antibonding state of Pt-H bond is shifted downwards, leading to a less occupation of antibonding state and a strong H binding on Pt surface.

2.1 Introduction

Dissociative adsorption of hydrogen is the first elementary step in hydrogenation and hydrogenolysis reactions on transition metals,^[1, 2] involving H₂ physisorption, cleavage of H-H bond and formation of H-metal bond.^[3] The heat of adsorption for H₂, also interpreted as hydrogen binding energy (HBE), is a key factor to evaluate the catalytic activity. As one of transition metals, Pt is used extensively as electrode material in electrochemistry or catalyst in conventional catalytic reactions.^[4-6]

The research on the adsorption of H₂ on Pt surface has been widely conducted in the gas phase, which means the direct exposition of transition metals to H₂ atmosphere, with the corresponding heat ranging from 44 to 178 kJ mol⁻¹H₂ experimentally and theoretically.^[7-19]

Understanding adsorption of H₂ in condensed phase, especially in the aqueous phase, has been mostly investigated in electrochemistry rather than synthetic chemistry, for which it is equally important since a mass of reactions like hydrogenation, hydrogenolysis, hydrodeoxygenation proceed in the aqueous phase for savings of cost and energy.^[20-22]

Yan and coworkers determined the adsorption heat of H₂ on Pt surface via cyclic voltammograms (CVs) method,^[23] in which the HBE has been evaluated by the equation (HBE = $-F \cdot E_{\text{peak}}$), whereas E_{peak} is the characteristic peak of underpotentially deposited hydrogen (H_{UPD}) and F is Faraday constant. However, this method is limited by the requirement of electrical conductivity for measured materials. Yang and coworkers established a kinetic method for determination of H₂ adsorption on Pt surface in the aqueous phase.^[24] The adsorption heat, as well as activation barrier for adsorption and desorption has been obtained regardless of conductivity of materials.

In this work, the adsorption heat of H₂ has been evaluated in the gas and aqueous phase by using calorimetry and kinetic method respectively.

2.2 Experimental and theoretical method

2.2.1 Preparation of catalyst materials

Synthesis for 1 wt% Pt/CNT

H₂PtCl₆ with amount of 13.4 mg was dissolved in 100 ml ethanol and 500 mg CNT was then added into the solution with stirring and ultrasonic treatment for three times respectively (each time for 15 minutes). After that, the solution was treated with reduced pressure distillation at 323 K until the ethanol completely vaporized. Then the solid sample was separated and dried at 373 K overnight. The solid was reduced under 100 mL·min⁻¹ H₂ at 623 K for 2 h with a heating rate of 0.4 K·min⁻¹. The obtained powder was 1wt% Pt/CNT.

2.2.2 Characterization of catalyst materials

Carbon nanotube (CNT)

The phenolic and carboxylic groups on the surface of CNT were quantified by Boehm titration, which is used to determine the concentrations of acidic and basic functional groups on the CNT surface. Due to the difference in their acidities, carboxyl, lactone and phenolic groups can be identified by neutralization with solutions of NaHCO₃, Na₂CO₃ and NaOH, respectively. Thus, 100 mg CNT was added into 200 mL NaHCO₃ (5 mM), Na₂CO₃ (5 mM) and NaOH (8.75 mM) solutions, respectively. Afterwards, the above solutions were dispersed by ultrasonication for 15 min and agitated by magnetic stirring for 48 h before filtration. 10 mL of the filtrates were taken from each sample for the neutralization titration with dilute HCl solution (3.6 mM). Then, the consumption of NaHCO₃, Na₂CO₃ and NaOH by CNT can be obtained. The NaHCO₃ consumption and the difference between Na₂CO₃ and NaHCO₃ consumption as well as the difference between NaOH and Na₂CO₃ consumption, corresponds to carboxyl and lactone and phenolic groups, respectively.

Pt/CNT (1 wt%)

Atomic Absorption Spectroscopy (AAS) was employed to analyze Pt content in catalyst with UNICAM 939 AA-Spectrometer. The catalyst was dissolved in mixture of hydrofluoric acid (48%) and nitrohydrochloric acid at its boiling point before measurement.

Hydrogen chemisorption was used to analyze the particle size and dispersion of Pt in the material.

2.2.3 Determination of H₂ adsorption heat in the gas phase

The adsorption heat of H₂ was measured calorimetrically by a Seteram TG-DSC 111 thermoanalyzer with a baratron pressure transducer. Typically, 4.55 mg of the platelet-shaped samples were placed in a quartz sample holder of the balance. Prior to measurement, the catalyst was activated in H₂ atmosphere at 573 K for 1 h before outgassing under vacuum ($P < 10^{-4}$ mbar). After cooling down to the desired temperature, H₂ was slowly introduced into the closed system until equilibrating under a certain pressure. The heat flux was recorded as the total heat (Q_{total}) of both chemisorbed (irreversibly) and physisorbed (reversibly adsorbed) H₂. Then the system was vacuumed at the same temperature for 12 hours to remove the physisorbed (reversibly adsorbed) H₂. Afterward, the same adsorption procedure of H₂ adsorption was repeated to obtain the heat of physisorbed (reversibly adsorbed) H₂, Q_{phy} . The adsorption heat of chemisorbed (irreversibly adsorbed) H₂, Q_{chem} , is obtained from the subtraction between total and physisorbed heats, $Q_{\text{chem}} = Q_{\text{total}} - Q_{\text{phy}}$.

2.2.4 Determination of H₂ adsorption heat in the aqueous phase by kinetic method of reaction of H₂ (g) with D₂O (l)

The reaction of H₂ (g) with D₂O (l) was performed in an autoclave (Parr Instrument, 100 mL). Typically, 5 mg Pt-CNT with 30 mL D₂O were added into the autoclave reactor before being heated to the reaction temperatures under 700 rpm agitation. When the required temperature was achieved, the reactor was quickly purged with H₂ gas for three times and pressurized to a certain H₂ pressures. The gas products were collected through a gas bag with a tap and analyzed by a Mass spectroscopy (OMNI Star GSD 320). The apparent and normalized formation rate of HD and D₂ are:

Apparent formation rate = Yield of HD or D₂ / Reaction time

Normalized formation rate to surface Pt atoms = Apparent formation rate / Number of surface Pt atoms in reaction

2.3 Results and discussion

2.3.1 Physicochemical properties of the catalyst

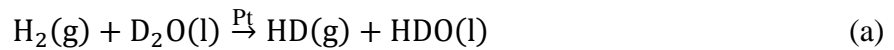
The functional groups on the surface of carbon nanotube (CNT) were determined by Boehm titration method. The concentration of phenolic and carboxylic groups is 29 and 7.2 $\mu\text{mol g}_{\text{CNT}}^{-1}$ (shown in Table 2.1), which means this kind of carbon nanotube has a clean surface with a very small amount of functional groups.

The metal dispersion of 1 wt% Pt/CNT sample is 12% with 9 nm Pt particle size.

2.3.2 Derivation of kinetic method and calculation of adsorption heat of H₂ in the aqueous phase

2.3.2.1 Derivation of kinetic method

In principle, the reaction of H₂ (g) with D₂O (l) on Pt/CNT catalyst could be described as :



For these two pathways, H₂ firstly adsorbs and dissociates into H atoms on Pt surface before partially exchanging to D atoms via interaction with adsorbed D₂O. The H and D atoms on Pt surface recombine into H₂, HD and D₂ and desorb from the surface. Table A2.1 summarizes the elementary steps involved in the reaction of D₂O (liquid) with H₂ (gas). Under a given H₂ pressure, the desorption rates of H₂ (r_{H_2}) HD (r_{HD}) and D₂ (r_{D_2}) follow Equations 2.1 and 2.2 (Derivation details are given in the Appendix).

$$(r_{\text{H}_2} + r_{\text{HD}} + r_{\text{D}_2})^{0.5} P_{\text{H}_2}^{-0.5} = k_a^{0.5} - K_a^{0.5} (r_{\text{H}_2}^{0.5} + r_{\text{D}_2}^{0.5} [\text{KIE}]_{\text{D}_2}^{0.5}) \quad (\text{Eq.2.1})$$

$$r_{\text{H}_2} = \frac{r_{\text{HD}}^2 [\text{KIE}]_{\text{D}_2}}{4r_{\text{D}_2} [\text{KIE}]_{\text{HD}}^2} \quad (\text{Eq. 2.2})$$

Adsorption rate constant: k_a

Equilibrium constant: K_a

$$\text{Kinetic isotope effect of HD: } [\text{KIE}]_{\text{HD}} = \frac{k_{\text{HD}}}{k_{\text{D}_2}}$$

$$\text{Kinetic isotope effect of D}_2: [\text{KIE}]_{\text{D}_2} = \frac{k_{\text{D}_2}}{k_{\text{H}_2}}$$

(KIE values are compiled in the Appendix Information, Section A2.2).

The values of r_{HD} and r_{D_2} were determined by the corresponding formation rates in the reaction, while for r_{H_2} , it could be obtained by using r_{HD} and r_{D_2} based on equation (2) instead of direct measurement due to the excess of H_2 .

According to equation (1), the term $(r_{\text{H}_2} + r_{\text{HD}} + r_{\text{D}_2})^{0.5} P_{\text{H}_2}^{-0.5}$ shows a linear correlation with the term $(r_{\text{H}_2}^{0.5} + r_{\text{D}_2}^{0.5} [\text{KIE}]_{\text{D}_2}^{0.5})$. K_a and k_a are the square of the slope and the intercept, respectively.

At 20 bar H_2 and 30 mL D_2O at 333 K, it is shown in the inset of Figure 3.3 (yields of HD and D_2 as a function of the reaction time), That HD and D_2 increased linearly from the starting point of the reaction until 20 min, indicating that the period to reach steady-state coverages of H and D on Pt surface is very short. Re-adsorption of HD and D_2 could be neglected during the reaction due to the large excess of H_2 causing D concentration in the gas phase being below 2 % even after 20 min. The formation rates of HD and D_2 were $64 \text{ mol}_{\text{HD}} \text{ mol}_{\text{Pt}}^{-1} \text{ s}^{-1}$ and $2.2 \text{ mol}_{\text{D}_2} \text{ mol}_{\text{Pt}}^{-1} \text{ s}^{-1}$ respectively according to the slopes.

Using the two values above in Equation 2.2, the formation rate of H_2 was calculated to be $5.6 \times 10^2 \text{ mol}_{\text{H}_2} \text{ mol}_{\text{Pt}}^{-1} \text{ s}^{-1}$. Similarly, the formation rates of H_2 , HD, and D_2 at different H_2 pressures and temperatures were measured and plotted according to Equation 2.1, as shown in Figure 2.1

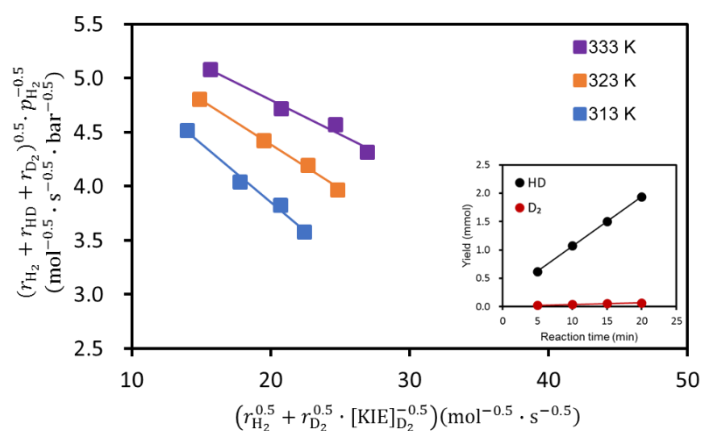


Figure 2.1. Reaction kinetic results over Pt/CNT at different pressures and temperatures plotted according to Equation (1). The inset shows the yield of HD and D_2 with reaction time at 333 K, 30 bar H_2 and 5 mg Pt/CNT.

The K_a and k_a were obtained from the corresponding slope and intercept according to Equation (1). Then, the desorption rate constant (k_{-a}) was calculated by division of k_a by K_a ($k_{-a} = \frac{k_a}{K_a}$). The summary of all adsorption rate constants and equilibrium constants on Pt/CNT are shown in Table 2.1.

Table 2.1. Adsorption and desorption rate constants and adsorption equilibrium constants over Pt/CNT at temperatures from 313 to 333 K. (Relative deviations: ca. 8%). [a] $E_{a, des}$: Activation energy of desorption, $E_{a, ads}$: activation energy of adsorption, Q_{ads} : heat of adsorption.

T [K]	K_a°	k_a [$s^{-1} \text{bar}^{-1}$]	k_{-a} [s^{-1}]
313	1.2×10^{-2}	36	3.1×10^3
323	6.7×10^{-3}	36	5.4×10^3
333	4.1×10^{-3}	37	9.0×10^3
	Q_{ads}	$E_{a, ads}$	$E_{a, des}$
Energy [$\text{kJ mol}_{\text{H}_2}^{-1}$] ^[a]	45 ± 1	1 ± 1	46 ± 1

According to Arrhenius plot and van't-Hoff plot, the activation energy of adsorption ($E_{a, ads}$) and desorption ($E_{a, des}$) as well as the heat of adsorption (Q_{ads}) were obtained (shown in Figure 2.2 and Table 2.1). The desorption rate constant k_{-a} shows an increasing trend with temperature, resulting in an activation energy of desorption being $46 \pm 1 \text{ kJ mol}_{\text{H}_2}^{-1}$. The equilibrium constant K_a° decreases with temperature, meaning an exothermic process with an adsorption heat of $45 \pm 1 \text{ kJ mol}_{\text{H}_2}^{-1}$. The activation energy of adsorption is nearly zero ($1 \pm 1 \text{ kJ mol}_{\text{H}_2}^{-1}$) since nearly no change appeared in the rate constant of H_2 adsorption k_a with temperature. This is in agreement with previous adsorption studies in the gas and aqueous phase that it is spontaneous for H_2 dissociative chemisorption process on Pt surface, which means no activation energy required for H_2 dissociative adsorption on Pt surface.

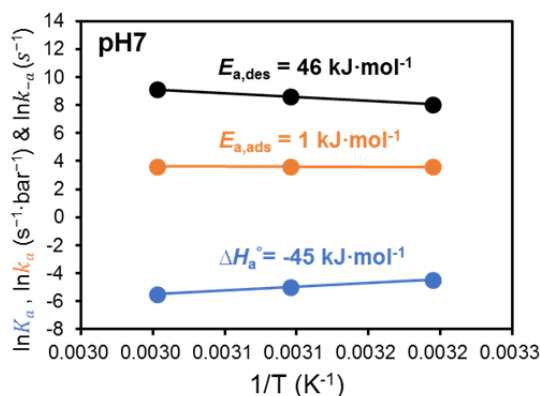


Figure 2.2. Arrhenius plots of adsorption and desorption rate constants and van't Hoff plot of adsorption equilibrium constants, in H_2 adsorption on Pt/CNT in the aqueous phase.

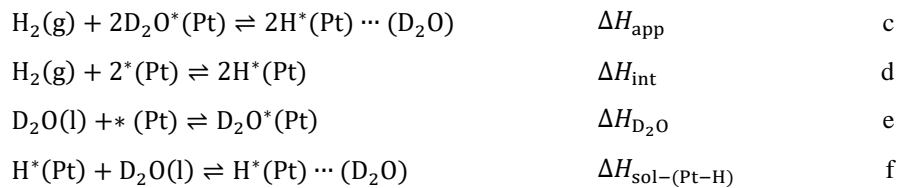
2.3.3 Adsorption heat of H₂ in the gas phase

By the difference between the heat of total adsorbed H atoms (1.9×10^{-6} kJ) and that (9.9×10^{-7} kJ) of the reversibly adsorbed H atoms. After normalized to the amount of surface Pt, the adsorption heat of H₂ on Pt/CNT in the gas phase was determined to be 70 ± 1 kJ mol_{H₂}⁻¹. This is higher than that in the aqueous phase, meaning the dissociative adsorption of H₂ on Pt in the gas phase is stronger than that in the aqueous phase. In this case, the influence of electronic structure of Pt on dissociative adsorption of H₂ will be introduced to explain the difference of H₂ adsorption between the gas phase and aqueous phase.

2.3.4 Influence of water on H₂ adsorption heat

In the aqueous phase, because of the existence of oriented and structured water molecules that covered Pt surface in forms of multilayers, the adsorption of H₂ on Pt surface goes through competition with that of water, displacing, disrupting or restructuring the water layers on Pt. In a thermodynamic cycle, three elementary steps are involved in H₂ adsorption on Pt in water (Reaction c, $\Delta H_{app} = -45$ kJ mol_{H₂}⁻¹):

- (1) Dissociative adsorption of H₂ on Pt (Reaction d, $\Delta H_{int} = -70$ kJ mol_{H₂}⁻¹)
- (2) Adsorption of D₂O from the liquid phase to Pt surface (Reaction e, $\Delta H_{D_2O} = -6$ kJ mol⁻¹)
- (3) Solvation of Pt-H within D₂O (Reaction f, $\Delta H_{sol-(Pt-H)}$)



Due to the solvation of Pt-H in liquid D₂O, the solvation enthalpy is obtained by

$$\Delta H_{sol-(Pt-H)} = \frac{(\Delta H_{app} - \Delta H_{int})}{2} + \Delta H_{D_2O} = 6.5 \text{ kJ mol}^{-1}$$

The positive value means the solvation of Pt-H within liquid D₂O is endothermic process, which is hypothesized to be resulted from both the solvation of Pt-H by D₂O and the change of electronic structure of Pt that is affected by the redox couple at the D₂O–Pt interface

2.3.5 Influence of Pt electronic structure on H₂ adsorption heat

Adsorbed H on Pt forms Pt-H bond. For a single Pt atom, the bond of Pt-H is formed by the combination of bonding and antibonding states which are resulted from the hybridization of its 5d orbital and the 1s orbital of H atom.^[25, 26] For a solid Pt metal, the 5d atomic orbitals of all Pt atoms constituting the solid overlap and form the 5d band. This 5d band hybridizes with 1s orbital of H atom to form bonding state and antibonding state. In molecular orbital theory (shown in Figure 2.3), a chemical bond has both bonding and antibonding states. The more filling of the antibonding state by electrons, the weaker the strength of a chemical bond. For the particular case, Pt-H bond at Pt surface, the more probabilities of antibonding state being occupied by electrons, the weaker the strength of Pt-H bond. The electron energy level could be described by Fermi level of Pt-H. The electron densities in the electronic band of metals are related to the corresponding Fermi levels.

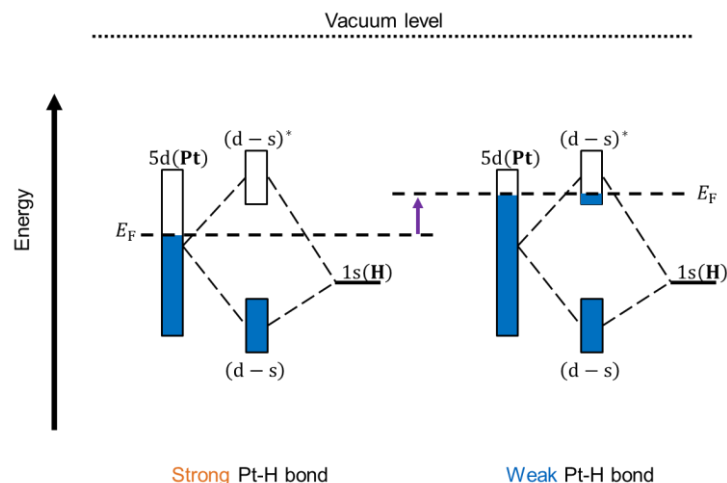


Figure 2.3. Filling of the antibonding state, (d-s)*, by fermi level of Pt-H bond. A less filling results in a strong Pt-H bond, while a more filling results in a weak Pt-H bond relatively. The green arrow indicates increase of energy.

The antibonding state of Pt-H is empty, and the Fermi level of Pt-H is located near the antibonding state hybridized by 5d band of Pt and 1s state of H atom. Thus, the filling of Pt-H antibonding state by electrons directly influences the strength of Pt-H bond. The less probability of the antibonding state being occupied by electrons, the stronger Pt-H bond and on the contrary, the more filling of Pt-H antibonding state leads to a weak Pt-H bond.

Pt/CNT catalyst in water and in presence of H₂ can be considered as a hydrogen electrode. At a certain temperature and pressure of hydrogen, the electrode potential of Pt/CNT can be obtained with pressure of hydrogen and pH. For instance, the electrode potential of Pt/CNT is

4.00 V (with respect of SHE as 4.44 V) under pH 7, 298 K and 10 bar H₂, which is also the work function of solution under the same conditions. The work function for pure Pt (111) surface is 5.6-5.8 eV.^[27]

Fermi level can be referenced to vacuum level and expressed as equation 3,

$$E_F = E_{V_{\text{vacuum}}} - \Phi \quad \text{Eq. 2.3}$$

Where E_F is Fermi level, $E_{V_{\text{vacuum}}}$ is energy of vacuum (0 eV) and Φ is work function.

Before the contact between Pt and electrolyte that shown in Figure 2.4(a), the Fermi level of Pt ($E_{F-\text{Pt}}$) is lower than that of $\text{H}^+(\text{H}_2\text{O})_n/\text{H}_2$ electrolyte ($E_{F-\text{redox}}$). $E_{F-\text{redox}}$ could be regarded as unchangeable due to the large amount of solution (30 mL) compared with 5 mg Pt/CNT catalysts. When Pt/CNT catalyst immersed in water, the junction is generated at the interface between $\text{H}^+(\text{H}_2\text{O})_n/\text{H}_2$ electrolyte and Pt surface. The change of electronic structure of Pt uppermost surface after immersion in water is shown in Figure 2.4 (b). When a contact is formed between two sides, the electrons start to flow from electrolyte side into Pt side (uppermost surface) until the Fermi level in both sides becoming equal. This leaves a negative charge accumulated on Pt side and a positive charge on electrolyte side with a contact potential, leading to the formation of an interface dipole layer (atomic scale, uppermost surface) at the junction. For small particle size catalysts (less than 2 nm), this model (model 1) can be well used to explain the change of electronic structure of metal in solution with redox couple.^[28] But to our knowledge, it is still unclear for the catalysts with large particle size by using this model.

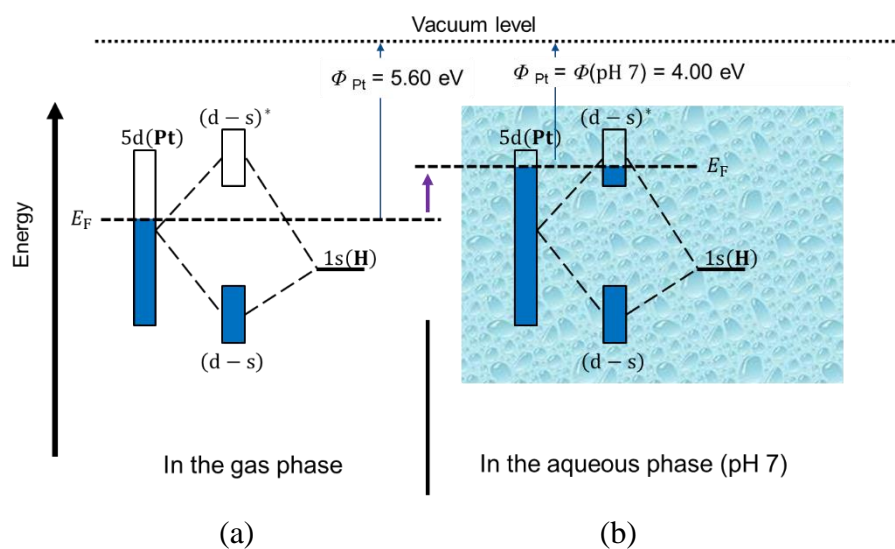


Figure 2.4. Schematic illustration: Comparison of electronic structure of uppermost surface Pt in the gas phase (a) and in the aqueous phase (b) under pH 7, 10 bar H₂ at 298 K.

If we treat the junction between metal and electrolyte with redox couple as the junction between dissimilar metals (model 2), the situation is like the model shown in Figure 2.5. It is reported that the Fermi level of two dissimilar metals would be aligned with each other at equilibrium after contact and a build-up of potential difference would be formed at the interface, which causes a sharp increase or decrease of the bands energy on the surface of two sides.^[29, 30]

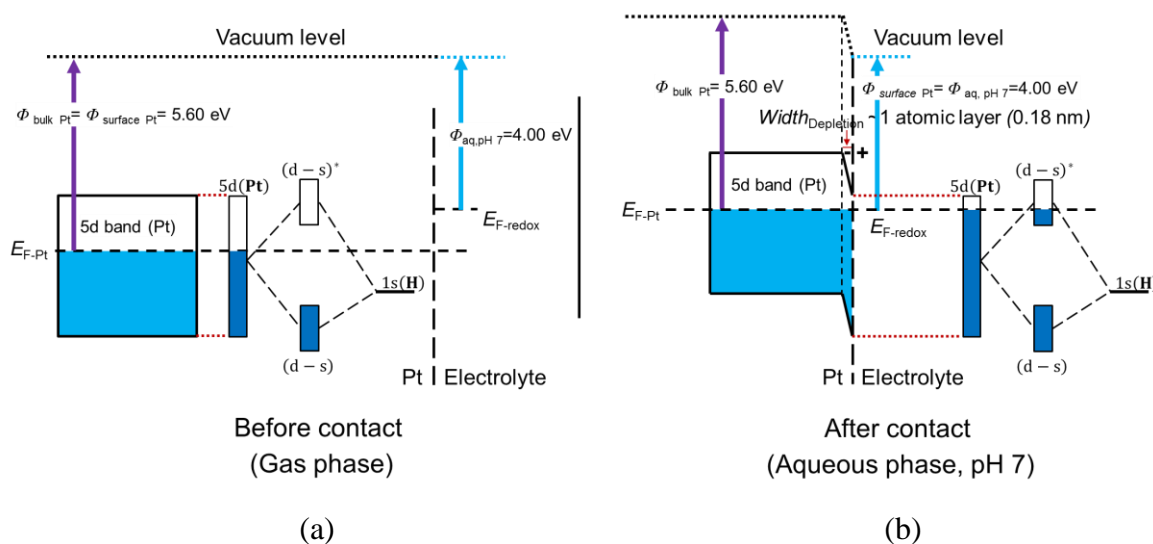


Figure 2.5. The change at Pt surface before (gas phase) (a) and after contact (aqueous phase) (b) with electrolyte with redox couple ($\text{H}_2/\text{H}_3\text{O}^+$) under pH 7, 298 K, 10 bar H_2 .

In addition, the excess electron is reported to be located at ~ 0.18 nm and ~ 0.13 nm from the uppermost layer of the Pt (111) surface for H_{ad} adsorbed at the top and hollow site, respectively.^[31]

As a result, the electronic bands at the interface bend down in the direction from Pt to electrolyte with the energy bands at Pt surface declining by the amount of the difference between $E_{\text{F-Pt}}$ and $E_{\text{F-redox}}$. This causes a part of Pt-H antibonding state being more filled by electrons, leading to a weaker Pt-H bond compared with the bond in the gas phase. However, it is still under debate for the change of electronic structure on metal uppermost surface by using band bending like p-n junction in semiconductor case.

It is notable that the band bending only occurred at the outmost surface of Pt after immersion into electrolyte. Band bending of metal can be neglected due to its small shift of energy levels resulted from small change in charge (depends on capacitance between the materials),^[32] and quite narrow depletion width (atomic scale) in comparison to that (10-200 nm^[33, 34]) of semiconductor. This is because of the much higher electron density in metal (10^{22} cm^{-3}) than in semiconductor (10^{17} cm^{-3}).^[35] But for heterogeneous catalysis the property of the outmost Pt

surface has a great impact on catalytic reactions. In Figure 2.5 (b), the up-shifting vacuum level for Pt bulk phase is drawn to assure the electron affinity of bulk phase Pt being constant, since no electric field existed in it.

Although the existence of defects when applying these two models to our work, there is no doubt on the change of electronic structure on the uppermost surface of Pt, which giving a tunable HBE on Pt by the Fermi level of redox couple or electrode potential.

2.4 Conclusions

In conclusion, the thermodynamic properties of H₂ adsorption on Pt surface in water were determined by reaction of H₂ (g) with D₂O (l) into D₂ (g) and HD (g) on Pt/CNT catalyst.

The adsorption of H₂ in the aqueous phase is much weaker in contrast to the adsorption at the gas–solid interface, which is mainly resulted from 1) water binding energy on Pt that competes with hydrogen; 2) variation of Pt electronic structure compared to adsorption at the gas–solid interface. The heat of H₂ adsorption on Pt in water and the gas phase are 45 ± 1 and 70 ± 1 kJ mol_{H₂}⁻¹, respectively.

At the established hydrogen electrode, adsorbed H atoms in liquid water are equilibrated with hydronium ions via a redox reaction at the Pt–water interface, inducing a more filling of Pt-H antibonding state by electrons with the antibonding state overwhelmed by fermi level after being equilibrated with H⁺(H₂O)_n/H₂ electrolyte under a certain condition.

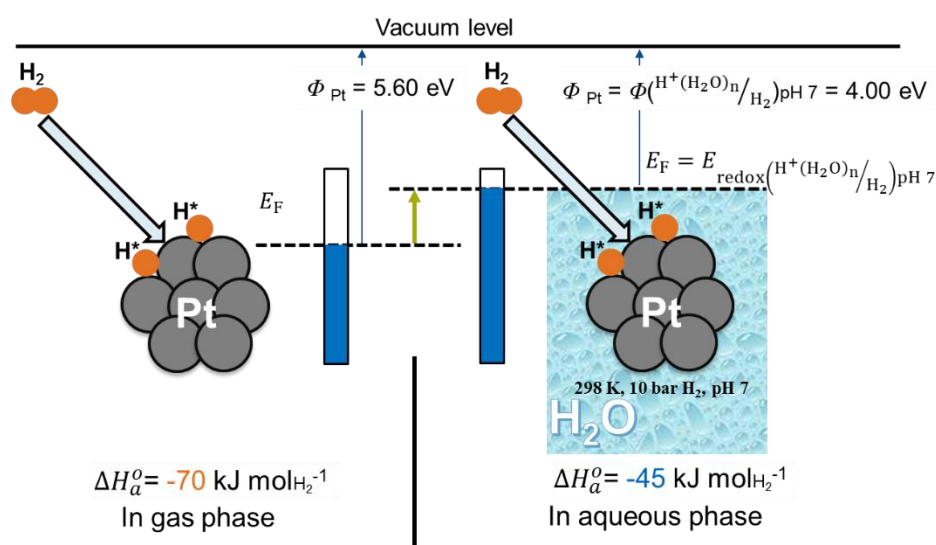


Figure 2.5. Schematic illustration: Influence of outmost surface Pt electronic structure on the dissociative adsorption of H₂ on Pt in the aqueous phase.

2.5 Appendix

Here, a novel kinetic method is used to evaluate the heat of adsorption for H₂ on Pt/CNT catalyst in the aqueous phase. (Adapted with permission from reference 24. Copyright © 2019 Wiley-VCH Verlag GmbH & Co. KGaA, Weinheim.)

The reactions involved in the method are shown in below (Eq. A2.1 and A2.2).



Table A2.1. Elementary steps in reaction of H₂ (g) with D₂O.(l)

Description	Elementary step	Rate constant	Rate equation
H ₂ adsorption	$\text{H}_2 + 2* \xrightarrow{k_a} 2\text{H}^*$ (Rxn A2.3)	k_a	$r_{\text{ads}} = k_a p_{\text{H}_2} \theta_*^2$ (Eq. A2.1)
D* generation	$\text{H}^* + \text{D}_2\text{O} \xrightarrow{k_{\text{exc}}} \text{D}^* + \text{HDO}$ (Rxn A2.4)	k_{exc}	$r_{\text{exc}} = k_{\text{exc}} \theta_{\text{H}} [\text{D}_2\text{O}]$ (Eq. A2.2)
H ₂ desorption	$\text{H}^* + \text{H}^* \xrightarrow{k_{-a}} \text{H}_2 + 2*$ (Rxn A2.5)	k_{-a}	$r_{\text{H}_2} = k_{-a} \theta_{\text{H}}^2$ (Eq. A2.3)
HD desorption	$\text{H}^* + \text{D}^* \xrightarrow{k_{\text{HD}}} \text{HD} + 2*$ (Rxn A2.6)	$k_{\text{HD}} = k_{-a} [\text{KIE}]_{\text{HD}}$	$r_{\text{HD}} = 2k_{\text{HD}} \theta_{\text{D}} \theta_{\text{H}}$ (Eq. A2.4)
D ₂ desorption	$\text{D}^* + \text{D}^* \xrightarrow{k_{\text{D}_2}} \text{D}_2 + 2*$ (Rxn A2.7)	$k_{\text{D}_2} = k_{-a} [\text{KIE}]_{\text{D}_2}$	$r_{\text{D}_2} = k_{\text{D}_2} \theta_{\text{D}}^2$ (Eq. A2.5)

* : Pt site uncovered by H or D;

p_{H_2} : H₂ pressure.

θ_{H} and θ_{D} are the coverage of Hydrogen and Deuterium.

θ_* is the fraction (coverage) of Pt sites uncovered by H or D.

[KIE] refers to the kinetic isotope effect. (Calculation of KIE in Supporting Information)

[KIE]_{HD} refers to k_{HD}/k_{-a} .

[KIE]_{D₂} refers to k_{HD}/k_{-a} .

[D₂O]: activity of D₂O in reaction solution.

Gaseous H₂ reacts with liquid D₂O, forming D₂, HD in gaseous state and HDO in liquid state. (Rxn A2.1 and A2.2).

Three elementary steps are involved:

- 1) Dissociative adsorption of H₂ on Pt surface (Rxn A2.3);
- 2) Active D atom generation on Pt surface via the reaction of D₂O with surface adsorbed H (Rxn. A2.4)
- 3) Desorption of HD, D₂ and H₂. (Rxn. A2.5 – A2.7).

Table A1 gives the detailed elementary steps and corresponding kinetic parameters.

The number of sites for adsorption on Pt surface is a constant, which equals to 1, including H coverage, D coverage and uncovered sites (Eq. A2.6).

$$\theta_{\text{H}} + \theta_{\text{D}} + \theta_{*} = 1 \quad (\text{Eq. A2.6})$$

Based on Equations A2.1, A2.3 and A2.5, the coverage of atomic H, atomic D and empty site can be expressed individually as:

$$\theta_{\text{H}} = r_{\text{H}_2}^{0.5} \cdot k_{-\text{a}}^{-0.5}; \quad (\text{Eq. A2.7})$$

$$\theta_{\text{D}} = r_{\text{D}_2}^{0.5} \cdot k_{-\text{a}}^{-0.5} \cdot [\text{KIE}]_{\text{D}_2}^{-0.5} \quad (\text{Eq. A2.8})$$

$$\theta_{*} = r_{\text{ads}}^{0.5} \cdot k_{\text{a}}^{-0.5} \cdot p_{\text{H}_2}^{-0.5} \quad (\text{Eq. A2.9})$$

Therefore, Equation A6 could be reformulated as Equation A2.10.

$$r_{\text{H}_2}^{0.5} \cdot k_{-\text{a}}^{-0.5} + r_{\text{D}_2}^{0.5} \cdot k_{-\text{a}}^{-0.5} \cdot [\text{KIE}]_{\text{D}_2}^{-0.5} + r_{\text{ads}}^{0.5} \cdot k_{\text{a}}^{-0.5} \cdot p_{\text{H}_2}^{-0.5} = 1 \dots (\text{Eq. A2.10})$$

In a steady state reaction, the adsorption rate of H₂ from the gas phase onto the surface of Pt is equivalent to the desorption rate of H₂, HD and D₂ from Pt into the gas phase (Eq. A2.11),

$$r_{\text{ads}} = r_{\text{H}_2} + r_{\text{HD}} + r_{\text{D}_2} \quad (\text{Eq. A2.11})$$

Equation A10 is further written as Equation A2.12 and reformulated as Equation A2.13.

$$r_{\text{D}_2}^{0.5} \cdot k_{-\text{a}}^{-0.5} \cdot [\text{KIE}]_{\text{D}_2}^{-0.5} + r_{\text{H}_2}^{0.5} \cdot k_{-\text{a}}^{-0.5} + (r_{\text{H}_2} + r_{\text{HD}} + r_{\text{D}_2})^{0.5} \cdot k_{\text{a}}^{-0.5} \cdot p_{\text{H}_2}^{-0.5} = 1 \dots (\text{Eq. A2.12})$$

$$(r_{\text{H}_2} + r_{\text{HD}} + r_{\text{D}_2})^{0.5} \cdot p_{\text{H}_2}^{-0.5} = k_{\text{a}}^{0.5} - (r_{\text{H}_2}^{0.5} + r_{\text{D}_2}^{0.5} \cdot [\text{KIE}]_{\text{D}_2}^{-0.5}) \cdot (k_{\text{a}}/k_{-\text{a}})^{0.5} \dots (\text{Eq. A2.13})$$

Note that the last term in Equation A2.13, $k_{\text{a}}/k_{-\text{a}}$, is actually the equilibrium constant of adsorption of H₂ on Pt, K_{a} (Eq. A2.14).

$$K_{\text{a}} = k_{\text{a}}/k_{-\text{a}} \quad (\text{Eq. A2.14})$$

Thus, Equation A2.14 is finally obtained from Equation A2.13 and A2.14.

$$(r_{\text{H}_2} + r_{\text{HD}} + r_{\text{D}_2})^{0.5} \cdot p_{\text{H}_2}^{-0.5} = k_{\text{a}}^{0.5} - (r_{\text{H}_2}^{0.5} + r_{\text{D}_2}^{0.5} \cdot [\text{KIE}]_{\text{D}_2}^{-0.5}) \cdot K_{\text{a}}^{0.5} \quad (\text{Eq. A2.15})$$

The form of Equation A2.15 shows that under constant k_{a} and K_{a} , which are typically fixed under a certain temperature, the term $(r_{\text{H}_2} + r_{\text{HD}} + r_{\text{D}_2})^{0.5} \cdot p_{\text{H}_2}^{-0.5}$ shows a negative linear correlation with the term $(r_{\text{H}_2}^{0.5} + r_{\text{D}_2}^{0.5} \cdot [\text{KIE}]_{\text{D}_2}^{-0.5})$, as the slope being the square root of K_{a} and the intercept being the square root of k_{a} . The desorption rate of HD (r_{HD}) and D₂ (r_{D_2}) are determined by the formation rates of HD and D₂ in the reaction. The desorption rate of H₂ (r_{H_2}) could not be directly obtained due to the large presence of gas H₂. According to the rate Equations A2.3, A2.4 and A2.5, the desorption rate of H₂ (r_{H_2}) can be calculated and expressed as a function of the measured r_{HD} and r_{D_2} (Eq. A2.16).

$$r_{H_2} = \frac{[KIE]_{D_2} \cdot r_{HD}^2}{4[KIE]_{HD}^2 \cdot r_{D_2}} \quad (\text{Eq. A2.16})$$

A practical method is given to determine K_a , k_a and k_{-a} from linear fitting Equation A2.15 via the measured data of r_{HD} and r_{D_2} under a certain temperature with a series of different pressure of H_2 (p_{H_2}) (**Table A2.2**). Moreover, all the relevant kinetic and thermodynamic parameters, e.g. heat of adsorption and energy barrier for adsorption and desorption, can be calculated via Arrhenius equation or Van't Hoff equation.

Table A2.2. Experimental method to determine the k_a , k_{-a} and K_a via the reaction of H_2 with liquid D_2O

Reaction	$H_2 (g) + 2D_2O (l) \xrightarrow{Pt} D_2 (g) + 2HDO (l)$	(Rxn A2.1)
	$H_2 (g) + D_2O (l) \xrightarrow{Pt} HD (g) + HDO (l)$	(Rxn A2.2)
Equation	$(r_{H_2} + r_{DH} + r_{D_2})^{0.5} \cdot p_{H_2}^{-0.5} = k_a^{0.5} - (r_{H_2}^{0.5} + r_{D_2}^{0.5} \cdot [KIE]_{D_2}^{-0.5}) \cdot K_a^{0.5}$	(Eq. A2.15)
Data acquisition	r_{HD} and r_{D_2} measured by HD and D_2 formation rate, r_{H_2} calculated by $r_{H_2} = \frac{[KIE]_{D_2} \cdot r_{HD}^2}{4[KIE]_{HD}^2 \cdot r_{D_2}}$	(Eq. A2.16)
Plot	Plotting $(r_{H_2} + r_{HD} + r_{D_2})^{0.5} \cdot p_{H_2}^{-0.5}$ against $(r_{H_2}^{0.5} + r_{D_2}^{0.5} \cdot [KIE]_{D_2}^{-0.5})$ gives a linear curve: $K_a = (\text{Slope})^2$; $k_a = (\text{Intercept})^2$; $k_{-a} = (\text{Slop/Intercept})^2$	

Calculation and values of kinetic isotope effect

(Adapted with permission from reference 24. Copyright © 2019 Wiley-VCH Verlag GmbH & Co. KGaA, Weinheim.)

It is known when an atom in a reactant molecule is replaced by one of its isotopes, rate constants for the reaction may change. The ratio between them is the kinetic isotope effect (KIE). This effect is normally weak for heavy atom isotopes, but is substantial for hydrogen isotopes (H, D and T). In the reaction of gas H₂ with liquid D₂O over Pt catalysts, the kinetic isotope effect in the formation rates of H₂, HD and D₂ involves the three elementary reactions in Table A2.3. The kinetic isotope effect [KIE]_{HD} and [KIE]_{D₂} are defined as their rate constant ratios:

$$[\text{KIE}]_{\text{HD}} = \frac{k_{\text{HD}}}{k_{\text{H}_2}}; [\text{KIE}]_{\text{D}_2} = \frac{k_{\text{D}_2}}{k_{\text{H}_2}} \quad (\text{Eq. A2.17})$$

In order to calculate the [KIE]_{HD} and [KIE]_{D₂} for HD and D₂, Bigeleisen's theoretical treatments were applied.^[36] The expression for calculating hydrogen/deuterium kinetic isotope effect is simplified as shown in the following Equation A2.18

$$\frac{k_{\text{H}}}{k_{\text{D}}} = S \cdot M \cdot I \cdot \text{EXC} \cdot \text{ZPE} \quad (\text{Eq. A2.18})$$

H or D in the subscript refers to hydrogen or deuterium containing species. Both S factor (symmetry number) and EXC factor (from the contributions of vibrationally excited molecules)

Table A3. Derivation of kinetic isotope effect (KIE) for the desorption of HD and D₂ on Pt.

Description	Reaction steps	Rate constant	Molecular mass	Moment of inertia	Zero point energy
H ₂ desorption	Pt-H + Pt-H $\xrightarrow{k_{\text{H}_2}}$ 2Pt + H ₂	k_{H_2} [a]	M_{H_2}	I_{H_2}	ZPE_{PtH} ; ZPE_{PtD}
HD desorption	Pt-H + Pt-D $\xrightarrow{k_{\text{HD}}}$ 2Pt + HD	k_{HD}	M_{HD}	I_{HD}	ZPE_{H_2}
D ₂ desorption	Pt-D + Pt-D $\xrightarrow{k_{\text{D}_2}}$ 2Pt + D ₂	k_{D_2}	M_{D_2}	I_{D_2}	ZPE_{HD} ; ZPE_{D_2}
Derivation of Kinetic isotope effects	$[\text{KIE}]_{\text{HD}} = \frac{k_{\text{HD}}}{k_{\text{H}_2}} = \left(\frac{M_{\text{HD}}^\ddagger}{M_{\text{H}_2}^\ddagger} \right)^{\frac{3}{2}} \left(\frac{(I_{\text{HD}}^\ddagger)^2}{(I_{\text{H}_2}^\ddagger)^2} \right)^{\frac{1}{2}} \exp\left(\frac{(ZPE_{\text{H}_2} - ZPE_{\text{HD}}) - (ZPE_{\text{PtH}} - ZPE_{\text{PtD}})}{RT} \right) \quad (\text{Eq. A2.19})$				
	$[\text{KIE}]_{\text{D}_2} = \frac{k_{\text{D}_2}}{k_{\text{H}_2}} = \left(\frac{M_{\text{D}_2}^\ddagger}{M_{\text{H}_2}^\ddagger} \right)^{\frac{3}{2}} \left(\frac{(I_{\text{D}_2}^\ddagger)^2}{(I_{\text{H}_2}^\ddagger)^2} \right)^{\frac{1}{2}} \exp\left(\frac{(ZPE_{\text{H}_2} - ZPE_{\text{D}_2}) - 2(ZPE_{\text{PtH}} - ZPE_{\text{PtD}})}{RT} \right) \quad (\text{Eq. A2.20})$				

[a] rate constants of H₂ desorption herein, i.e. k_{H_2} , is the same to k_{a} used in the main context.

are ignorable in this work, hence only molecular mass (M factor), the moment of inertia (I factor) and zero point energy (ZPE) of corresponding species will be considered. Notably, the late transition state was proposed for desorptions of H₂, HD and D₂ from Pt surface, as the reverse process, based on the fact that adsorption of H₂ on Pt surface is almost barrierless.^[37-39] In

addition, translational and rotational degrees of freedom for surface H and D species (Pt-H and Pt-D) is neglected. Eventually, the kinetic isotope effects of HD and D₂ is expressed as Equation A2.19 and A2.20 in Table A2.3. The values of corresponding *M*, *I* and *ZPE* factors involved in the calculation of kinetic isotope effects are listed in the Table A2.4.

Table A2.4. *M*, *I* and *ZPE* values of H and D-containing species involved in the calculation for the KIE.

Species	<i>M</i> (g·mol ⁻¹)	<i>I</i> (x10 ⁻¹⁴ g·cm ²)	<i>ZPE</i> [a](kJ·mol ⁻¹)	Ref.
Pt-H	[d]	[d]	17.4 [b]	[40]
Pt-D	[d]	[d]	12.3 [c]	
H ₂	2	4.67	26.1	[41]
HD	3	6.21	22.6	
D ₂	4	9.31	18.5	

[a] $ZPE = 0.5hv$ (*v* is the fundamental vibrational frequency)

[b] Calculated on the basis of vibrations both normal and parallel to the surface.

[c] The vibrational frequency of this mode was estimated from that of Pt-H bond, based on $\frac{\nu_{Pt-D}}{\nu_{Pt-H}} =$

$\sqrt{\frac{\mu_{Pt-H}}{\mu_{Pt-D}}}$ (μ is the reduced mass).

[d] Translational and rotational degrees of freedom for surface H and D are ignored.

Therefore, [KIE]_{HD} and [KIE]_{D₂} can be calculated using the values in Table A2.4, according to Equation A2.19 and A2.20. Their values vary with the temperature, as shown in Table A2.5.

Table A2.5. [KIE]_{HD} and [KIE]_{D₂} values at temperature of 313 – 333 K.

Temp (K)	[KIE] _{HD}	[KIE] _{D₂}
313	1.32	2.08
323	1.35	2.14
333	1.37	2.20

Desorption rate of HD, D₂ and H₂ in the reaction of H₂ (g) with D₂O (I).

The desorption rate of H₂, HD and D₂ normalized to the number of surface Pt over Pt/CNT at 313 – 333 K are summarized in Tables A2.6-A2.8 respectively. The rates of HD and D₂ have relative deviations of 5%, and rate of H₂ has relative deviations of 10%.

Table A2.6 (313 K)

Pressure (bar)	Desorption rate (mol·mol _{Pt surf.} ⁻¹ ·s ⁻¹)		
	HD	D ₂	H ₂
10	31.8	1.76	171
20	38.5	1.54	286
30	44.5	1.49	394
40	44.7	1.27	467

Table A2.7 (323 K)

Pressure (bar)	Desorption rate (mol·mol _{Pt surf.} ⁻¹ ·s ⁻¹)		
	HD	D ₂	H ₂
10	36.6	2.06	192
20	44.2	1.67	346
30	49.6	1.52	477
40	52.6	1.42	576

Table A2.8 (333 K)

Pressure (bar)	Desorption rate (mol·mol _{Pt surf.} ⁻¹ ·s ⁻¹)		
	HD	D ₂	H ₂
10	46.1	2.98	209
20	55.7	2.35	387
30	64.0	2.15	560
40	66.8	1.94	676

2.6 References

- [1] A. M. Ruppert, K. Weinberg, R. Palkovits, *Angewandte Chemie* **2012**, *124*, 2614-2654.
- [2] B. Delmon, *Catalysis letters* **1993**, *22*, 1-32.
- [3] K. Christmann, *Surface Science Reports* **1988**, *9*, 1-163.
- [4] N. Marković, T. Schmidt, V. Stamenković, P. Ross, *Fuel cells* **2001**, *1*, 105-116.
- [5] G. Samjeské, M. Osawa, *Angewandte Chemie International Edition* **2005**, *44*, 5694-5698.
- [6] H. Zhang, M. Jin, Y. Xia, *Chemical Society Reviews* **2012**, *41*, 8035-8049.
- [7] P. Norton, P. Richards, *Surface Science* **1974**, *44*, 129-140.
- [8] J. B. Lantz, R. D. Gonzalez, *Journal of Catalysis* **1976**, *41*, 293-302.
- [9] X. Liu, H. Dilger, R. Eichel, J. Kunstmann, E. Roduner, *The journal of physical chemistry B* **2006**, *110*, 2013-2023.
- [10] Y. Okamoto, *Chemical physics letters* **2006**, *429*, 209-213.
- [11] C. Zhou, J. Wu, A. Nie, R. C. Forrey, A. Tachibana, H. Cheng, *The Journal of Physical Chemistry C* **2007**, *111*, 12773-12778.
- [12] S. M. Kozlov, H. A. Aleksandrov, K. M. Neyman, *The Journal of Physical Chemistry C* **2015**, *119*, 5180-5186.
- [13] S. K. Ignatov, A. I. Okhapkin, O. B. Gadzhiev, A. G. Razuvaev, S. Kunz, M. Bäumer, *The Journal of Physical Chemistry C* **2016**, *120*, 18570-18587.
- [14] R. Olsen, G. Kroes, E. Baerends, *The Journal of Chemical Physics* **1999**, *111*, 11155-11163.
- [15] G. W. Watson, R. P. Wells, D. J. Willock, G. J. Hutchings, *The Journal of Physical Chemistry B* **2001**, *105*, 4889-4894.
- [16] S. Gudmundsdóttir, E. Skúlason, K.-J. Weststrate, L. Juurlink, H. Jónsson, *Physical Chemistry Chemical Physics* **2013**, *15*, 6323-6332.
- [17] J. Greeley, M. Mavrikakis, *The Journal of Physical Chemistry B* **2005**, *109*, 3460-3471.
- [18] J. Fearon, G. W. Watson, *Journal of Materials Chemistry* **2006**, *16*, 1989-1996.
- [19] A. Zyubin, T. Zyubina, Y. A. Dobrovol'skii, V. Volokhov, *Russian Journal of Inorganic Chemistry* **2012**, *57*, 1460-1469.
- [20] U. Sanyal, Y. Song, N. Singh, J. L. Fulton, J. Herranz, A. Jentys, O. Y. Gutiérrez, J. A. Lercher, *ChemCatChem* **2019**, *11*, 575-582.
- [21] N. Li, G. W. Huber, *Journal of Catalysis* **2010**, *270*, 48-59.

- [22] E. P. Maris, R. J. Davis, *Journal of Catalysis* **2007**, *249*, 328-337.
- [23] W. Sheng, Z. Zhuang, M. Gao, J. Zheng, J. G. Chen, Y. Yan, *Nature communications* **2015**, *6*, 5848.
- [24] G. Yang, S. A. Akhade, X. Chen, Y. Liu, M. S. Lee, V. A. Glezakou, R. Rousseau, J. A. Lercher, *Angewandte Chemie* **2019**, *58*, 3527-3532.
- [25] B. Hammer, J. K. Norskov, *Nature* **1995**, *376*, 238-240.
- [26] B. Hammer, J. Nørskov, *Surface Science* **1995**, *343*, 211-220.
- [27] G. Bramley, M.-T. Nguyen, V.-A. Glezakou, R. Rousseau, C.-K. Skylaris, *Journal of chemical theory and computation* **2020**, *16*, 2703-2715.
- [28] M. D. Scanlon, P. Peljo, M. A. Méndez, E. Smirnov, H. H. Girault, *Chemical science* **2015**, *6*, 2705-2720.
- [29] C. Örnek, C. Leygraf, J. Pan, *Corrosion Engineering, Science and Technology* **2019**, *54*, 185-198.
- [30] M. Rohwerder, F. Turcu, *Electrochimica Acta* **2007**, *53*, 290-299.
- [31] J.-B. Le, A. Chen, L. Li, J.-F. Xiong, J. Lan, Y.-P. Liu, M. Iannuzzi, J. Cheng, *JACS Au* **2021**.
- [32] V. S. Bagotsky, *Fundamentals of electrochemistry, Vol. 44*, John Wiley & Sons, **2005**.
- [33] A. Twitchett, R. Dunin-Borkowski, P. Midgley, *Physical review letters* **2002**, *88*, 238302.
- [34] A. Takshi, A. Dimopoulos, J. D. Madden, *Applied Physics Letters* **2007**, *91*, 083513.
- [35] H. Lüth, in *Solid Surfaces, Interfaces and Thin Films*, Springer, **2010**, pp. 323-376.
- [36] E. Buncl, C. C. Lee, in *Isotopes in organic chemistry, Vol. 5*, Elsevier: Amsterdam., **1977**.
- [37] R. A. Olsen, G. J. Kroes, E. J. Baerends, *J. Chem. Phys.* **1999**, *111*, 11155-11163.
- [38] A. S. Zyubin, T. S. Zyubina, Y. A. Dobrovolskii, V. M. Volokhov, *Russ J Inorg Chem+* **2012**, *57*, 1460-1469.
- [39] C. G. Zhou, J. P. Wu, A. H. Nie, R. C. Forrey, A. Tachibana, H. S. Cheng, *J Phys Chem C* **2007**, *111*, 12773-12778.
- [40] J. Greeley, M. Mavrikakis, *J. Phys. Chem. B* **2005**, *109*, 3460-3471.
- [41] K. K. Irikura, *J. Phys. Chem. Ref. Data* **2009**, *38*, 749-749.

Chapter 3

Impact of pH on H₂ adsorption on Pt in the aqueous phase

Impact of pH on adsorption of H₂ was evaluated by using a kinetic method. As pH decreasing from 7 to 2, the adsorption heat of H₂ decreases from 45 to 38 kJ·mol⁻¹. In addition, the activation energy of adsorption increases from 1 to 8 kJ·mol⁻¹, whereas the activation energy of desorption remains constant with the variation of pH. Due to the decrease of pH, an increase of work is required to shift the electric double layer away from the surface of Pt, leading to a decrease of the adsorption heat of H₂ on Pt surface and a weaker strength of Pt-H bond as pH decreasing from 7 to 2 in the aqueous phase.

3.1 Introduction

The concentration of hydronium ions in the aqueous phase is of vital importance on many catalytic hydrogenation reactions. Recent studies have focused on the hydrogenation activity of Pt at different pH . It was found that the activity of the hydrogen oxidation and evolution reaction (HOR/HER) on platinum group metals was higher at lower pH,^[1-4] suggesting that the pH of solution has an impact on its activity by modulating the hydrogen binding energy (HBE) of the catalysts.^[5-11]

The interpretation for such a dependence of the HBE on the pH is still under debate in electrochemistry, due to a pH-dependent behavior of water at Pt-H₂O interface^[12-14] or due to a change in the near-interface ions.^[15-18] Furthermore, these studies determined the heat of adsorption of H₂ in the aqueous phase by electrochemical methods, which is limited the requirement that the catalyst materials must be conductive.^[5, 19]

In our previous work, a kinetic method was established to determine the thermodynamic properties of adsorbed H atoms by means of the adsorption of H₂ (g) on supported Pt nanoparticles immersed in D₂O (l), monitoring the formation rate of HD and D₂ in comparison with H₂ adsorption in the gas phase.^[20]

This work determined the adsorption heat for H₂ on Pt/CNT with variation of pH in the aqueous phase in the absence of buffer electrolyte ions under a high pressure of H₂ and proved that dissociative adsorption of H₂ on Pt is influenced by the concentration of hydronium ions in the aqueous phase. The decrease of adsorption heat of H₂ on Pt surface is due to the increase of activation energy of adsorption for H₂ with pH decreasing.

3.2 Experimental and theoretical method

3.2.1 Preparation and characterization of catalyst materials

Synthesis for 1 wt% Pt/CNT

1% Pt/CNT was chosen as the catalyst for determining impact of pH on H₂ adsorption on Pt in the aqueous phase. The methods of preparation and characterization were described in detail in Chapter 2 (Part 2.2)

3.2.2 Determination of H₂ adsorption heat in the aqueous phase Kinetic method-reaction of H₂ (g) with D₂O (l)

The procedure for the reaction of H₂ (g) with D₂O (l) has been introduced in Chapter 2 (part 2.2.4)

3.3 Results and discussion

3.3.1 Thermodynamic and kinetic properties of H₂ adsorption on Pt under different pH

A kinetic method is established to determine the thermodynamic properties of adsorbed H atoms through the adsorption of H₂ (g) on carbon nanotube supported Pt (Pt/CNT) with 1 wt.% loading in D₂O (l) with variation of pH, by monitoring the formation rate of HD and D₂.

Figure 3.1a shows the definition of adsorption enthalpy that is equal to the sum of the adsorption barrier minus the desorption barrier for H₂ on Pt surface. The adsorption enthalpy increases from -45 to -38 kJ mol_{H₂}⁻¹ with decrease of pH from 7 to 2, showing that the concentration of hydronium ions influences dissociative adsorption of H₂ in the aqueous phase. The adsorption enthalpy as well as the activation energy of adsorption and desorption at pH from 2 to 7 are shown in Figure 3.1b. The dissociative adsorption of H₂ is an exothermic process, which could be proved by the equilibrium constant of adsorption K_a° as well as the desorption rate constant k_{-a} showing a declining trend with temperature under a certain pH.

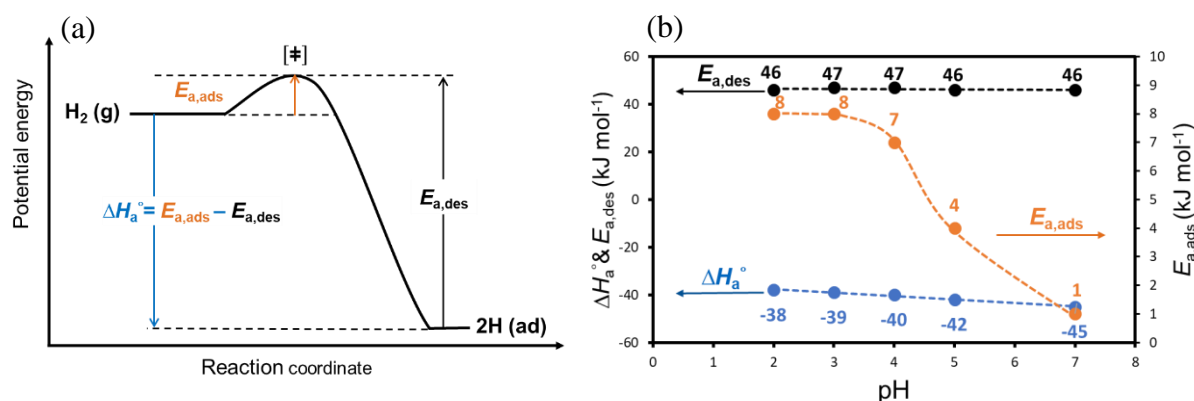


Figure 3.1. (a) Energy diagram of dissociative adsorption of H₂ on Pt/CNT in water; and (b) impact of pH on ΔH_a° (apparent enthalpy of adsorption), $E_{a,des}$ (apparent activation energy of desorption) and $E_{a,ads}$ (apparent activation energy of adsorption).

There is almost no activation barrier (1 ± 1 kJ mol_{H₂}⁻¹) for the adsorption of H₂ on Pt/CNT at pH 7, which is consistent with our previous study that no activation energy is required for the adsorption of H₂ on Pt/Silicalite-1 (1 ± 2 kJ mol_{H₂}⁻¹).^[20] However, the activation energy of adsorption rises from 1 to 8 kJ mol_{H₂}⁻¹ with pH decreasing from 7 to 2. On the contrary, the activation energy of sorbed H desorption to H₂ (g) almost keeps constant within pH 2-7. Thus, we conclude that the concentration of hydronium ions has a remarkable influence on activation energy of adsorption, which results in the difference of adsorption heat with pH.

CNT was chosen as the support of Pt catalyst in this work due to its clean surface with very small amount of functional groups including carboxylic groups (7.2 μmol / g CNT) and phenolic groups (29.3 μmol / g CNT) which would influence the PZC of CNT,^[20] HOR rates^[21] or the cation concentration near to the surface of Pt^[22] and as a result, affect the measured results. Thus, the change on the heat of adsorption and other thermodynamic properties of H₂ on Pt/CNT are mainly resulted from the variation of pH in the aqueous phase.

The coverage of H atom on Pt is affected by pH. As shown in Figure 3.2, the adsorption isotherms of H₂ on Pt/CNT at 313 K were derived with the equilibrium constants of adsorption under different pH in the aqueous phase. The adsorption isotherm shift downwards gradually with pH decreasing from 7 to 3.

The adsorption isotherms in Figure 3.2 show that H₂ adsorption on Pt/CNT in water is weaker at a lower pH compared to higher pH. This is also reflected by the smaller equilibrium constant at a lower pH. K_a° is 0.01 at pH 7 while it is 0.003 at pH 2. These results indicates a

destabilization of H atoms adsorbed on Pt due to the higher concentration of hydronium ions at low pH in the aqueous phase.

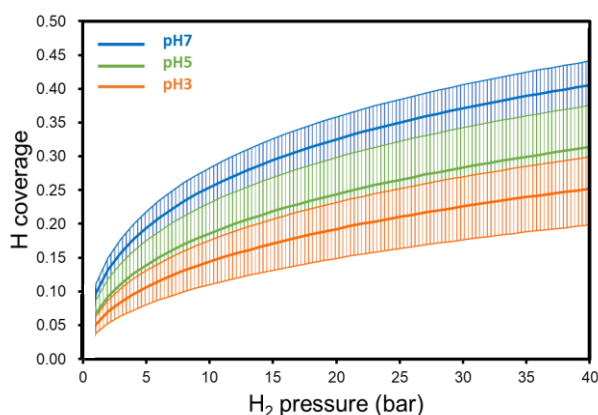


Figure 3.2. Adsorption isotherms of H₂ on Pt/CNT at 313 K in the aqueous phase under different pH (based on K_a^{\ominus}). Shaded regions for isotherms in water at different pH represent the 95% confidence interval.

With the measured barrier for H₂ adsorption and desorption, we illustrate the potential energy (PE) curves of dissociative adsorption of H₂ (g) on Pt in water solution (Figure 3.3a). It shows the variation of potential energy of the system as a function of the distance of H₂ molecule from the surface of Pt particle. In the aqueous phase under pH 7, the only attraction between H₂ (g) and the Pt surface is from weak, van der Waals forces in the case of pure physisorption (dashed blue curve). These forces give rise to a shallow minimum in the PE curve at a relatively long distance from the Pt surface. The solid blue curve in the diagram is the chemisorption PE of H atom to the Pt surface. The starting point on the right side of solid blue curve represents two separated H atoms before approaching to the Pt surface. The H forms strong chemical bonds to Pt surface, which corresponds to the minimum in this curve with accounting the Point of Zero Energy (PZE). In reality, a physisorbed H₂ molecule undergoes a transition state (the blue crossing point of the solid and dashed curve), from which it can either desorb back as a H₂ molecule, or cross over the barrier into the dissociated, chemisorbed H. The adsorption barrier is the difference of energy between the transient state and the H₂ in the gas phase, and the desorption barrier is the difference of energy between the transient state and the PZE level above the minimum point of the blue curve. It is seen that under pH 7 almost no adsorption barrier (1 kJ mol_{H₂}⁻¹) exists for H₂ molecule, while the desorption barrier is significant (46 kJ mol_{H₂}⁻¹).

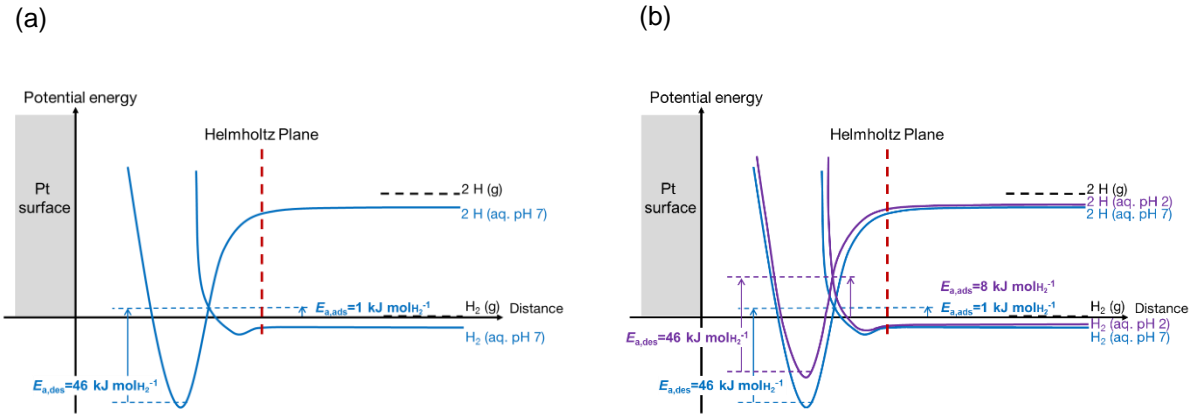


Figure 3.3. Potential energy curve of H₂ adsorption on Pt/CNT in the aqueous phase at pH 7 (a) and pH 2 (b). The solid blue curve and dashed blue curve represent the chemisorption and physisorption PE curve under pH 7, respectively. The solid purple curve and dashed purple curve represent the chemisorption and physisorption PE curve under pH 2, respectively. The dashed line in red represents the Helmholtz plane at the Pt-water interface.

Under pH 2 (Figure 3.3b), both the transition and final states (chemisorption state) go up to a high energy position by same amount. The adsorption barrier increases to 8 kJ molH_2^{-1} , whereas the desorption barrier remains unchanged ($46 \text{ kJ molH}_2^{-1}$). As a result, the adsorption enthalpy increases to $-38 \text{ kJ molH}_2^{-1}$.

3.3.2 Influence of pH dependent electronic structure of surface Pt on Pt-H bond strength

In chapter 2, the two models established based on molecular orbital theory have been introduced in detail for explanation of H₂ adsorption in water. Several studies have pointed out that the electronic structure of Pt can be altered by electrode potential, via applying external potential^[23] or changing pH.^[11] Here, we use the model in chapter 1 for further discussion on impact of pH on electronic structure of Pt surface in water. According to Nernst equation in equation 3.1 ($E^{(\text{SHE})} = 4.44 \text{ V}$ vs. vacuum level),

$$E = E^{(\text{SHE})} + \frac{RT}{F} \ln \left(\frac{[\text{H}^+]}{P_{\text{H}_2}^{0.5}} \right) \quad \text{Eq. 3.1}$$

The variation of electrode potential with pH are calculated and shown in Table 3.1.

Fermi level can be expressed as equation 3.2,

$$E_{\text{F}} = E_{\text{Vacuum}} - \Phi \quad \text{Eq. 3.2}$$

Where E_F is Fermi level, E_{vacuum} is the energy of vacuum (defined as 0 eV) and Φ is the work function.

Table 3.1. Electrode potential with variation of pH

pH	2	3	4	5	7
Absolute Electrode potential (V) SHE (4.44 V) 10 bar H ₂ , 298 K	4.29	4.23	4.17	4.11	4.00

After immersion of Pt into electrolyte under pH 7 (10 bar H₂, 298 K), Fermi level of Pt is aligned with that of electrolyte (-4.00 eV). The variation of electronic structure at Pt surface is shown in Figure 2.4, Chapter 2. While under pH 2 (10 bar H₂, 298 K), the electronic structure of Pt surface is shown in Figure 3.4 (model 1). After contact with electrolyte, Fermi level of Pt is in line with that of electrolyte (-4.29 eV), with a formation of interface dipole layer under an equilibrium junction between Pt and electrolyte.

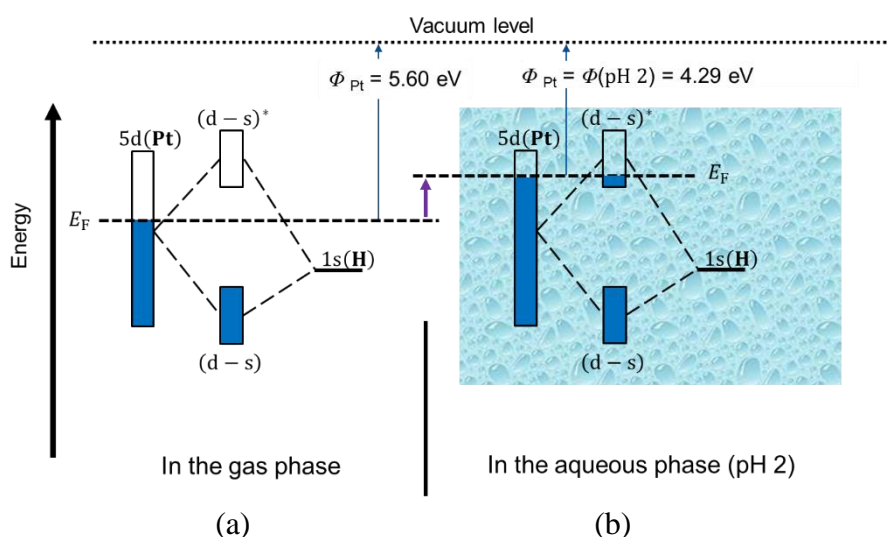


Figure 3.4. Schematic illustration: Comparison of electronic structure of uppermost surface Pt in the gas phase (a) and in the aqueous phase (b) under pH 2, 10 bar H₂ at 298 K.

If we treat the junction between metal and electrolyte with redox couple as the junction between dissimilar metals (model 2), the situation is like the model shown in Figure 3.5. The Fermi level of two sides would be aligned with each other at equilibrium after contact and a build-up of potential difference would be formed at the interface, which causes a sharp increase or decrease of the bands energy on the surface of two sides.

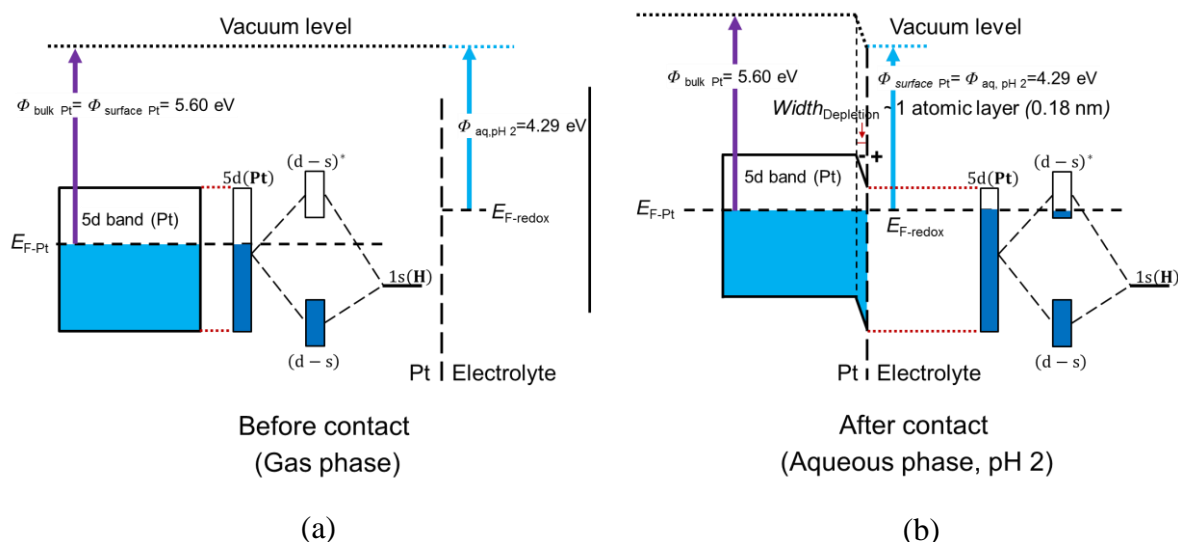


Figure 3.5. The change at Pt surface before (a) and after contact (b) with electrolyte with redox couple ($\text{H}_2/\text{H}_3\text{O}^+$) under pH 2, 298 K, 10 bar H_2 .

Comparison of Pt surface electronic structure between pH 2 and pH 7 is shown in Figure 3.6 and 3.7. Due to the higher electrolyte Fermi level under pH 7, the antibonding state of Pt-H bond has a more filling by electrons, resulting in a weaker Pt-H bond compared to that under pH 2. Shao and coworkers have directly monitored the H binding strength by using surface-enhanced infrared absorption spectroscopy (SEIRAS) with the attenuated total reflection (ATR) configuration,^[24] through which monotonously weakened HBE is observed as pH increased. This is consistent with the tendency derived from this model.

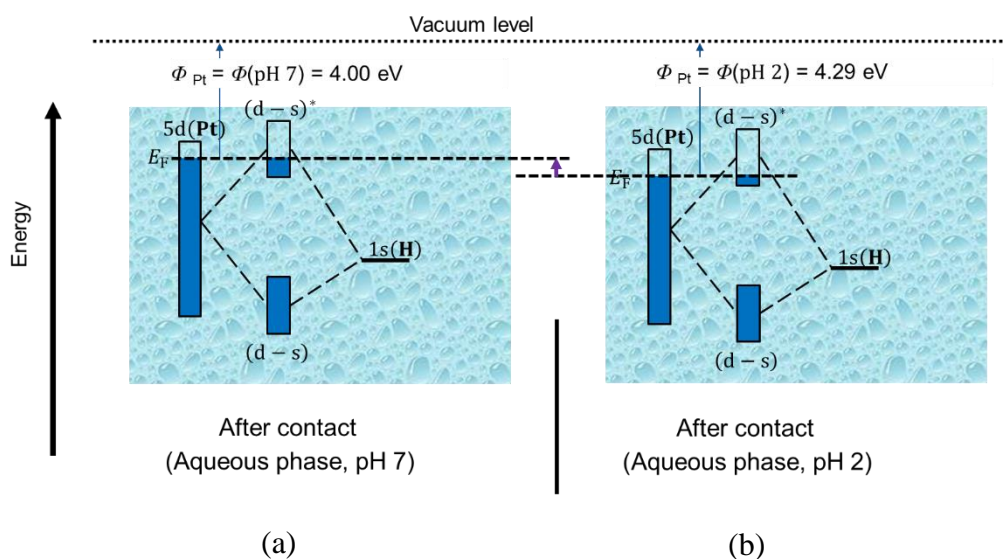


Figure 3.6. Model 1-Comparison of Pt surface electronic structure between (a) pH 7 and (b) pH 2 with redox couple ($\text{H}_2/\text{H}_3\text{O}^+$), 10 bar H_2 .

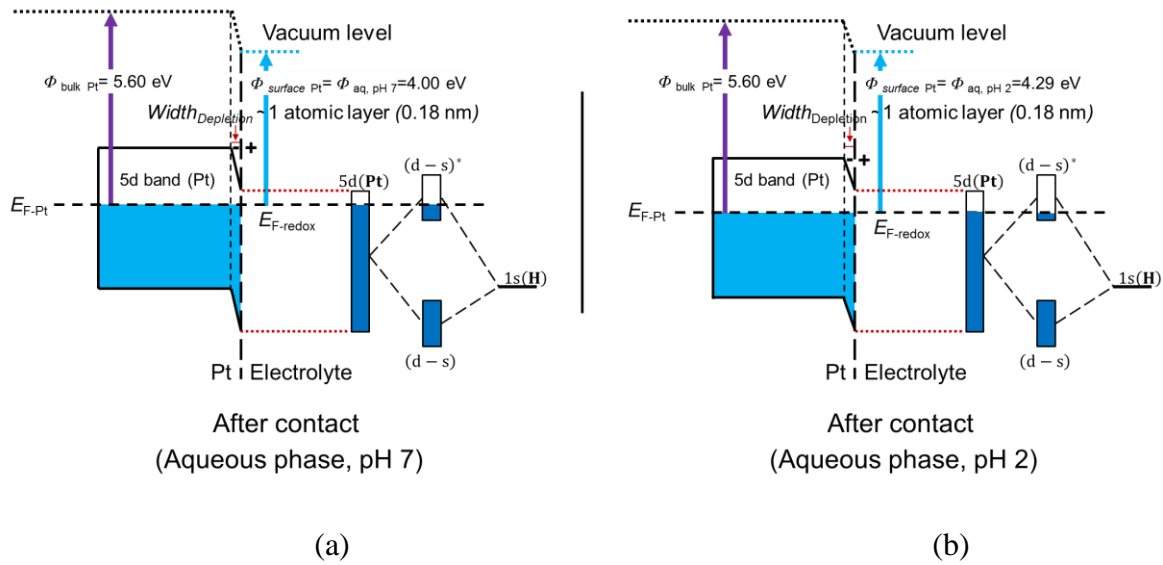


Figure 3.7. Model 2-Comparison of Pt surface electronic structure between (a) pH 7 and (b) pH 2 with redox couple ($\text{H}_2/\text{H}_3\text{O}^+$), 10 bar H_2 .

3.3.3 Influence from water layer

Since the adsorption of H_2 is competitive to that of water on Pt surface, adsorption of water on Pt is a factor that can't be neglected. Several studies ascribed water binding energy on metal as the main factor that influence apparent HBE with variation of pH in water. It was reported that increase of apparent HBE with increase of pH is resulted from decrease of water binding energy, whereas measured HBE shows a reverse tendency, decreasing with increase of pH. The weakening strength of water-metal bond is resulted from the negatively charged Pt surface, which is induced from the larger difference of Fermi level between Pt and electrolyte under high pH. Goddard group reported that as applied potential is made more negative for simulating pH dependent electrode potential, the electrode has a tendency to repel water, which in turn strengthen the hydrogen binding.^[11] As pH increases from 0.2 to 12.8, a 0.13 eV increase was predicted in hydrogen binding with a slope of 10 meV/pH that is close to the experimental observation of 8 to 12 meV/pH.

However, due to large amount of hydronium ions existing under low pH, whether the water layer adsorbed on Pt is a part of hydronium ions inside inner Helmholtz plane or not, is still under estimated. Thus, the contribution from electrical double layer should be considered.

3.3.4 Influence of electrical double layer

At low pH (e.g. pH 2), a large amount of hydronium ions in water enriched at the Pt-water interface, forming a dense layer known as Helmholtz Plane. We hypothesize that such dense layer increases the potential energy (PE) of all the H species between the Pt surface and this plane, including both H₂ molecule and H atom, while does not affect those species outside the plane in the bulk solution. For the physisorption of H₂, its PE curve at pH 2 remains almost unchanged outside the Helmholtz Plane while shifts up compared to that at pH 7 (see the changes from the dashed blue curve to the dashed purple curve, Fig. 3.3). The same is for the PE curve of chemisorption of H that the part outside Helmholtz Plane is unchanged and the part inside shift up (see the changes from the solid blue curve to the solid purple curve, Fig. 3.3). As the consequence, the crossing point of two curves shifting up as well, leading to a higher transition state between physisorbed H₂ and chemisorbed H on Pt. The adsorption barrier is then increased (8 kJ mol_{H₂}⁻¹ at pH 2 vs. 1 kJ mol_{H₂}⁻¹ at pH 7). On the contrary, the barrier of desorption is barely changed (46 kJ mol_{H₂}⁻¹ at both pH 2 and 7) because the energy increase of transition state is compensated by the energy increase of adsorbed H.

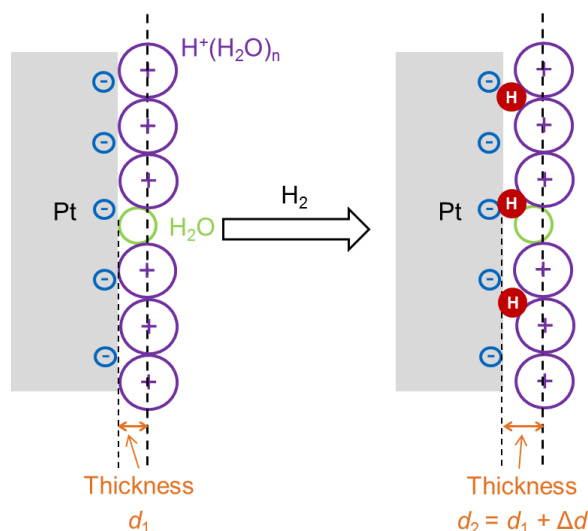


Figure 3.6. The comparison of the distance between Pt surface and electronic double layer in presence and absence of adsorbed H atom on Pt surface in the aqueous phase.

As shown in Figure 3.6, the thickness between EDL and Pt surface should be larger in the presence than that in the absence of adsorbed H atom. In other words, adsorption of H₂ on Pt shifts the EDL away from the Pt surface. It is noticed from the previous study that the distribution of water molecules shifts away from the surface of Pt in presence of adsorbed H, which enlarges the distance of the first water layer from Pt surface.^[25] The capacitance of the

work (W) being paid to shift the EDL away from the surface of Pt, should be equal to the change of electrostatic energy stored in the capacitor., and can be calculated by the equation below:

$$E_e = \frac{1}{4\pi\epsilon} qQ \left(\frac{1}{d_2} - \frac{1}{d_1} \right) \quad \text{Eq. 3.3}$$

Where q is the surface charge of Pt, Q is the charge (positive) at Helmholtz layer, d_1 is the distance between q and Q before adsorption of H_2 , d_2 is the distance between q and Q after adsorption of H_2 , ϵ is the permittivity of water ($716.85 \times 10^{-12} \text{ F m}^{-1}$).

By using equation 1, the increase of electrostatic energy could be compared under different pH. As pH decreasing (in Figure 3.7), the variable Q would much increase and q would less decrease while the other variables could be considered as constants. Thus, the electrostatic energy stored in EDL would be larger in low pH (e.g. pH 2) than that in neutral pH (pH 7). This means that part of the energy in the adsorption of H is consumed by the work to increase the electrostatic energy in EDL, resulting in a smaller adsorption heat of H_2 and weaker H binding of Pt as decreasing of pH.

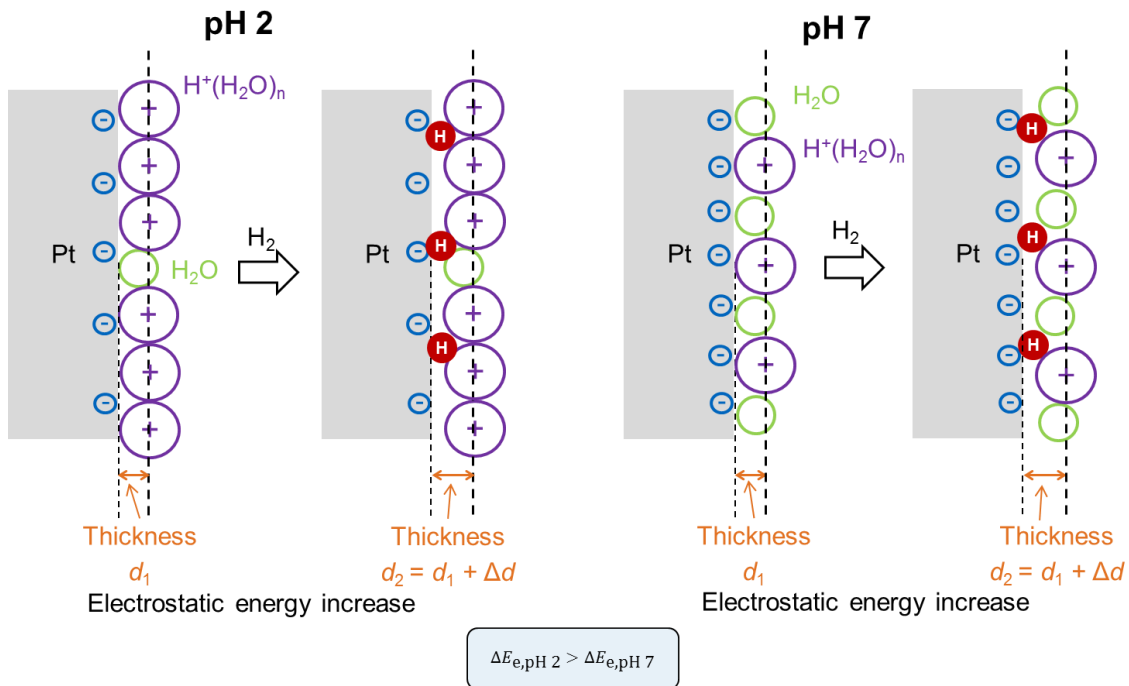


Figure 3.7. Schematic illustration of the shift of EDL during the adsorption of hydrogen on Pt surface at pH 2 and pH 7.

3.4 Conclusions

In conclusion, the impact of pH on adsorption of H₂ on Pt in water was determined by the kinetic method. With variation of pH from 7 to 2, the heat of adsorption of H₂ decreases from 45 to 38 kJ·mol⁻¹ while the activation energy of adsorption increases from 1 to 8 kJ·mol⁻¹. The activation energy of desorption is constant with the variation of pH. The decrease of pH causes 1) an increase of strength of water binding on Pt and 2) a work being paid to shift the EDL away from the surface of Pt. These resulted in a decrease of the adsorption heat of H₂ on Pt surface and a weaker strength of Pt-H bond as pH decreasing from 7 to 2 in the aqueous phase.

3.5 Appendix

Derivation of electrostatic potential energy:

The electrostatic potential energy stored is given by:

$$\begin{aligned} E_e &= E_{e2} - E_{e1} = \frac{qQ}{4\pi\epsilon} \cdot \frac{1}{d_2} - \frac{qQ}{4\pi\epsilon} \cdot \frac{1}{d_1} \\ &= \frac{1}{4\pi\epsilon} qQ \left(\frac{1}{d_2} - \frac{1}{d_1} \right) \end{aligned}$$

Where q is the surface charge of Pt, Q is the charge (positive) at Helmholtz layer, d_1 is the distance between q and Q before adsorption of H₂, d_2 is the distance between q and Q after adsorption of H₂, E_{e1} and E_{e2} are the electrostatic potential energy stored at d_1 and d_2 , respectively, ϵ is the permittivity of water (716.85×10^{-12} F m⁻¹).

Table A3.1-A3.5 shows rate constants of adsorption and desorption and adsorption equilibrium constants on Pt/CNT at temperature from 313 to 333 K under different pH.

Table A3.1 Under pH 2.

Temp. (K)	pH 2		
	K_a°	k_a (bar ⁻¹)	k_{-a} (s ⁻¹)
313	3.4×10^{-3}	25	7.4×10^3
323	2.3×10^{-3}	28	1.2×10^4
333	1.4×10^{-3}	30	2.2×10^4
Energy (kJ molH ₂ ⁻¹)	Adsorption heat -38 ± 3	Adsorption Barrier 8 ± 1	Desorption barrier 46 ± 3

Table A3.2 Under pH 3.

Temp. (K)	pH 3		
	K_a°	k_a (bar ⁻¹)	k_{-a} (s ⁻¹)
313	2.8×10^{-3}	27	9.4×10^3
323	1.9×10^{-3}	29	1.5×10^4
333	1.1×10^{-3}	32	2.8×10^4
Energy (kJ molH ₂ ⁻¹)	Adsorption heat -39 ± 3	Adsorption Barrier 8 ± 1	Desorption barrier 47 ± 4

Table A3.3 Under pH 4.

Temp. (K)	pH 4		
	K_a°	k_a (bar ⁻¹)	k_{-a} (s ⁻¹)
313	3.9×10^{-3}	29	7.2×10^3
323	2.5×10^{-3}	30	1.2×10^4
333	1.6×10^{-3}	34	2.2×10^4
Energy (kJ molH ₂ ⁻¹)	Adsorption heat -40 ± 2	Adsorption Barrier 7 ± 2	Desorption barrier 47 ± 4

Table A3.4 Under pH 5.

Temp. (K)	pH 5		
	K_a°	k_a (bar ⁻¹)	k_{-a} (s ⁻¹)
313	5.2×10^{-3}	33	6.4×10^3
323	3.2×10^{-3}	34	1.1×10^4
333	2.0×10^{-3}	37	1.9×10^4
Energy (kJ molH ₂ ⁻¹)	Adsorption heat -42 ± 1	Adsorption Barrier 4 ± 1	Desorption barrier 46 ± 1

Table A3.5 Under pH 7.

Temp. (K)	pH 7		
	K_a°	k_a (bar ⁻¹)	k_{-a} (s ⁻¹)
313	1.2×10^{-2}	36	3.1×10^3
323	6.7×10^{-3}	36	5.4×10^3
333	4.1×10^{-3}	37	9.0×10^3
Energy (kJ molH ₂ ⁻¹)	Adsorption heat -45 ± 1	Adsorption Barrier 1 ± 1	Desorption barrier 46 ± 1

Reaction kinetic results over 1 wt% Pt/CNT at different pressures and temperatures plotted according to Equation (left) and Arrhenius plots of adsorption and desorption rate constants and van't Hoff plot of adsorption equilibrium constants, in H₂ adsorption on Pt/CNT in the aqueous phase.(right)

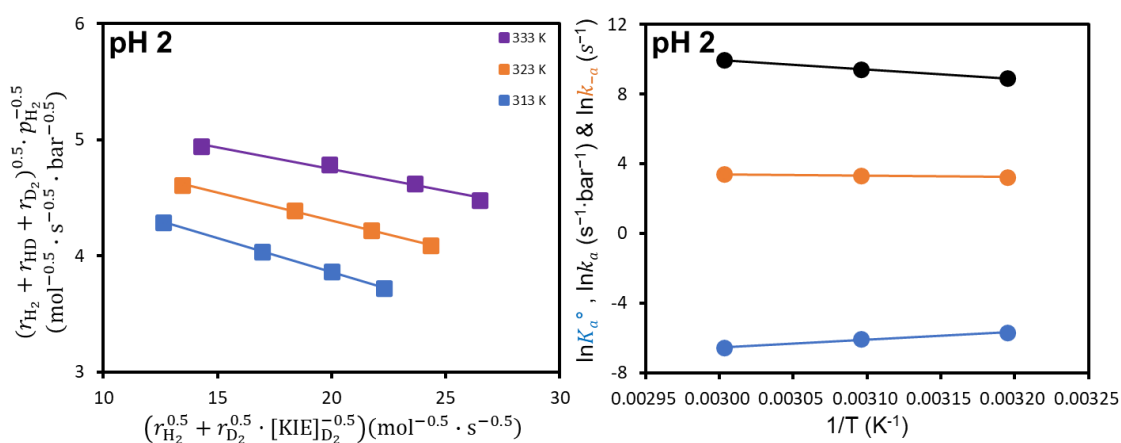


Figure A3.1. Under pH 2.

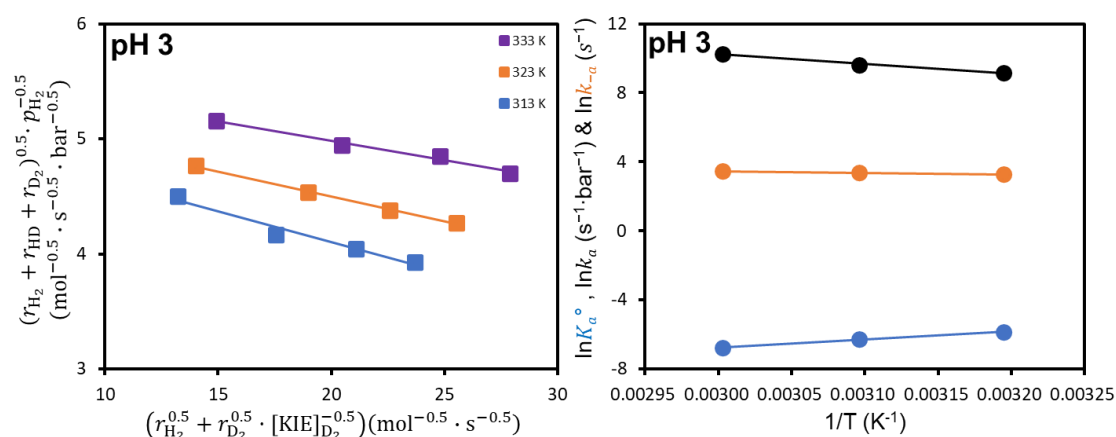


Figure A3.2. Under pH 3.

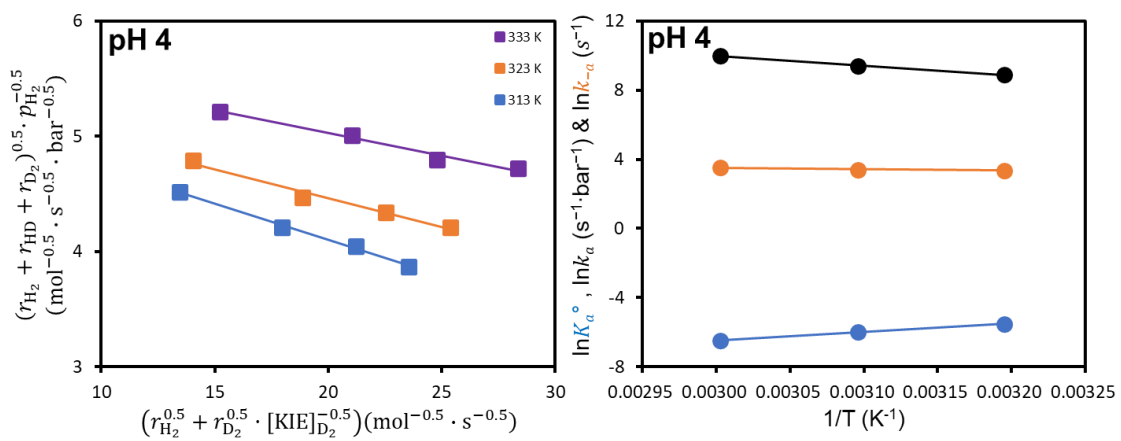


Figure A3.3. Under pH 4.

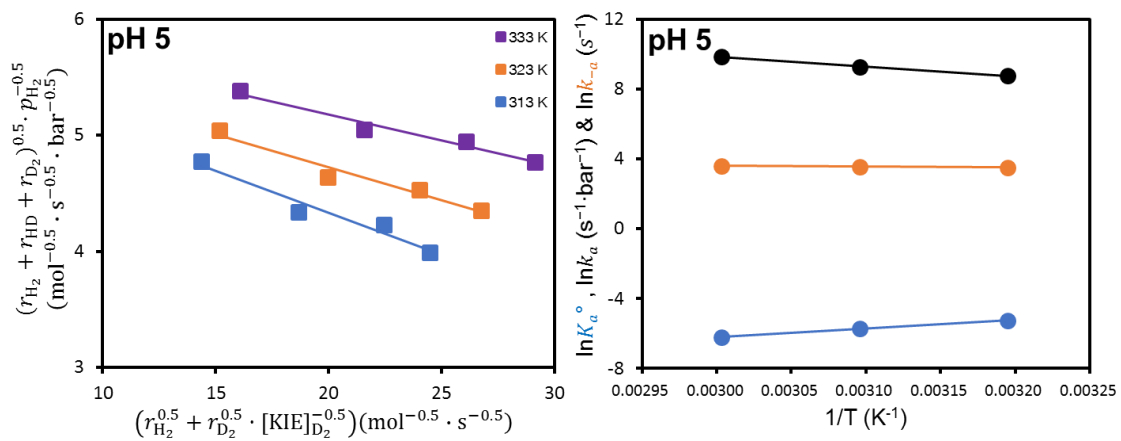


Figure A3.4. Under pH 5.

Desorption rate of HD, D₂ and H₂ in the reaction of H₂ (g) with D₂O (I).

The desorption rate of H₂, HD and D₂ normalized to the number of surface Pt over Pt/CNT at 313 – 333 K are summarized in Tables A3.6-A3.17 respectively. The rates of HD and D₂ have relative deviations of 5%, and rate of H₂ has relative deviations of 10%.

Table A3.6 (pH 2, 313 K)

Pressure (bar)	Desorption rate (mol·mol _{Pt surf.} ⁻¹ ·s ⁻¹)		
	HD	D ₂	H ₂
10	69.8	14.5	99.8
20	113	19.5	193
30	147	23.1	278
40	178	26.8	350

Table A3.7 (pH 2, 323 K)

Pressure (bar)	Desorption rate (mol·mol _{Pt surf.} ⁻¹ ·s ⁻¹)		
	HD	D ₂	H ₂
10	83.4	18.5	111
20	136	24.2	226
30	182	30.3	323
40	224	36.1	410

Table A3.8 (pH 2, 333 K)

Pressure (bar)	Desorption rate (mol·mol _{Pt surf.} ⁻¹ ·s ⁻¹)		
	HD	D ₂	H ₂
10	99.5	24.0	121
20	167	31.7	259
30	225	39.5	377
40	279	47.7	478

Table A3.9 (pH 3, 313 K)

Pressure (bar)	Desorption rate (mol·mol _{Pt surf.} ⁻¹ ·s ⁻¹)		
	HD	D ₂	H ₂
10	78.3	17.0	107
20	118	19.7	210
30	150	20.8	321
40	181	23.5	413

Table A3.10 (pH 3, 323 K)

Pressure (bar)	Desorption rate (mol·mol _{Pt surf.} ⁻¹ ·s ⁻¹)		
	HD	D ₂	H ₂
10	84.8	17.0	125
20	146	26.1	240
30	192	31.0	352
40	228	32.9	467

Table A3.11 (pH 3, 333 K)

Pressure (bar)	Desorption rate (mol·mol _{Pt surf.} ⁻¹ ·s ⁻¹)		
	HD	D ₂	H ₂
10	108	25.5	133
20	185	37.7	267
30	249	43.9	413
40	295	47.4	540

Table A3.12 (pH 4, 313 K)

Pressure (bar)	Desorption rate (mol·mol _{Pt surf.} ⁻¹ ·s ⁻¹)		
	HD	D ₂	H ₂
10	70.0	12.0	122
20	103	13.4	237
30	131	14.9	344
40	149	15.2	434

Table A3.13 (pH 4, 323 K)

Pressure (bar)	Desorption rate (mol·mol _{Pt surf.} ⁻¹ ·s ⁻¹)		
	HD	D ₂	H ₂
10	86.3	17.6	125
20	129	19.5	252
30	171	23.3	371
40	199	24.1	486

Table A3.14 (pH 4, 333 K)

Pressure (bar)	Desorption rate (mol·mol _{Pt surf.} ⁻¹ ·s ⁻¹)		
	HD	D ₂	H ₂
10	104	21.8	146
20	165	25.8	311
30	218	31.7	441
40	254	31.3	605

Table A3.15 (pH 5, 313 K)

Pressure (bar)	Desorption rate ($\text{mol}\cdot\text{mol}_{\text{Pt surf.}}^{-1}\cdot\text{s}^{-1}$)		
	HD	D ₂	H ₂
10	68.5	9.29	150
20	94.3	9.73	272
30	114	9.36	414
40	127	9.65	499

Table A3.16 (pH 5, 323 K)

Pressure (bar)	Desorption rate ($\text{mol}\cdot\text{mol}_{\text{Pt surf.}}^{-1}\cdot\text{s}^{-1}$)		
	HD	D ₂	H ₂
10	74.6	9.65	170
20	105	10.2	315
30	129	10.4	477
40	146	10.4	602

Table A3.17 (pH 5, 333 K)

Pressure (bar)	Desorption rate ($\text{mol}\cdot\text{mol}_{\text{Pt surf.}}^{-1}\cdot\text{s}^{-1}$)		
	HD	D ₂	H ₂
10	89.2	12.4	188
20	134	14.6	361
30	167	14.9	552
40	195	16.0	698

3.6 Reference

- [1] J. Durst, A. Siebel, C. Simon, F. Hasché, J. Herranz, H. A. Gasteiger, *Energy Environ. Sci.* **2014**, *7*, 2255-2260.
- [2] K. C. Neyerlin, W. Gu, J. Jorne, H. A. Gasteiger, *Journal of The Electrochemical Society* **2007**, *154*, B631.
- [3] W. Sheng, H. A. Gasteiger, Y. Shao-Horn, *Journal of The Electrochemical Society* **2010**, *157*, B1529.
- [4] T. Bhowmik, M. K. Kundu, S. Barman, *Acs Catalysis* **2016**, *6*, 1929-1941.
- [5] W. Sheng, Z. Zhuang, M. Gao, J. Zheng, J. G. Chen, Y. Yan, *Nature communications* **2015**, *6*, 5848.
- [6] J. K. Nørskov, T. Bligaard, A. Logadottir, J. Kitchin, J. G. Chen, S. Pandelov, U. Stimming, *Journal of The Electrochemical Society* **2005**, *152*, J23.
- [7] W. Sheng, M. Myint, J. G. Chen, Y. Yan, *Energy & Environmental Science* **2013**, *6*, 1509-1512.
- [8] Y. Wang, G. Wang, G. Li, B. Huang, J. Pan, Q. Liu, J. Han, L. Xiao, J. Lu, L. Zhuang, *Energy & Environmental Science* **2015**, *8*, 177-181.
- [9] J. Zheng, J. Nash, B. Xu, Y. Yan, *Journal of The Electrochemical Society* **2018**, *165*, H27.
- [10] R. Parsons, *Transactions of the Faraday Society* **1958**, *54*, 1053-1063.
- [11] T. Cheng, L. Wang, B. V. Merinov, W. A. Goddard III, *Journal of the American Chemical Society* **2018**, *140*, 7787-7790.
- [12] S. A. Giles, J. C. Wilson, J. Nash, B. J. Xu, D. G. Vlachos, Y. S. Yan, *J Catal* **2018**, *367*, 328-331.
- [13] S. Trasatti, *Journal of Electroanalytical Chemistry and Interfacial Electrochemistry* **1972**, *39*, 163-184.
- [14] R. Gisbert, G. García, M. T. Koper, *Electrochimica acta* **2011**, *56*, 2443-2449.
- [15] M. J. Janik, I. T. McCrum, M. T. M. Koper, *J Catal* **2018**, *367*, 332-337.
- [16] E. P. Maris, R. J. Davis, *Journal of Catalysis* **2007**, *249*, 328-337.
- [17] M. T. Koper, *Nature chemistry* **2013**, *5*, 255-256.
- [18] L. Zhuang, J. Jin, H. D. Abruna, *Journal of the American Chemical Society* **2007**, *129*, 11033-11035.
- [19] J. Zheng, W. Sheng, Z. Zhuang, B. Xu, Y. Yan, *Science advances* **2016**, *2*, e1501602.

- [20] G. Yang, S. A. Akhade, X. Chen, Y. Liu, M. S. Lee, V. A. Glezakou, R. Rousseau, J. A. Lercher, *Angewandte Chemie* **2019**, *58*, 3527-3532.
- [21] D. Strmcnik, M. Uchimura, C. Wang, R. Subbaraman, N. Danilovic, D. van der Vliet, A. P. Paulikas, V. R. Stamenkovic, N. M. Markovic, *Nature chemistry* **2013**, *5*, 300-306.
- [22] X. Chen, I. T. McCrum, K. A. Schwarz, M. J. Janik, M. T. M. Koper, *Angewandte Chemie* **2017**, *56*, 15025-15029.
- [23] I. Hamada, Y. Morikawa, *The Journal of Physical Chemistry C* **2008**, *112*, 10889-10898.
- [24] S. Zhu, X. Qin, Y. Yao, M. Shao, *Journal of the American Chemical Society* **2020**, *142*, 8748-8754.
- [25] G. J. Yang, S. A. Akhade, X. Chen, Y. Liu, M. S. Lee, V. A. Glezakou, R. Rousseau, J. A. Lercher, *Angew Chem Int Edit* **2019**, *58*, 3527-3532.

Chapter 4

Impact of pH on hydrogenation of phenol on Pt in the aqueous phase

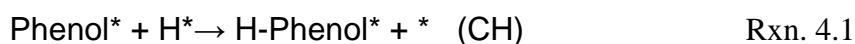
Two reaction pathways, conventional hydrogenation (CH) and proton coupled electron transfer (PCET) are demonstrated to occur in phenol hydrogenation, with the dominated route transforming from CH to PCET as pH decreasing. Notably, all the reactions were carried out in absence of electric over potential, that only open circuit potential (OCP) drove the PCET pathway. When pH decreases, the reaction rate of CH is enhanced by the decrease of activation energy that is caused by decrease of adsorption heat of H₂ on Pt. The reaction rate of PCET is promoted by decrease of pH because of the largely increased hydronium ion concentration even though the activation Gibbs free energy increased in parallel. These results demonstrate that an electrocatalytic hydrogenation reaction can still occur under OCP.

4.1 Introduction

As the simplest phenolic compound, phenol has been extensively tested for bio-oil upgrading.^[1-10] In comparison to the gas phase, hydrogenation reaction in liquid water has several factors that would affect the reaction rate such as solvation, electric double layer, ionic strength and pH.^[11-14] Among them, the impact of pH in the aqueous phase plays a key role on many catalytic hydrogenation reactions.

Song reported that the intrinsic rate of phenol hydrogenation increased accordingly with the concentration of Brønsted acid site of Ni/HZSM-5 catalyst, which was ascribed to not only the enrichment of both phenol and the intermediates in pores with high Brønsted acid concentration, but also the active H atom derived from the available protons adjacent to Ni particles.^[15] Recent studies have focused on the phenol hydrogenation on Pt under different pH in water and found that the hydrogenation activity of phenol on Pt catalysts increases exponentially with the thermodynamic activity of hydronium ions, which is ascribed to the dependence of H binding strength of Pt on pH, since the pH of solution has an impact on its activity by modulating the heat of adsorption for H₂.^[16]

Besides the pathway of conventional hydrogenation (CH) that takes place in thermal hydrogenation reactions in which sorbed organic substrate reacts with sorbed H atom on the surface of transition metal (shown in Rxn. 4.1),^[17-25] proton coupled electron transfer (PCET) is a pathway typically occurring in electrocatalytic hydrogenation by the simultaneous or sequential attack of hydronium ions with electron on organic substrate under an overpotential (shown in Rxn. 4.2).^[13, 26-30] By taking these two pathways into consideration, the reaction pathway for phenol hydrogenation in this work is proposed to be the combination of two pathways, since in presence of H⁺(H₂O)_n and H₂, the Pt catalyst itself is a hydrogen electrode with an open-circuit potential (OCV), which may trigger the PCET pathway in hydrogenation of phenol in the aqueous phase.



This work determined thermodynamic and kinetic properties of the adsorption of H₂, hydrogenation of phenol on Pt/CNT with variation of pH in the aqueous phase and proved that dissociative adsorption of H₂ on Pt and the main reaction pathway for phenol hydrogenation are influenced by the concentration of hydronium ions in the aqueous phase.

4.2 Experimental and theoretical method

4.2.1 Preparation and characterization of catalyst materials

Chemical and materials

The following chemicals were used as received in this work: phenol (99.0 %, Sigma-Aldrich), Cyclohexanol (99.0 %, Sigma-Aldrich), Cyclohexanone (99.0 %, Sigma-Aldrich), D₂O (99.9 atom % D, Sigma-Aldrich), ethyl acetate (Chromasolv, 99.9 %, Sigma-Aldrich), nitrogen (99.999 %, Westfalen), hydrogen (99.999 %, Westfalen), D₂ (99.8 atom % D, Sigma-Aldrich) and oxygen (99.9999 %, Westfalen), Perchloric acid (70 wt.%, Sigma-Aldrich), Hydrochloric acid (36.5-38 wt.%, Sigma-Aldrich), Sodium hydroxide (≥98%, Sigma-Aldrich), Sodium bicarbonate (≥99.7%, Sigma-Aldrich), Sodium carbonate (≥99.0%, Sigma-Aldrich).

Preparation of Pt/CNT catalyst

1 wt% Pt/CNT catalyst was used in this chapter. The synthesis procedure is reported in chapter 2.

4.2.2 Catalytic tests

Hydrogenation of phenol. The aqueous-phase hydrogenation of phenol was performed in an autoclave (Parr Instrument, 300 mL). Typically, 1.0 - 2.0 g phenol, 0.005 g Pt/CNT catalyst, and 100 mL distilled H₂O were charged into the autoclave followed by pressurizing with H₂. Subsequently, it was heated to desired reaction temperature. After a certain reaction time, the autoclave was quenched by fast cooling to 278 K in an ice bath. The organic products were extracted from the aqueous phase with 20 mL ethyl acetate for three times, and sodium chloride was added to the mixture during extraction to promote the extraction ratio. Products were qualitatively and quantitatively analyzed by a GC (Shimadzu 2010 Plus) equipped with an DB-WAX UI column (30 m × 250 μm × 0.25 μm). Before the analysis, the ethyl acetate solutions were dried with sodium sulfate.

The KIE experiment of phenol hydrogenation. These reactions to determine KIE were carried out in an autoclave (Parr Instrument, 100 mL). Typically, 10-50 mg of catalyst and 0.3 g phenol were mixed with the 30 mL H₂O or D₂O. H₂ or D₂ was charged in the autoclave (ambient temperature). Then, after the required temperature was reached, the stirring was started and the reaction time was recorded from that moment. Eventually, the organic products and phenol were extracted with ethyl acetate for analysis by GC (Shimadzu 2010 Plus).

Reaction of H₂ with D₂O. The reaction of gas H₂ with liquid D₂O over Pt/CNT catalyst was carried out in an autoclave (Parr Instrument, 100 mL). Typically, 5.0 mg Pt/CNT catalyst and 30 ml D₂O were added to the reactor. The reactor was heated to the required temperature under 780 rpm agitation. When the temperature is stable, the reactor was purged with H₂ for three times and pressurized to a required H₂ pressure. After a certain reaction time, the gas was collected in a gas bag and analyzed by a mass spectrometer (OmniStar GSD 320). The apparent reaction rate is:

$$\text{Apparent rate} = \text{Product yield} / \text{Reaction time}$$

Conversion, reaction rate, turnover frequency (TOF) and carbon balance were calculated according to the following equations:

$$\text{Conversion} = (\text{weight of converted reactant} / \text{weight of the starting reactant}) \times 100\%.$$

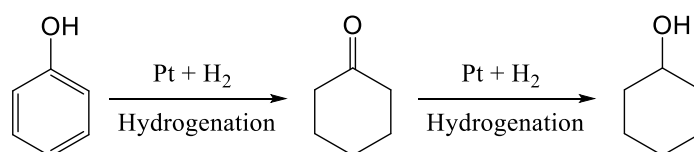
$$\text{TOF} = \text{mole of converted reactant} / (\text{mole of active metal site} \times \text{reaction time}).$$

$$\text{The carbon balance} = \text{mole of carbon in starting reactant} / \text{mole of carbon in the product}.$$

4.3 Results and discussions

4.3.1 Impact of pH on hydrogenation of phenol over Pt/CNT in the aqueous phase

Hydrogenation of phenol goes through the following pathway (scheme 4.1). The products of this reaction under conditions (313-333 K, 1-10 bar H₂) are only cyclohexanone and cyclohexanol.



Scheme 4.1. Reaction pathway of phenol hydrogenation in the aqueous phase.

No cyclohexene or cyclohexane were observed. Figure 4.1 shows the apparent hydrogenation rate of phenol on Pt/CNT at different pH in the aqueous phase. The initial turnover frequency of phenol hydrogenation (TOF, converted phenol per Pt surface atom per second) shows a clear escalating trend as pH decreasing from 5 to 2, growing by one order of magnitude when pH decreasing from 5.3 to 2 at a certain temperature. This phenomenon is also observed by other

studies that pH has a great impact on phenol hydrogenation rate over Pt catalyst in the aqueous phase.^[2-3] As pH decreases from 5.3 to 2, the reaction order of H₂ (ranging from 1 to 10 bar) becomes more positive from 0.2 to 0.5 (in Figure. A4.2), while the reaction order of phenol (ranging from 0.106 to 0.212 M) maintains close to zero .

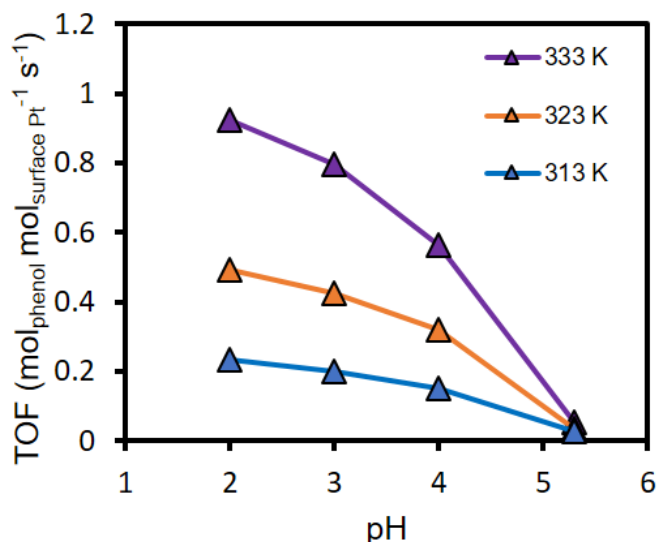


Figure 4.1. TOFs of phenol hydrogenation at 313-333 K with 10 bar H₂ and HBEs on 1 wt % Pt/CNT plotted as a function of pH.

The rate-determining step of phenol hydrogenation was reported to be the first H addition step based on a broad range of kinetic measurements on Pt/C.^[14, 16, 31] Therefore, the rate-determining step in this work is assumed to be the first addition of a sorbed H atom to a sorbed phenol on Pt/CNT catalyst.

4.3.2 Reaction pathway with pH

Conventional hydrogenation (CH) is the classic pathway for phenol hydrogenation in thermal catalytic hydrogenation (TCH). In CH pathway, active H atom on metal surface is derived from dissociative adsorption of H₂ before further reaction with adsorbed phenol. Singh's work has discussed the impact of pH on phenol hydrogenation in the aqueous phase and ascribes the change in hydrogenation rate of phenol to the change in HBE with pH under CH pathway.^[16] In electrocatalytic hydrogenation (ECH), if hydrogenation of phenol proceeds via proton coupled electron transfer (PCET) pathway, phenol molecule would be attacked simultaneously or sequentially by hydronium ions with electron under an overpotential. In view of the positive

correlation between the concentration of hydronium ion and the rate of phenol hydrogenation, PCET pathway is suspected to participate in phenol hydrogenation in the aqueous phase.

Taking the mechanism difference between CH and PCET in account, kinetic isotope effect experiments ($KIE_{CH} = k_{H_2}/k_{D_2}$ and $KIE_{PCET} = k_{H_2O}/k_{D_2O}$) were designed to determine the

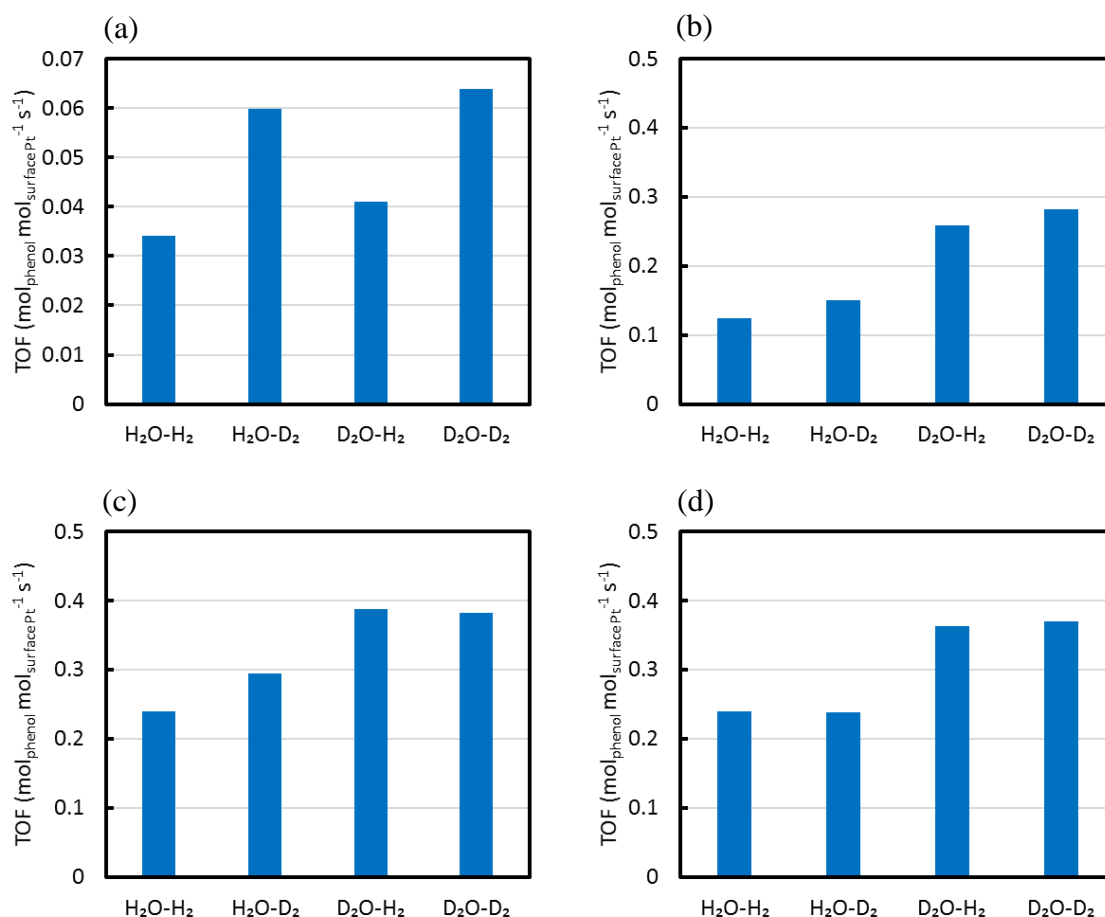


Figure 4.2. Comparison of phenol conversion rate among H₂-H₂O, D₂-H₂O, H₂-D₂O, D₂-D₂O over 50 mg 1 wt % Pt/CNT for pH 5.3 (no HClO₄) (a); 10 mg Pt/CNT for pH 4 (b), pH 3(c) and pH 2 (d), 313 K, 10 bar H₂ / D₂, 30 mL H₂O / D₂O, 0.106 M phenol.

dominated reaction pathway in phenol hydrogenation with pH by comparing the corresponding apparent hydrogenation rate under a certain pH at 313 K. As hypothesized, the dominated pathway would be CH in case of the main difference coming from r_{H_2}/r_{D_2} , because the active H or D atom is derived from dissociative adsorption of H₂ or D₂ in CH pathway. If the main difference were between r_{H_2O} and r_{D_2O} , it would be PCET as the dominated pathway, since the H or D for addition into phenol is formed from H⁺ or D⁺ in water. All the comparison experiments were carried out at low temperature (313 K) under 10 bar H₂ or D₂ to avoid the

influence e.g., formed D_2 on reaction of phenol with H_2 . The percentage of formed D_2 (H_2 reacts with D_2O) is below 8% in the reacting time. It can be seen from Figure 4.2(a) that the main difference in hydrogenation of phenol is coming from r_{H_2}/r_{D_2} instead of r_{H_2O}/r_{D_2O} under pH 5.3.

Under pH 4 in Figure 4.2(b), the main difference is shifting from r_{H_2}/r_{D_2} to r_{H_2O}/r_{D_2O} . While under pH 3 and 2 in Figure 4.2(c) and (d), there is nearly only difference between r_{H_2O} and r_{D_2O} (shown in Figure 4.3). The obvious shift of *KIE* difference from CH to PCET with pH decreasing provides a strong clue that the dominated reaction pathway changed with pH. The hydrogenation of phenol is dominated by conventional hydrogenation under pH 5.3 and by proton coupled electron transfer under low pH (e.g. pH 2).

4.3.3 Adsorption model for H_2 and phenol

Based on the previous work in our group,^[2] the rate-determining step is ascribed to the first H addition to phenol in phenol hydrogenation over Pt. For hydrogenation of phenol, two adsorption models are proposed for H_2 and phenol. One is competitive adsorption, in which the adsorption site for phenol is the same as for H_2 . Another one is non-competitive adsorption, with the adsorption site for phenol different from the one for H_2 . The elementary steps of phenol hydrogenation are deduced in CH or PCET pathway in SI. Due to the independence of adsorption model on reaction pathway, the discussion of adsorption model below is based on CH reaction pathway.

Firstly, the elementary steps of phenol hydrogenation in CH and PCET are deduced and summarized in Table 4.1.

Table 4.1. Elementary steps and rate equations of phenol hydrogenation via CH and PCET pathway ^a (Derivation is in Appendix)

Conventional hydrogenation (CH)				Proton coupled electron transfer (PCET)	
Rxn.	Description	Elementary steps	Rate and equilibrium constants	Elementary steps	Rate and equilibrium constants
(4.3)	H ₂ adsorption	H ₂ + 2 * \rightleftharpoons 2 H*	K _{H₂}	H ₂ + 2 * \rightleftharpoons 2 H*	K _{H₂}
				Electrode reaction H ⁺ + e ⁻ \rightleftharpoons $\frac{1}{2}$ H ₂ (Rxn. 4.3b)	E (electrode potential)
(4.4)	Phenol adsorption	Ph + * \rightleftharpoons Ph*	K _{Ph}	Ph + * \rightleftharpoons Ph*	K _{Ph}
(4.5)	1 st H addition	Ph* + H* \rightarrow HPh* + *	k _{CH}	Ph* + H ⁺ + e ⁻ \rightarrow HPh*	k _{PCET} k _{PCET} ^(SHE) rate constants at SHE
Eq. (4.6)	Empty site	(4.6a) H	$\theta_* = (1 + K_{H_2}^{0.5} P_{H_2}^{0.5})^{-1}$	(4.6c) H	$\theta_* = (1 + K_{H_2}^{0.5} P_{H_2}^{0.5})^{-1}$
		(4.6b) Phenol	$\theta_* = (1 + K_{Ph} C_{Ph})^{-1}$	(4.6d) Phenol	$\theta_* = (1 + K_{Ph} C_{Ph})^{-1}$
(4.7)	Coverage	(4.7a) H	$\theta_H = K_{H_2}^{0.5} P_{H_2}^{0.5} \theta_*$	(4.7c) H	$\theta_H = K_{H_2}^{0.5} P_{H_2}^{0.5} \theta_*$
		(4.7b) Phenol	$\theta_{Ph} = K_{Ph} C_{Ph} \theta_*$	(4.7d) Phenol	$\theta_{Ph} = K_{Ph} C_{Ph} \theta_*$
(4.8)	Overall rate	(4.8a) $r_{CH} = k_{CH} \theta_H \theta_{Ph} = \frac{k_{CH} K_{H_2}^{0.5} P_{H_2}^{0.5} K_{Ph} C_{Ph}}{(1 + K_{H_2}^{0.5} P_{H_2}^{0.5})(1 + K_{Ph} C_{Ph})}$		(4.8b) $r_{PCET} = k_{PCET}^{(SHE)} \exp\left[\frac{-\alpha(E-E^{(SHE)})F}{RT}\right] \theta_{Ph} [H^+] = k_{PCET}^{(SHE)} \exp\left[\frac{-\alpha(E-E^{(SHE)})F}{RT}\right] \frac{K_{Ph} C_{Ph} [H^+]}{(1 + K_{Ph} C_{Ph})}$	
				(4.8c) $\exp\left[\frac{-\alpha(E-E^{(SHE)})F}{RT}\right] = \left(\frac{P_{H_2}^{0.5}}{[H^+]}\right)^\alpha$	
(4.9)	Reaction order	(4.9a) H ₂	$\frac{\partial \ln r_{CH}}{\partial \ln P_{H_2}} = 0.5(1 - \theta_H)$	(4.9c) H ₂	$\frac{\partial \ln r_{PCET}}{\partial \ln P_{H_2}} = 0.5\alpha$
		(4.9b) Phenol	$\frac{\partial \ln r_{CH}}{\partial \ln C_{Ph}} = 1 - \theta_{Ph}$	(4.9d) Phenol	$\frac{\partial \ln r_{PCET}}{\partial \ln C_{Ph}} = 1 - \theta_{Ph}$

^aKey to symbols: *, accessible Pt site for H; *, accessible Pt site for Phenol; Ph, phenol; \rightleftharpoons , an equilibrated step; \rightarrow , an irreversible step; SHE, standard hydrogen electrode; P_{H₂}, H₂ pressure; C_{Ph}, phenol concentration; [H⁺] hydronium ion concentration; α, cathodic transfer coefficient.

In competitive adsorption model, the rate-determining step for CH pathway could be expressed as equation 4.10 (deduction is shown in SI)

$$r_{\text{CH}} = k_{\text{CH}}\theta_{\text{H}}\theta_{\text{Ph}} = \frac{k_{\text{CH}}K_{\text{H}_2}^{0.5}P_{\text{H}_2}^{0.5}K_{\text{Ph}}C_{\text{Ph}}}{(1+K_{\text{H}_2}^{0.5}P_{\text{H}_2}^{0.5}+K_{\text{Ph}}C_{\text{Ph}})^2} \quad \text{Eq. 4.10}$$

The reaction order of phenol would be -1 when $K_{\text{Ph}}C_{\text{Ph}}$ is much larger than $K_{\text{H}_2}^{0.5}P_{\text{H}_2}^{0.5}$. But in the testing range of pH, we did not observe the reaction order of phenol appearing as negative, indicating non-competitive adsorption of phenol with H_2 .

In non-competitive adsorption model, the rate-determining step for CH pathway could be expressed as equation (4.8a).

$$r_{\text{CH}} = k_{\text{CH}}\theta_{\text{H}}\theta_{\text{Ph}} = \frac{k_{\text{CH}}K_{\text{H}_2}^{0.5}P_{\text{H}_2}^{0.5}K_{\text{Ph}}C_{\text{Ph}}}{(1+K_{\text{H}_2}^{0.5}P_{\text{H}_2}^{0.5})(1+K_{\text{Ph}}C_{\text{Ph}})} \quad \text{Eq. (4.8a)}$$

The reaction order of phenol would be zero when $K_{\text{Ph}}C_{\text{Ph}}$ is much larger than $K_{\text{H}_2}^{0.5}P_{\text{H}_2}^{0.5}$. This is consistent with the reaction order of phenol observed in this work.

To further verify the adsorption model for H_2 and phenol, the formation rates of HD and D_2 in presence or absence of phenol were compared via the reaction of H_2 (g) with D_2O (l) under a certain condition. If phenol and H_2 adsorb competitively, the HD, H_2 , D_2 and total formation rate would decrease continuously as increase of phenol concentration. If phenol adsorption were not compete with H_2 , these rates would remain unchanged approximately.

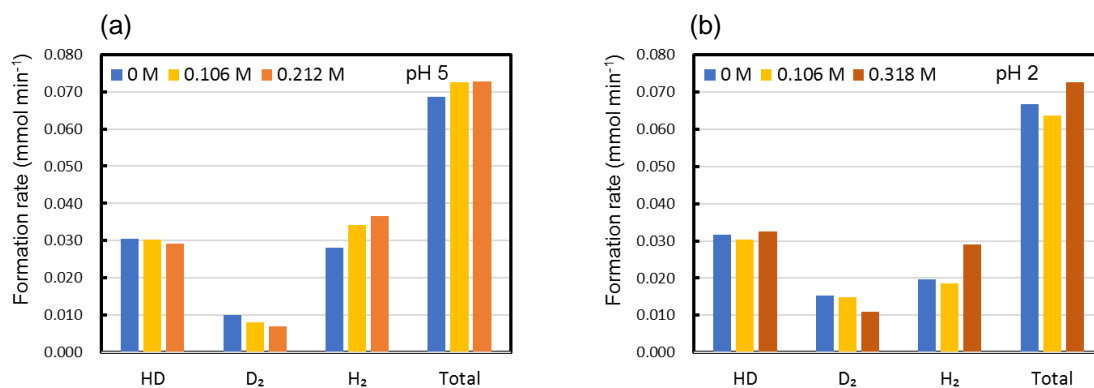


Figure 4.3. Formation rate of HD, D_2 and H_2 under (a) pH 5.3 and (b) pH 2 in the presence or absence of phenol (0.106 – 0.318 M) on 1 wt % Pt/CNT (5 mg), 298 K, 30 mL D_2O , 10 bar H_2 , HClO_4 .

As shown in Figure 4.3, each formation rate of HD, D_2 and H_2 does not show a noticeable decrease after adding phenol (0.106 – 0.318 M) under pH 5 and 2, which gives a strong evidence that adsorptions of phenol and H_2 are not competitive on Pt/CNT.

According to the equations of rate-determining step in CH (Eq. 4.8a) and PCET (Eq. 4.8b) pathways, the adsorption constant of H_2 and phenol on Pt/CNT are necessary for obtaining the kinetic parameters of each pathway. Thus, we determined the impact of pH on H_2 and phenol

adsorption on Pt/CNT in the aqueous phase.

4.3.4 Impact of pH on adsorption of H₂ on Pt/CNT in the aqueous phase

The impact of pH on H₂ dissociative adsorption on Pt in the aqueous phase has been discussed in detail in Chapter 2.

Table 4.2. Thermodynamic properties of the adsorption of H₂ on Pt/CNT.

T [K]	K_a°				
	pH 2	pH 3	pH 4	pH 5	pH 7
313	3.4×10^{-3}	2.8×10^{-3}	3.9×10^{-3}	5.2×10^{-3}	1.2×10^{-2}
323	2.3×10^{-3}	1.9×10^{-3}	2.5×10^{-3}	3.2×10^{-3}	6.7×10^{-3}
333	1.4×10^{-3}	1.1×10^{-3}	1.6×10^{-3}	2.0×10^{-3}	4.1×10^{-3}
ΔH_a° [kJ mol _{H₂} ⁻¹]	-38 ± 3	-39 ± 3	-40 ± 2	-42 ± 1	-45 ± 1

Table 4.2 shows the adsorption equilibrium constants that decreases as pH decreasing. The K_a° under different pH is then employed for calculation of kinetic parameters in phenol hydrogenation.

4.3.5 Impact of pH on adsorption of phenol on Pt in the aqueous phase

The reaction order of phenol in hydrogenation of phenol is observed to be zero on Pt/CNT under pH ranging from 5.3 to 2 (shown in Figure 4.4).

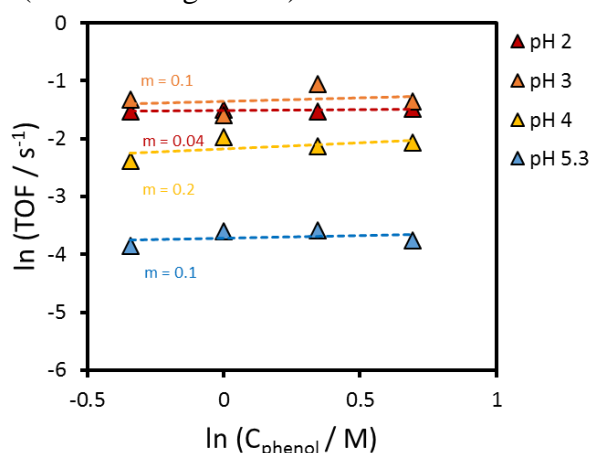


Figure 4.4. Reaction order of phenol (m) in phenol hydrogenation by plotting $\ln(\text{TOF} / \text{s}^{-1})$ as a function of $\ln(C_{\text{phenol}} / \text{M})$ over 1% Pt/CNT at 313 K, 10 bar H₂ under pH 2, 3, 4 and 5.3.

This indicates that the coverage of phenol is saturated and remain unchanged when modulating the pH in 0.106 mol L⁻¹ phenol concentration. It is reported that the reaction rate is zero order for phenol under conditions with variation of pH on Pt/C (0.172 mol L⁻¹ phenol, 80 °C, 20 bar H₂).^[2] Then, the coverage of phenol would be considered as 1 for further calculation of kinetic parameters in CH and PCET pathways.

Based on the mentioned results, the kinetic parameters of phenol hydrogenation could be obtained under different reaction pathways as discussed next.

4.3.6 Conventional hydrogenation

The first H addition step (Rxn. 1) is the rate-determining step of phenol hydrogenation, in which the reaction enthalpy could be described as the equation 11 below:

$$\begin{aligned}\Delta H_{\text{rds}} &= \Delta H_{\text{f, Ph-H}^*}^0 - \Delta H_{\text{f, Ph}^*}^0 - \Delta H_{\text{f, H}^*}^0 \\ &= \Delta H_{\text{f, Ph-H}^*}^0 - \Delta H_{\text{f, Ph}^*}^0 - HBE_{\text{app}}\end{aligned}\quad \text{Eq. 4.11}$$

H*, Ph* and Ph – H* represent adsorbed H, phenol and H-phenol respectively. In this step, the effect of pH on adsorptions of both phenol and hydrogenated phenol are likely to be in a similar extent. So $\Delta H_{\text{f, Ph-H}^*}^0 - \Delta H_{\text{f, Ph}^*}^0$ could be considered as a constant with pH. Based on Bell–Evans–Polanyi (BEP) principle, the activation energy of rate-determining step is linearly proportional to the reaction enthalpy, shown as:

$$E_a = c + \beta \Delta H_{\text{rds}} \quad \text{Eq. 4.12}$$

Where c is a constant and β is a constant between 0 and 1. Use equation 11 and equation 4.12, gives the expression of difference between two activation energies, e.g., E_a and E_0 (reference point) in equation 4.13:

$$E_a - E_0 = \beta (HBE_{\text{a,app}} - HBE_{\text{0,app}}) \quad \text{Eq. 4.13}$$

According to Arrhenius equation, the rate constant k_a could be obtained by equation 4.14:

$$k_a = k_0 \cdot e^{\frac{-\beta(HBE_{\text{a,app}} - HBE_{\text{0,app}})}{RT}} \quad \text{Eq. 4.14}$$

where k_0 is a referenced rate constant of the rate-determining step in conventional hydrogenation pathway. The value of β , i.e. the slope of BEP relations, is reported to be 1 for Pt/C catalyst with pH variation.^[2] Thus, the value of β in this work is assumed to be 1. Since nearly no hydrogenation of phenol occurring through proton coupled electron transfer pathway under pH 5.3, the apparent rate under pH 5.3 ($r_{\text{pH 5.3}}$) is assumed to be the rate in CH under pH 5.3 ($r_{\text{CH-pH 5.3}}$). Thus, the rate constant in CH under pH 5.3 ($k_{\text{CH-pH 5}}$) can be calculated by equation 4.13. The rate constant in CH pathway under pH 4-2 ($k_{\text{CH-pH 4}}$, $k_{\text{CH-pH 3}}$ and

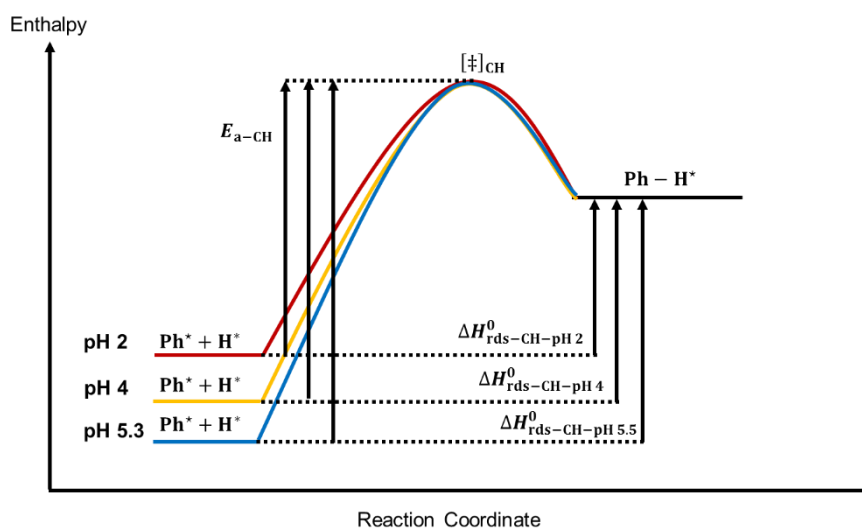
$k_{\text{CH-pH } 2}$) can be obtained by equation 4.14 (k_0 is assumed to $k_{\text{CH-pH } 5.3}$). The enthalpy, entropy and Gibbs energy of activation can be calculated by using Eyring equation for the rate-determining step.

Table 4.3 gives apparent HBE and kinetic parameters of phenol hydrogenation on Pt/CNT catalyst with pH in the aqueous phase. The rate constant shows an increasing trend with decrease of pH, while the enthalpy of activation is constant. We assumed that the coverage of phenol on Pt under 0.106 mol L^{-1} concentration is 1 for pH 2 – 5.3 at 313 – 333 K.

Table 4.3. HBE and kinetic parameters in conventional hydrogenation over Pt/CNT with pH in water.

pH	Apparent HBE (kJ mol ⁻¹)	k_{CH} (s ⁻¹)			E_a (kJ mol ⁻¹)
		313 K	323 K	333 K	
2	-19.0	0.32	0.51	0.93	44.8
3	-19.5	0.26	0.42	0.77	45.3
4	-20.0	0.22	0.34	0.63	45.8
5.3	-21.0	0.15	0.23	0.43	46.8

Scheme 4.2 gives the enthalpy diagram of the rate-determining step in CH under three pH values. For conventional hydrogenation pathway, a weaker H binding energy increases the total energy of adsorbed reactants, leading to a shrinking E_a with decrease of pH.



Scheme 4.2. Enthalpy of rate-determining step in CH pathway under different pH

4.3.7 Proton coupled electron transfer

The rate of proton coupled electron transfer could be determined by subtraction of total rate with that of conventional hydrogenation under a certain pH. Figure 4.5 gives the phenol

hydrogenation rate of apparent, CH and PCET as a function of pH at 313 K (The cases at 323 and 333 K are shown in Figure A1). Besides the reaction rate of apparent and CH, PCET also shows a pH-dependence in phenol hydrogenation.

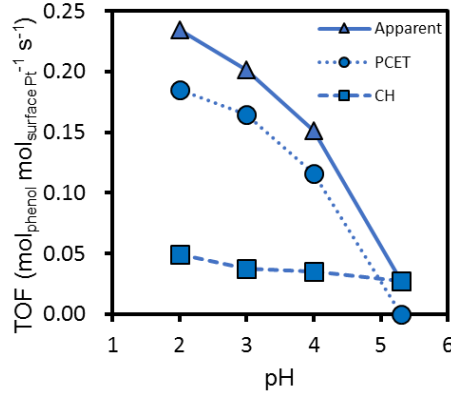


Figure 4.5. Phenol hydrogenation rate of apparent, CH and PCET as a function of pH over 1% Pt/CNT at 313 K.

The rate-determining step in PCET is expressed as equation 4.8b in table 4.1.

$$r_{\text{PCET}} = k_{\text{PCET}}^{(\text{SHE})} \exp\left[\frac{-\alpha(E-E^{(\text{SHE})})F}{RT}\right] \theta_{\text{Ph}}[\text{H}^+] \quad \text{Eq.(4.8b)}$$

Based on equation (4.8b) and (4.8c),

$$\frac{r_{\text{PCET}}}{[\text{H}^+]} = \left(\frac{P_{\text{H}_2}^{0.5}}{[\text{H}^+]}\right)^\alpha \quad \text{Eq. 4.15}$$

Taking natural logarithm on both sides, equation 4.15 could be transferred to equation 4.16:

$$\ln\left(\frac{r_{\text{PCET}}}{[\text{H}^+]}\right) = \alpha \ln\left(\frac{P_{\text{H}_2}^{0.5}}{[\text{H}^+]}\right) \quad \text{Eq. 4.16}$$

According to equation 4.16, the cathodic transfer coefficient α in PCET could be obtained from the slope by plotting $\ln\left(\frac{r_{\text{PCET}}}{[\text{H}^+]}\right)$ as a function of $\ln\left(\frac{P_{\text{H}_2}^{0.5}}{[\text{H}^+]}\right)$, which is shown in Figure 4.6.

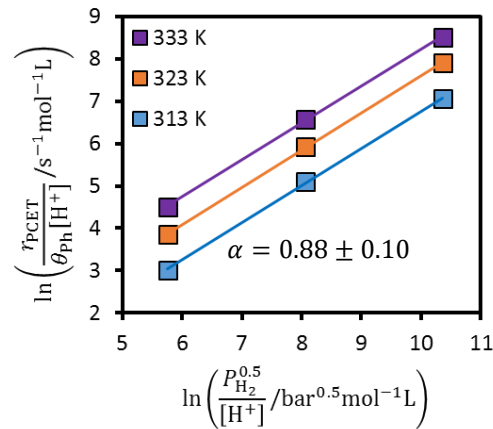


Figure 4.6. Cathodic transfer coefficient results, α , over Pt/CNT at different temperatures, plotted according to Equation 16.

Table 4.4 summarizes the reaction rates in PCET pathway under different pH and cathodic transfer coefficient. In PCET pathway, the hydrogen electrode reaction (Rxn. 4.3 in Table 4.1) establishes an equilibrium of H₂ and H⁺, generating an OCP on Pt, which is also recognized as reversible hydrogen electrode (RHE) potential.

Table 4.4. Kinetic parameters in proton coupled electron transfer over Pt/CNT with pH in the aqueous phase.

pH	r_{PCET} (s ⁻¹)			α
	313 K	323 K	333 K	
2	0.19	0.43	0.83	0.88 ± 0.10
3	0.16	0.37	0.72	
4	0.12	0.27	0.49	

By Nernst equation, the OCP (E) relates to the H₂ pressure and H⁺ activity (Eq. 17).

$$E = E^{(\text{SHE})} + \frac{RT}{F} \ln \left(\frac{[\text{H}^+]}{P_{\text{H}_2}^{0.5}} \right) \quad \text{Eq. 4.17}$$

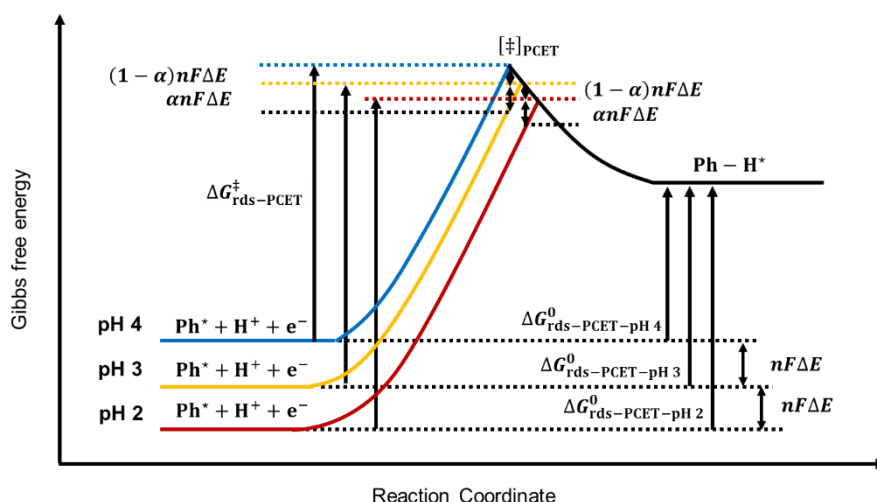
The $E^{(\text{SHE})}$ is the standard hydrogen electrode potential. The H addition step goes via PCET, with the first H addition as the rate-determining step. The rate constant of the first H addition is derived based on Butler-Volmer equation, which gives the following expressions (see Kinetic Derivation session in Supporting Information for details).

$$k_{\text{PCET}} = k_{\text{PCET}}^{(\text{SHE})} \exp \left[\frac{-\alpha(E - E^{(\text{SHE})})F}{RT} \right] = k_{\text{PCET}}^{(\text{SHE})} \exp \left[\frac{-\alpha E^{(\text{RHE})}F}{RT} \right] \quad \text{Eq. 4.18}$$

Here, k_{PCET} is the rate constant of the first H addition step in PCET at the reaction OCP (E); while $k_{\text{PCET}}^{(\text{SHE})}$ is the counterpart at SHE potential.

Scheme 4.3 shows the Gibbs free energy diagram of the rate-determining step in PCET under different pH. When pH decreases by one unit at 313 K with 10 bar H₂, the OCP would increase by 0.062 V (ΔE), leading to decrease of energy in ground state of reactant by 6 kJ mol⁻¹, whereas the transition state will decrease by $(1 - \alpha)nF\Delta E$. The Gibbs energy of activation then will increase by 6α based on equation 4.19.

$$\begin{aligned} \Delta G_{\text{pH } n}^{\ddagger} - \Delta G_{\text{pH } n+1}^{\ddagger} &= \alpha n F (E_{\text{pH } n} - E_{\text{pH } n+1}) \\ &= \alpha n F \Delta E \\ &= 6\alpha \end{aligned} \quad \text{Eq. 4.19}$$



Scheme 4.3. Gibbs free energy of rate-determining step in PCET pathway under pH 2, 3 and 4. $\Delta G_{\text{rds-PCET}}^{\ddagger}$ and $\Delta G_{\text{rds-PCET}}^{\circ}$ are Gibbs energy of activation for transition state and reaction in RDS under PCET pathway, respectively.

When pH decreases from 4 to 2, the rate of PCET increases from 0.10 to 0.18 s⁻¹, but the Gibbs energy of activation of PCET shows an increasing tendency with decrease of pH. The rate constant of PCET is greatly reduced by decreasing pH, which is caused by the electrode potential getting positive. The higher the electrode potential of Pt, the more activation energy required for PCET pathway. However, due to the exponentially increased concentration of hydronium ions as pH decreasing, the rate of phenol hydrogenation in PCET pathway is still promoted even with higher activation energy.

In this work, the reaction order of H₂ increases from 0.2 to 0.5 with pH decreasing from 5 to 2. The correlation of H₂ reaction order with H coverage in CH or PCET pathway can be expressed in equation 4.9 in table 4.1.

$$\frac{\partial \ln r_{\text{CH}}}{\partial \ln P_{\text{H}_2}} = 0.5(1 - \theta_{\text{H}}) \quad \text{Eq. (4.9a)}$$

$$\frac{\partial \ln r_{\text{PCET}}}{\partial \ln P_{\text{H}_2}} = 0.5\alpha \quad \text{Eq. (4.9b)}$$

Under pH 2 to 4, PCET is the dominated reaction pathway. The reaction order of H₂ measured experimentally is 0.5-0.4, which is in line with the calculated order 0.5 based on equation (4.9b). Under pH 5.3, CH is the dominated pathway, with the reaction order predicted to be 0.4 based on equation (4.9a), which is larger than the value 0.2 from experimental. This contradictory is probably caused for simplification of the reaction model by using Langmuir adsorption model

in this work. But this does not affect the results of non-competitive adsorption model. With decrease of pH, the increase of H_2 order on Pt/CNT arises from 1) the shift of dominated reaction pathway from CH to PCET and 2) decrease of adsorption constant of H_2 on Pt.

4.4 Conclusions

In conclusion, apparent hydrogenation rate of phenol is greatly by decreasing pH in water. Two reaction pathways, CH and PCET, are involved in the reaction. As pH decreasing from 5 to 2, the main reaction pathway shifts from CH to PCET. The activation energy in CH decreased due to the weakening HBE on Pt/CNT, leading to an increasing tendency of reaction rate in CH. The activation Gibbs free energy in PCET increases by reason of the increase of electrode potential. Despite of this, the reaction rate of PCET is still promoted by decrease of pH because of the exponential increase of hydronium ion concentration. Both impact of pH on reaction rate in CH and PCET lead to an increasing trend of apparent hydrogenation rate of phenol.

4.5 Appendix

Table A4.1a. TOFs of phenol hydrogenation at 313-333 K with 10 bar H₂ on 1 wt % Pt/CNT in 100 mL H₂O under pH 2 and 3.

T / K	pH 2			pH 3		
	TOF / s ⁻¹			TOF / s ⁻¹		
	1 bar	3 bar	10 bar	1 bar	3 bar	10 bar
313	0.073	0.16	0.23	0.084	0.12	0.20
323	0.15	0.35	0.49	0.16	0.22	0.42
333	0.30	0.61	0.92	0.26	0.42	0.79

Table A4.1b. TOFs of phenol hydrogenation at 313-333 K with 10 bar H₂ on 1 wt % Pt/CNT in 100 mL H₂O under pH 4 and 5.3.

T / K	pH 4			pH 5.3		
	TOF / s ⁻¹			TOF / s ⁻¹		
	1 bar	3 bar	10 bar	1 bar	3 bar	10 bar
313	0.068	0.11	0.15	0.018	0.025	0.027
323	0.12	0.20	0.32	0.023	0.031	0.036
333	0.19	0.41	0.56	0.033	0.043	0.053

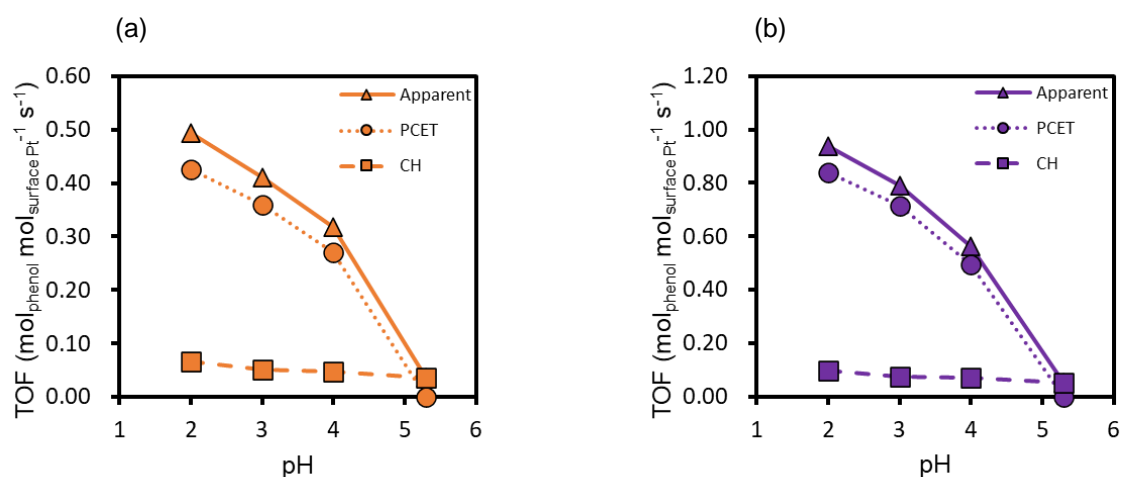


Figure A4.1. Phenol hydrogenation rate of apparent, CH and PCET as a function of pH over 1% Pt/CNT at (a) 323 K and (b) 333 K.

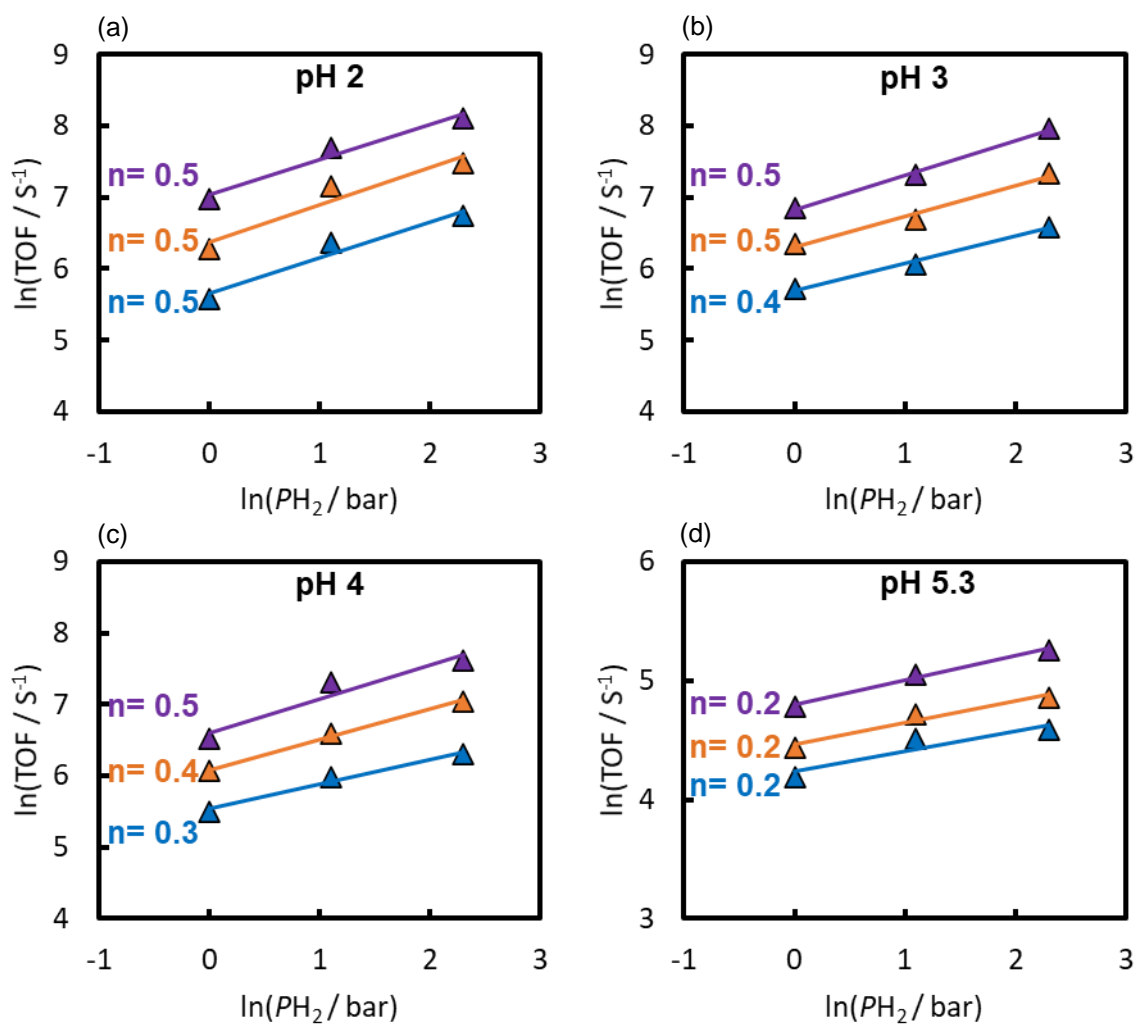
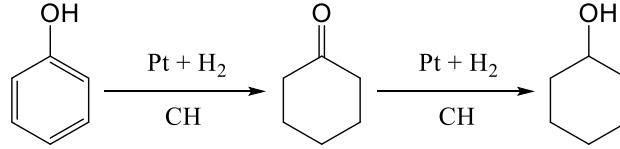


Figure A4.2. Reaction order H_2 (n) in phenol hydrogenation by plotting $\ln(\text{TOF} / \text{s}^{-1})$ as a function of $\ln(P_{H_2} / \text{bar})$ over 1% Pt/CNT at 313 K (blue) 323 K (orange) and 333 K (purple) under (a) pH 2, (b) pH 3, (c) pH 4 and (d) pH 5.3.

Conventional hydrogenation pathway

Hydrogenation of phenol on Pt/CNT in the aqueous phase proceeds via CH pathway shown below:



Non-competitive adsorption model

The adsorbed phenol and H₂ follow the equilibrium equation with the respective constant K_{Ph} , and K_{H_2} .

$$K_{H_2} = \frac{\theta_H^2}{P_{H_2} \theta_*^2} \quad (\text{Eq. A4.1a})$$

$$K_{Ph} = \frac{\theta_{Ph}}{C_{Ph} \theta_*} \quad (\text{Eq. A4.1b})$$

The coverage of hydrogen and phenol are given as following:

$$\theta_H = K_{H_2}^{0.5} P_{H_2}^{0.5} \theta_* \quad (\text{Eq. A4.2a})$$

$$\theta_{Ph} = K_{Ph} C_{Ph} \theta_* \quad (\text{Eq. A4.2b})$$

The adsorptions of phenol and H₂ are non-competitive. All the coverages of surface species add up to unity, giving Equation A4.3.

$$\theta_H + \theta_* = 1 \quad (\text{Eq. A4.3a})$$

$$\theta_{Ph} + \theta_* = 1 \quad (\text{Eq. A4.3b})$$

Taking Equation A4.2a and A4.2b to Equation A4.3a and A4.3b, gives the coverage of surface species

$$\theta_* = \frac{1}{(1 + K_{H_2}^{0.5} P_{H_2}^{0.5})} \quad (\text{Eq. A4.4a})$$

$$\theta_* = \frac{1}{(1 + K_{Ph} C_{Ph})} \quad (\text{Eq. A4.4b})$$

Therefore, the coverage of surface species are expressed as

$$\theta_H = \frac{K_{H_2}^{0.5} P_{H_2}^{0.5}}{(1 + K_{H_2}^{0.5} P_{H_2}^{0.5})} \quad (\text{Eq. A4.5a})$$

$$\theta_{Ph} = \frac{K_{Ph} C_{Ph}}{(1 + K_{Ph} C_{Ph})} \quad (\text{Eq. A4.5b})$$

The reaction rate of phenol hydrogenation (normalized to Pt sites concentration) should be proportional to θ_H and θ_{Ph} with a rate constant k_{CH} . Using the equations of S5a and A4.5b, the normalized hydrogenation rate in conventional hydrogenation pathway (over Pt/CNT) is calculated as following:

$$r_{CH} = k_{CH}\theta_H\theta_{Ph} = \frac{k_{CH}K_{H_2}^{0.5}P_{H_2}^{0.5}K_{Ph}C_{Ph}}{(1+K_{H_2}^{0.5}P_{H_2}^{0.5})(1+K_{Ph}C_{Ph})} \quad (\text{Eq. A4.6})$$

The reaction order with respect to phenol on Pt/CNT is expressed as equation A4.7.

$$\frac{\partial \ln r_{CH}}{\partial \ln C_{Ph}} = \frac{\partial C_{Ph}}{\partial \ln C_{Ph}} \cdot \frac{\partial \ln r_{CH}}{\partial C_{Ph}} = C_{Ph} \cdot \frac{\partial \ln r_{CH}}{\partial C_{Ph}} \quad (\text{Eq. A4.7})$$

Equation A4.7 can be expressed further with Equation A4.6, gives:

$$\begin{aligned} \frac{\partial \ln r_{CH}}{\partial \ln C_{Ph}} &= C_{Ph} \cdot \frac{\partial \ln r_{CH}}{\partial C_{Ph}} = C_{Ph} \cdot \frac{\partial}{\partial C_{Ph}} \ln \left[\frac{k_{CH}K_{H_2}^{0.5}P_{H_2}^{0.5}K_{Ph}C_{Ph}}{(1+K_{H_2}^{0.5}P_{H_2}^{0.5})(1+K_{Ph}C_{Ph})} \right] \\ &= C_{Ph} \cdot \frac{\partial}{\partial C_{Ph}} \left[\ln(k_{CH}K_{H_2}^{0.5}P_{H_2}^{0.5}K_{Ph}C_{Ph}) - \ln(1+K_{H_2}^{0.5}P_{H_2}^{0.5}) - \ln(1+K_{Ph}C_{Ph}) \right] \\ &= C_{Ph} \cdot \left[\frac{1}{C_{Ph}} - \frac{K_{Ph}}{1+K_{Ph}C_{Ph}} \right] \\ &= 1 - \frac{K_{Ph}C_{Ph}}{1+K_{Ph}C_{Ph}} \end{aligned} \quad (\text{Eq. A4.8a})$$

Note that the term, $\frac{K_{Ph}C_{Ph}}{1+K_{Ph}C_{Ph}}$, in Equation A4.8a is actually θ_{Ph} (see Eq. A4.5c and A4.5d), it is finally expressed as

$$\frac{\partial \ln r_{CH}}{\partial \ln C_{Ph}} = 1 - \theta_{Ph} \quad (\text{Eq. A4.8b})$$

In the same way, the reaction order with of H_2 the similar derivation is shown as following:

$$\begin{aligned} \frac{\partial \ln r_{CH}}{\partial \ln P_{H_2}} &= P_{H_2} \cdot \frac{\partial \ln r_{CH}}{\partial P_{H_2}} = P_{H_2} \cdot \frac{\partial}{\partial P_{H_2}} \ln \left[\frac{k_{CH}K_{H_2}^{0.5}P_{H_2}^{0.5}K_{Ph}C_{Ph}}{(1+K_{H_2}^{0.5}P_{H_2}^{0.5})(1+K_{Ph}C_{Ph})} \right] \\ &= P_{H_2} \cdot \frac{\partial}{\partial P_{H_2}} \left[\ln(k_{CH}K_{H_2}^{0.5}P_{H_2}^{0.5}K_{Ph}C_{Ph}) - \ln(1+K_{H_2}^{0.5}P_{H_2}^{0.5}) - \ln(1+K_{Ph}C_{Ph}) \right] \\ &= P_{H_2} \left[\frac{0.5}{P_{H_2}} - \frac{0.5K_{H_2}^{0.5}P_{H_2}^{-0.5}}{1+K_{H_2}^{0.5}P_{H_2}^{0.5}} \right] \\ &= 0.5 - \frac{0.5K_{H_2}^{0.5}P_{H_2}^{0.5}}{1+K_{H_2}^{0.5}P_{H_2}^{0.5}} \\ &= 0.5(1 - \theta_H) \end{aligned} \quad (\text{Eq. A4.9})$$

Competitive adsorption model

The adsorbed phenol and H₂ follow the equilibrium equation with the respective constant K_{Ph} , and K_{H_2} .

$$K_{H_2} = \frac{\theta_H^2}{P_{H_2} \theta_*^2} \quad (\text{Eq. A4.10a})$$

$$K_{Ph} = \frac{\theta_{Ph}}{C_{Ph} \theta_*} \quad (\text{Eq. A4.10b})$$

The coverage of hydrogen and phenol are given as following:

$$\theta_H = K_{H_2}^{0.5} P_{H_2}^{0.5} \theta_* \quad (\text{Eq. A4.11a})$$

$$\theta_{Ph} = K_{Ph} C_{Ph} \theta_* \quad (\text{Eq. A4.11b})$$

The adsorptions of phenol and H₂ are competitive. All the coverages of surface species add up to unity, giving Equation A4.12.

$$\theta_H + \theta_{Ph} + \theta_* = 1 \quad (\text{Eq. A4.12})$$

Taking Equation A4.11a and A4.11b to Equation A4.12, gives the coverage of surface species

$$\theta_* = \frac{1}{(1 + K_{H_2}^{0.5} P_{H_2}^{0.5} + K_{Ph} C_{Ph})} \quad (\text{Eq. A4.13})$$

Therefore, the coverage of surface species could be expressed as

$$\theta_H = \frac{K_{H_2}^{0.5} P_{H_2}^{0.5}}{(1 + K_{H_2}^{0.5} P_{H_2}^{0.5} + K_{Ph} C_{Ph})} \quad (\text{Eq. A4.14a})$$

$$\theta_{Ph} = \frac{K_{Ph} C_{Ph}}{(1 + K_{H_2}^{0.5} P_{H_2}^{0.5} + K_{Ph} C_{Ph})} \quad (\text{Eq. A4.14b})$$

The reaction rate of phenol hydrogenation (normalized to Pt sites concentration) should be proportional to θ_H and θ_{Ph} with a rate constant k_{CH} . Using the equations of A4.14a and A4.14b, the normalized hydrogenation rate in conventional hydrogenation pathway (over Pt/CNT) is calculated as following:

$$r_{CH} = k_{CH} \theta_H \theta_{Ph} = \frac{k_{CH} K_{H_2}^{0.5} P_{H_2}^{0.5} K_{Ph} C_{Ph}}{(1 + K_{H_2}^{0.5} P_{H_2}^{0.5} + K_{Ph} C_{Ph})^2} \quad (\text{Eq. A4.15})$$

The reaction order with respect to phenol on Pt/CNT is expressed as equation A4.16.

$$\frac{\partial \ln r_{CH}}{\partial \ln C_{Ph}} = \frac{\partial C_{Ph}}{\partial \ln C_{Ph}} \cdot \frac{\partial \ln r_{CH}}{\partial C_{Ph}} = C_{Ph} \cdot \frac{\partial \ln r_{CH}}{\partial C_{Ph}} \quad (\text{Eq. A4.16})$$

Equation A4.16 can be expressed further with Equation A4.15, gives:

$$\frac{\partial \ln r_{CH}}{\partial \ln C_{Ph}} = C_{Ph} \cdot \frac{\partial \ln r_{CH}}{\partial C_{Ph}} = C_{Ph} \cdot \frac{\partial}{\partial C_{Ph}} \ln \left[\frac{k_{CH} K_{H_2}^{0.5} P_{H_2}^{0.5} K_{Ph} C_{Ph}}{(1 + K_{H_2}^{0.5} P_{H_2}^{0.5} + K_{Ph} C_{Ph})^2} \right]$$

$$\begin{aligned}
&= C_{\text{Ph}} \cdot \frac{\partial}{\partial C_{\text{Ph}}} \left[\ln(k_{\text{CH}} K_{\text{H}_2}^{0.5} P_{\text{H}_2}^{0.5} K_{\text{Ph}} C_{\text{Ph}}) - 2 \ln(1 + K_{\text{H}_2}^{0.5} P_{\text{H}_2}^{0.5} + K_{\text{Ph}} C_{\text{Ph}}) \right] \\
&= C_{\text{Ph}} \cdot \left[\frac{1}{C_{\text{Ph}}} - 2 \cdot \frac{K_{\text{Ph}}}{1 + K_{\text{H}_2}^{0.5} P_{\text{H}_2}^{0.5} + K_{\text{Ph}} C_{\text{Ph}}} \right] \\
&= 1 - 2 \cdot \frac{K_{\text{Ph}} C_{\text{Ph}}}{1 + K_{\text{H}_2}^{0.5} P_{\text{H}_2}^{0.5} + K_{\text{Ph}} C_{\text{Ph}}} \tag{Eq. A4.17a}
\end{aligned}$$

Note that the term, $\frac{K_{\text{Ph}} C_{\text{Ph}}}{1 + K_{\text{H}_2}^{0.5} P_{\text{H}_2}^{0.5} + K_{\text{Ph}} C_{\text{Ph}}}$, in Equation A4.17a is actually θ_{Ph} (see Eq. A4.14a and A4.14b), it is finally expressed as

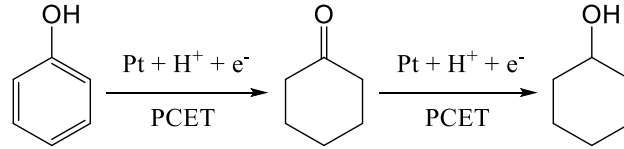
$$\frac{\partial \ln r_{\text{CH}}}{\partial \ln C_{\text{Ph}}} = 1 - 2\theta_{\text{Ph}} \tag{Eq. A4.17b}$$

In the same way, the reaction order with of H₂ the similar derivation is shown as following:

$$\begin{aligned}
\frac{\partial \ln r_{\text{CH}}}{\partial \ln P_{\text{H}_2}} &= P_{\text{H}_2} \cdot \frac{\partial \ln r_{\text{CH}}}{\partial P_{\text{H}_2}} = P_{\text{H}_2} \cdot \frac{\partial}{\partial P_{\text{H}_2}} \ln \left[\frac{k_{\text{CH}} K_{\text{H}_2}^{0.5} P_{\text{H}_2}^{0.5} K_{\text{Ph}} C_{\text{Ph}}}{(1 + K_{\text{H}_2}^{0.5} P_{\text{H}_2}^{0.5} + K_{\text{Ph}} C_{\text{Ph}})^2} \right] \\
&= P_{\text{H}_2} \cdot \frac{\partial}{\partial P_{\text{H}_2}} \left[\ln(k_{\text{CH}} K_{\text{H}_2}^{0.5} P_{\text{H}_2}^{0.5} K_{\text{Ph}} C_{\text{Ph}}) - 2 \ln(1 + K_{\text{H}_2}^{0.5} P_{\text{H}_2}^{0.5} + K_{\text{Ph}} C_{\text{Ph}}) \right] \\
&= P_{\text{H}_2} \left[\frac{0.5}{P_{\text{H}_2}} - \frac{K_{\text{H}_2}^{0.5} P_{\text{H}_2}^{-0.5}}{1 + K_{\text{H}_2}^{0.5} P_{\text{H}_2}^{0.5} + K_{\text{Ph}} C_{\text{Ph}}} \right] \\
&= 0.5 - \frac{K_{\text{H}_2}^{0.5} P_{\text{H}_2}^{0.5}}{1 + K_{\text{H}_2}^{0.5} P_{\text{H}_2}^{0.5} + K_{\text{Ph}} C_{\text{Ph}}} \\
&= 0.5 - \theta_{\text{H}} \tag{Eq. A4.18}
\end{aligned}$$

Proton coupled electron transfer pathway

Hydrogenation of phenol on Pt/CNT in the aqueous phase proceeds via PCET pathway shown below:



Non-competitive adsorption model

If the phenol hydrogenation reaction follows the PCET pathway, the elementary steps of which are shown in Table 4.1 (in the main text). The adsorbed phenol and H₂ follow the equilibrium equation with the respective constant K_{Ph} , and K_{H_2} . The coverage of hydrogen and phenol can be deduced as following:

$$K_{H_2} = \frac{\theta_H^2}{P_{H_2} \theta_*^2} \quad (\text{Eq. A4.19a})$$

$$K_{Ph} = \frac{\theta_{Ph}}{C_{Ph} \theta_*} \quad (\text{Eq. A4.19b})$$

Where K_{Ph} , and K_{H_2} represent the equilibrium constants of adsorbed phenol and H₂. The coverage of hydrogen and phenol can be individually expressed as:

$$\theta_H = K_{H_2}^{0.5} P_{H_2}^{0.5} \theta_* \quad (\text{Eq. A20a})$$

$$\theta_{Ph} = K_{Ph} C_{Ph} \theta_* \quad (\text{Eq. A20b})$$

In PCET pathway, the hydrogen electrode reaction (Rxn 4.3) establishes an equilibrium of H₂ and H⁺, generating an Open Circuit Potential (OCP) on Pt, which is also recognized as reversible hydrogen electrode (RHE) potential. By Nernst Equation, the OCP (E) relates to the H₂ pressure and H⁺ concentration (Eq. A4.21).

$$E = E^{(SHE)} + \frac{RT}{F} \ln \frac{[H^+]}{P_{H_2}^{0.5}} \Leftrightarrow \frac{[H^+]}{P_{H_2}^{0.5}} = \exp \left[\frac{(E - E^{(SHE)})F}{RT} \right] \quad (\text{Eq. A4.21})$$

The $E^{(SHE)}$ is the standard hydrogen electrode (SHE) potential. For the case that the H addition to phenol goes via PCET, the first H addition is rate-determining step. The rate constant of PCET is derived based on Butler-Volmer equation. So the rate constants (k_{PCET}) can be deduced as the following:

$$k_{PCET} = \frac{k_B T}{h} \exp \left[-\frac{\Delta G_{SHE}^\ddagger + \alpha E F}{RT} \right] = \frac{k_B T}{h} \exp \left[-\frac{\Delta G_{SHE}^\ddagger + \alpha E^{(SHE)} F}{RT} \right] \exp \left[\frac{\alpha (E^{(SHE)} - E) F}{RT} \right] \quad (\text{Eq. A4.22})$$

The $\Delta G_{\text{SHE}}^\ddagger$ is the activation free energy for the corresponding PCET reaction at zero electrode potential ($E^{(\text{SHE})} = 0$ V); α is the cathodic transfer coefficient. By defining their first exponential terms as the rate constant when the electrode potential is at SHE potential, $k_{\text{PCET}}^{(\text{SHE})}$ can be expressed:

$$k_{\text{PCET}}^{(\text{SHE})} = \frac{k_B T}{h} \exp \left[-\frac{\Delta G_{\text{SHE}}^\ddagger + \alpha E^{(\text{SHE})} F}{RT} \right] \quad (\text{Eq. A4.23})$$

the Equations A4.22 reduce to Equation A4.24a.

$$k_{\text{PCET}} = k_{\text{PCET}}^{(\text{SHE})} \exp \left[\frac{-\alpha (E - E^{(\text{SHE})}) F}{RT} \right] \quad (\text{Eq. A4.24a})$$

$$E - E^{(\text{SHE})} = \frac{RT}{F} \ln \frac{[\text{H}^+]}{P_{\text{H}_2}^{0.5}} \quad (\text{Eq. A4.24b})$$

$$k_{\text{PCET}} = k_{\text{PCET}}^{(\text{SHE})} \left(\frac{P_{\text{H}_2}^{0.5}}{[\text{H}^+]} \right)^\alpha \quad (\text{Eq. A4.24c})$$

Therefore, the rate equation can be expressed based on the above rate constants.

$$r_{\text{PCET}} = k_{\text{PCET}} \theta_{\text{Ph}} [\text{H}^+] = k_{\text{PCET}}^{(\text{SHE})} \left(\frac{P_{\text{H}_2}^{0.5}}{[\text{H}^+]} \right)^\alpha [\text{H}^+] \theta_{\text{Ph}} \quad (\text{Eq. A4.25})$$

All the coverages of surface species add up to unity, giving Equation A4.26

$$\theta_{\text{H}} + \theta_* = 1 \quad (\text{Eq. A4.26a})$$

$$\theta_{\text{Ph}} + \theta_* = 1 \quad (\text{Eq. A4.26b})$$

Use equations A4.20 into equation A4.26, gives

$$\theta_* = \frac{1}{(1 + K_{\text{H}_2}^{0.5} P_{\text{H}_2}^{0.5})} \quad (\text{Eq. A4.27a})$$

$$\theta_* = \frac{1}{(1 + K_{\text{Ph}} C_{\text{Ph}})} \quad (\text{Eq. A4.27b})$$

Therefore, the coverages of surface species are expressed as

$$\theta_{\text{H}} = K_{\text{H}_2}^{0.5} P_{\text{H}_2}^{0.5} \theta_* = \frac{K_{\text{H}_2}^{0.5} P_{\text{H}_2}^{0.5}}{1 + K_{\text{H}_2}^{0.5} P_{\text{H}_2}^{0.5}} \quad (\text{Eq. A4.28a})$$

$$\theta_{\text{Ph}} = K_{\text{Ph}} C_{\text{Ph}} \theta_* = \frac{K_{\text{Ph}} C_{\text{Ph}}}{1 + K_{\text{Ph}} C_{\text{Ph}}} \quad (\text{Eq. A4.28b})$$

The reaction rate of phenol hydrogenation via PCET pathway is proportional to θ_{Ph} and $[\text{H}^+]$ with a rate constant k_{PCET} , which can be written in Equation A4.29a.

$$r_{\text{PCET}} = r_{\text{PCET}} = k_{\text{PCET}} \theta_{\text{Ph}} [\text{H}^+] \quad (\text{Eq. A4.29a})$$

Using expression of θ_{Ph} in Equation A4.20b and k_{PCET} in Equation A4.24c, the rate in Equation A4.29a is reformulated into Equation A4.29b

$$r_{\text{PCET}} = k_{\text{PCET}}^{(\text{SHE})} \left(\frac{P_{\text{H}_2}^{0.5}}{[\text{H}^+]} \right)^\alpha \frac{K_{\text{Ph}} C_{\text{Ph}}}{1 + K_{\text{Ph}} C_{\text{Ph}}} [\text{H}^+] \quad (\text{Eq. A4.29b})$$

The reaction order with respect to phenol (via PCET pathway) can be deduced as bellow:

$$\begin{aligned} \frac{\partial \ln r_{\text{PCET}}}{\partial \ln C_{\text{Ph}}} &= C_{\text{Ph}} \cdot \frac{\partial \ln r_{\text{PCET}}}{\partial C_{\text{Ph}}} = C_{\text{Ph}} \cdot \frac{\partial}{\partial C_{\text{Ph}}} \ln \left[k_{\text{PCET}}^{(\text{SHE})} \left(\frac{P_{\text{H}_2}^{0.5}}{[\text{H}^+]} \right)^\alpha \frac{K_{\text{Ph}} C_{\text{Ph}}}{1 + K_{\text{Ph}} C_{\text{Ph}}} [\text{H}^+] \right] \\ &= C_{\text{Ph}} \cdot \frac{\partial}{\partial C_{\text{Ph}}} \left[\ln \left(k_{\text{PCET}}^{(\text{SHE})} \left(\frac{P_{\text{H}_2}^{0.5}}{[\text{H}^+]} \right)^\alpha \right) + \ln \left(\frac{K_{\text{Ph}} C_{\text{Ph}}}{1 + K_{\text{Ph}} C_{\text{Ph}}} \right) + \ln [\text{H}^+] \right] \\ &= C_{\text{Ph}} \cdot \frac{\partial}{\partial C_{\text{Ph}}} [\ln(K_{\text{Ph}} C_{\text{Ph}}) - \ln(1 + K_{\text{Ph}} C_{\text{Ph}})] \\ &= C_{\text{Ph}} \cdot \left[\frac{1}{C_{\text{Ph}}} - \frac{K_{\text{Ph}}}{1 + K_{\text{Ph}} C_{\text{Ph}}} \right] \\ &= 1 - \frac{K_{\text{Ph}} C_{\text{Ph}}}{1 + K_{\text{Ph}} C_{\text{Ph}}} \\ &= 1 - \theta_{\text{Ph}} \end{aligned} \quad (\text{Eq. A4.30a})$$

While the reaction order of H₂ (via PCET pathway) is derived as bellow

$$\begin{aligned} \frac{\partial \ln r_{\text{PCET}}}{\partial \ln P_{\text{H}_2}} &= P_{\text{H}_2} \cdot \frac{\partial \ln r_{\text{PCET}}}{\partial P_{\text{H}_2}} = P_{\text{H}_2} \cdot \frac{\partial}{\partial P_{\text{H}_2}} \ln \left[k_{\text{PCET}}^{(\text{SHE})} \left(\frac{P_{\text{H}_2}^{0.5}}{[\text{H}^+]} \right)^\alpha \frac{K_{\text{Ph}} C_{\text{Ph}}}{1 + K_{\text{Ph}} C_{\text{Ph}}} [\text{H}^+] \right] \\ &= P_{\text{H}_2} \cdot \frac{\partial}{\partial P_{\text{H}_2}} [\ln(P_{\text{H}_2}^{0.5\alpha})] \\ &= P_{\text{H}_2} \left[\frac{0.5\alpha}{P_{\text{H}_2}} \right] \\ &= 0.5\alpha \end{aligned} \quad (\text{Eq. A4.30b})$$

Competitive adsorption model

The adsorbed phenol and H₂ follow the equilibrium equation with the respective constant K_{Ph} , and K_{H_2} . The coverage of hydrogen and phenol can be deduced as following:

$$K_{H_2} = \frac{\theta_H^2}{P_{H_2} \theta_*^2} \quad (\text{Eq. A4.31a})$$

$$K_{Ph} = \frac{\theta_{Ph}}{C_{Ph} \theta_*} \quad (\text{Eq. A4.31b})$$

Where K_{Ph} , and K_{H_2} represent the equilibrium constants of adsorbed phenol and H₂. The coverage of hydrogen and phenol can be individually expressed as:

$$\theta_H = K_{H_2}^{0.5} P_{H_2}^{0.5} \theta_* \quad (\text{Eq. A4.32a})$$

$$\theta_{Ph} = K_{Ph} C_{Ph} \theta_* \quad (\text{Eq. A4.32b})$$

The rate equation of PCET in competitive adsorption model is the same as that in Equations A4.25.

$$r_{PCET} = k_{PCET} \theta_{Ph} [H^+] = k_{PCET}^{(SHE)} \left(\frac{P_{H_2}^{0.5}}{[H^+]} \right)^\alpha [H^+] \theta_{Ph} \quad (\text{Eq. A4.33a})$$

All the coverages of surface species add up to unity, giving Equation A4.34

$$\theta_H + \theta_{Ph} + \theta_* = 1 \quad (\text{Eq. A4.34})$$

Use equations A4.32 into equation A4.34, gives

$$\theta_* = \frac{1}{(1 + K_{Ph} C_{Ph} + K_{H_2}^{0.5} P_{H_2}^{0.5})} \quad (\text{Eq. A4.35a})$$

Therefore, the coverages of surface species are expressed as

$$\theta_H = K_{H_2}^{0.5} P_{H_2}^{0.5} \theta_* = \frac{K_{H_2}^{0.5} P_{H_2}^{0.5}}{(1 + K_{Ph} C_{Ph} + K_{H_2}^{0.5} P_{H_2}^{0.5})} \quad (\text{Eq. A4.35c})$$

$$\theta_{Ph} = K_{Ph} C_{Ph} \theta_* = \frac{K_{Ph} C_{Ph}}{(1 + K_{Ph} C_{Ph} + K_{H_2}^{0.5} P_{H_2}^{0.5})} \quad (\text{Eq. A4.35d})$$

The reaction rate of phenol hydrogenation via PCET pathway is proportional to θ_{Ph} and $[H^+]$ with a rate constant k_{PCET} , which can be written in Equation A4.36a.

$$r_{PCET} = r_{PCET} = k_{PCET} \theta_{Ph} [H^+] \quad (\text{Eq. A4.36a})$$

Using expression of θ_{Ph} in Equation A4.35d and k_{PCET} in Equation A4.24c, the rate in Equation A4.36a is reformulated into Equation A4.36b

$$r_{\text{PCET}} = k_{\text{PCET}}^{(\text{SHE})} \left(\frac{P_{\text{H}_2}^{0.5}}{[\text{H}^+]} \right)^\alpha \frac{K_{\text{Ph}} C_{\text{Ph}}}{(1 + K_{\text{Ph}} C_{\text{Ph}} + K_{\text{H}_2}^{0.5} P_{\text{H}_2}^{0.5})} [\text{H}^+] \quad (\text{Eq. A4.36b})$$

The reaction order with respect to phenol (via PCET pathway) can be deduced as bellow:

$$\begin{aligned} \frac{\partial \ln r_{\text{PCET}}}{\partial \ln C_{\text{Ph}}} &= C_{\text{Ph}} \cdot \frac{\partial \ln r_{\text{PCET}}}{\partial C_{\text{Ph}}} = C_{\text{Ph}} \cdot \frac{\partial}{\partial C_{\text{Ph}}} \ln \left[k_{\text{PCET}}^{(\text{SHE})} \left(\frac{P_{\text{H}_2}^{0.5}}{[\text{H}^+]} \right)^\alpha \frac{K_{\text{Ph}} C_{\text{Ph}}}{(1 + K_{\text{Ph}} C_{\text{Ph}} + K_{\text{H}_2}^{0.5} P_{\text{H}_2}^{0.5})} [\text{H}^+] \right] \\ &= C_{\text{Ph}} \cdot \frac{\partial}{\partial C_{\text{Ph}}} \left[\ln \left(k_{\text{PCET}}^{(\text{SHE})} \left(\frac{P_{\text{H}_2}^{0.5}}{[\text{H}^+]} \right)^\alpha \right) + \ln \left(\frac{K_{\text{Ph}} C_{\text{Ph}}}{1 + K_{\text{Ph}} C_{\text{Ph}} + K_{\text{H}_2}^{0.5} P_{\text{H}_2}^{0.5}} \right) + \ln [\text{H}^+] \right] \\ &= C_{\text{Ph}} \cdot \frac{\partial}{\partial C_{\text{Ph}}} \left[\ln(K_{\text{Ph}} C_{\text{Ph}}) - \ln(1 + K_{\text{Ph}} C_{\text{Ph}} + K_{\text{H}_2}^{0.5} P_{\text{H}_2}^{0.5}) \right] \\ &= C_{\text{Ph}} \cdot \left[\frac{1}{C_{\text{Ph}}} - \frac{K_{\text{Ph}}}{1 + K_{\text{Ph}} C_{\text{Ph}} + K_{\text{H}_2}^{0.5} P_{\text{H}_2}^{0.5}} \right] \\ &= 1 - \frac{K_{\text{Ph}} C_{\text{Ph}}}{1 + K_{\text{Ph}} C_{\text{Ph}} + K_{\text{H}_2}^{0.5} P_{\text{H}_2}^{0.5}} \\ &= 1 - \theta_{\text{Ph}} \end{aligned} \quad (\text{Eq. A4.37a})$$

While the reaction order of H₂ (via PCET pathway) is derived as bellow

$$\begin{aligned} \frac{\partial \ln r_{\text{PCET}}}{\partial \ln P_{\text{H}_2}} &= P_{\text{H}_2} \cdot \frac{\partial \ln r_{\text{PCET}}}{\partial P_{\text{H}_2}} = P_{\text{H}_2} \cdot \frac{\partial}{\partial P_{\text{H}_2}} \ln \left[k_{\text{PCET}}^{(\text{SHE})} \left(\frac{P_{\text{H}_2}^{0.5}}{[\text{H}^+]} \right)^\alpha \frac{K_{\text{Ph}} C_{\text{Ph}}}{(1 + K_{\text{Ph}} C_{\text{Ph}} + K_{\text{H}_2}^{0.5} P_{\text{H}_2}^{0.5})} [\text{H}^+] \right] \\ &= P_{\text{H}_2} \cdot \frac{\partial}{\partial P_{\text{H}_2}} \left[\ln(P_{\text{H}_2}^{0.5\alpha}) - \ln(1 + K_{\text{Ph}} C_{\text{Ph}} + K_{\text{H}_2}^{0.5} P_{\text{H}_2}^{0.5}) \right] \\ &= P_{\text{H}_2} \left[\frac{0.5\alpha}{P_{\text{H}_2}} - \frac{0.5 K_{\text{H}_2}^{0.5} P_{\text{H}_2}^{-0.5}}{(1 + K_{\text{Ph}} C_{\text{Ph}} + K_{\text{H}_2}^{0.5} P_{\text{H}_2}^{0.5})} \right] \\ &= \left[0.5\alpha - \frac{0.5 K_{\text{H}_2}^{0.5} P_{\text{H}_2}^{0.5}}{(1 + K_{\text{Ph}} C_{\text{Ph}} + K_{\text{H}_2}^{0.5} P_{\text{H}_2}^{0.5})} \right] \\ &= 0.5(\alpha - \theta_{\text{H}}) \end{aligned} \quad (\text{Eq. A4.37b})$$

Kinetic isotope effect in hydrogenation of phenol

The kinetic isotope effect $[KIE]_{CH}$ and $[KIE]_{PCET}$ are defined as their rate constant ratios:

$$[KIE]_{CH} = \frac{k_{H-CH}}{k_{D-CH}} \quad (\text{Eq. A4.38a})$$

$$[KIE]_{PCET} = \frac{k_{H-PCET}}{k_{D-PCET}} \quad (\text{Eq. A4.38b})$$

The symbol H or D in the subscript refers to the species containing H or D. Bigeleisen's theoretical treatments were applied for the calculation of KIE in CH and PCET pathways.^[32] The equation is simplified in order to calculate hydrogen/deuterium kinetic isotope effect as shown in the following Equation A4.39

$$\frac{k_H}{k_D} = S \cdot M \cdot I \cdot EXC \cdot ZPE \quad (\text{Eq. A4.39})$$

Where S is symmetry number; M is molecular mass; I is the moment of inertial; EXC is from the contribution of vibrationally excited molecules; ZPE is zero-point energy of corresponding species in reaction. Both S and I factors are assumed to be unity and neglected in this work. In addition, the degrees of freedom in translation and rotation for H and D species in surface (Pt-H and Pt-D), transition (Ph-H[‡] and Ph-D[‡], late transition state^[16]) and final states (Ph-H and Ph-D) are neglected. The values for mentioned parameters are listed in Table A4.2.

Table A4.2. M, I and ZPE values of H and D-containing species involved in the calculation for the KIE.

Species	M (g·mol ⁻¹)	I (×10 ⁻⁴¹ g·cm ²)	ZPE [a](kJ·mol ⁻¹)	Ref.
Pt-H	[d]	[d]	17.4 [b]	[33]
Pt-D	[d]	[d]	12.3 [c]	
Ph-H	[d]	[d]	18.4 [b]	[34]
Ph-D	[d]	[d]	13.1 [c]	
H ₂	2.00	4.67	26.1	[35]
D ₂	4.00	9.31	18.5	
[a] $ZPE = 0.5h\nu$ (ν is the fundamental vibrational frequency)				
[b] Calculated on the basis of vibrations both normal and parallel to the species.				
[c] The vibrational frequency of this mode was estimated from that of Pt-H or Ph-H bond, based on $\frac{\nu_{Pt-D}}{\nu_{Pt-H}} = \sqrt{\frac{\mu_{Pt-H}}{\mu_{Pt-D}}}$, $\frac{\nu_{Ph-D}}{\nu_{Ph-H}} = \sqrt{\frac{\mu_{Ph-H}}{\mu_{Ph-D}}}$ (μ is the reduced mass)				
[d] Translational and rotational degrees of freedom for H and D on surface and transition species are ignored.				

Table A4.3. Derivation of kinetic isotope effect (KIE) for the adsorption and reaction of H₂ and D₂ on Pt.

Description	Reaction steps	Equilibrium and Rate constants	Zero-point energy
H ₂ adsorption	$\frac{1}{2} \text{H}_2 + \text{Pt} \rightleftharpoons \text{Pt} - \text{H}$	K_{H_2}	$ZPE_{\text{H}}^{\text{IS}-1}$
D ₂ adsorption	$\frac{1}{2} \text{D}_2 + \text{Pt} \rightleftharpoons \text{Pt} - \text{D}$	K_{D_2}	$ZPE_{\text{D}}^{\text{IS}-1}$
H ₂ reaction	$\text{Pt} - \text{H} + \text{Ph} \rightarrow \text{Pt} + \text{Ph} - \text{H}$	k_{H}	$ZPE_{\text{H}}^{\text{IS}-2}, ZPE_{\text{H}}^{\text{TS}}$
D ₂ reaction	$\text{Pt} - \text{D} + \text{Ph} \rightarrow \text{Pt} + \text{Ph} - \text{D}$	k_{D}	$ZPE_{\text{D}}^{\text{IS}-2}, ZPE_{\text{D}}^{\text{TS}}$
$\Delta ZPE_{\text{IS}-1} = ZPE_{\text{H}}^{\text{IS}-1} - ZPE_{\text{D}}^{\text{IS}-1}$			
$\Delta ZPE_{\text{IS}-2} = ZPE_{\text{H}}^{\text{IS}-2} - ZPE_{\text{D}}^{\text{IS}-2}$			
$\Delta ZPE_{\text{TS}} = ZPE_{\text{H}}^{\text{TS}} - ZPE_{\text{D}}^{\text{TS}}$			
Equilibrium isotope effect (EIE)	$\frac{K_{\text{H}_2}}{K_{\text{D}_2}} = \left(\frac{M_{\text{D}_2}}{M_{\text{H}_2}}\right)^{\frac{3}{2}} \cdot \left(\frac{I_{\text{D}_2}}{I_{\text{H}_2}}\right)^{\frac{1}{2}} \cdot \exp\left(\frac{\Delta ZPE_{\text{IS}-1} - \Delta ZPE_{\text{IS}-2}}{RT}\right)$		Eq. A4.40
Kinetic isotope effect (KIE)	$\frac{k_{\text{H}}}{k_{\text{D}}} = \exp\left(\frac{\Delta ZPE_{\text{IS}-2} - \Delta ZPE_{\text{TS}}}{RT}\right)$		Eq. A4.41
Reaction rate ratio ($\theta_{\text{H}} \cong 1$)	$\frac{r_{\text{H}}}{r_{\text{D}}} = \frac{k_{\text{H}}}{k_{\text{D}}}$		Eq. A4.42
Reaction rate ratio ($\theta_{\text{H}} \cong 0$)	$\frac{r_{\text{H}}}{r_{\text{D}}} = \left(\frac{k_{\text{H}}}{k_{\text{D}}} \cdot \sqrt{\frac{K_{\text{H}_2}}{K_{\text{D}_2}}}\right)$		Eq. A4.43

Scheme A4.1 shows the diagram of normal and inverse kinetic isotope effect for the rate-determining step of phenol hydrogenation on Pt/CNT.

For CH pathway, the rate equation of rate-determining step is $r_{\text{CH}} = k_{\text{CH}}\theta_{\text{H}}\theta_{\text{Ph}}$

- 1) When θ_{H} is 1 (θ_{Ph} is 1 under 0.106 M concentration of phenol), the rate equation can be simplified to: $r_{\text{CH}} = k_{\text{CH}}$

Then,

$$\frac{r_{\text{H-CH}}}{r_{\text{D-CH}}} = \frac{k_{\text{H-CH}}}{k_{\text{D-CH}}}$$

There is a negligible difference in the molecular masses and moments of inertia between H and D containing species since H and D are much lighter in comparison to the reactants and transition species. So, M and I factors are also approximated as unity. Then, the rate constant ratio is dominated by ZPE factor:

$$\begin{aligned} \frac{k_{\text{H-CH}}}{k_{\text{D-CH}}} &= \exp\left(\frac{ZPE_{\text{D}}^{\text{TS}} - ZPE_{\text{D}}^{\text{IS}-2} - ZPE_{\text{H}}^{\text{TS}} + ZPE_{\text{H}}^{\text{IS}-2}}{RT}\right) \\ &= \exp\left(\frac{(ZPE_{\text{H}}^{\text{IS}-2} - ZPE_{\text{D}}^{\text{IS}-2}) - (ZPE_{\text{H}}^{\text{TS}} - ZPE_{\text{D}}^{\text{TS}})}{RT}\right) \\ &= \exp\left(\frac{\Delta ZPE_{\text{IS}-2} - \Delta ZPE_{\text{TS}}}{RT}\right) \end{aligned} \quad (\text{Eq. A4.44})$$

From the ZPE value in Table S1, $\Delta ZPE_{\text{IS}-2}$ is larger than ΔZPE_{TS} , so

$$\frac{r_{\text{H-CH}}}{r_{\text{D-CH}}} = \frac{k_{\text{H-CH}}}{k_{\text{D-CH}}} < 1$$

2) When the coverage of H₂ tends to be 0 (θ_{ph} is 1 under 0.106 M concentration of phenol), the rate equation could be simplified to:

$$r_{\text{CH}} = k_{\text{CH}}\theta_{\text{H}} = \frac{k_{\text{CH}}K_{\text{H}_2}^{0.5}P_{\text{H}_2}^{0.5}}{(1+K_{\text{H}_2}^{0.5}P_{\text{H}_2}^{0.5})} \quad (\text{Eq. A4.45})$$

Where $1 + K_{\text{H}_2}^{0.5}P_{\text{H}_2}^{0.5}$ could be approximated as 1, then:

$$r_{\text{CH}} = k_{\text{CH}}K_{\text{H}_2}^{0.5}P_{\text{H}_2}^{0.5} \quad (\text{Eq. A4.46})$$

Then, the reaction rate ratio is expressed as Equation A4.47:

$$\frac{r_{\text{H-CH}}}{r_{\text{D-CH}}} = \left(\frac{k_{\text{H}}}{k_{\text{D}}} \cdot \sqrt{\frac{K_{\text{H}_2}}{K_{\text{D}_2}}} \right) \quad (\text{Eq. A4.47})$$

Since $\Delta ZPE_{\text{IS-1}} > \Delta ZPE_{\text{IS-2}}$, the equilibrium isotope effect, $\frac{K_{\text{H}_2}}{K_{\text{D}_2}} > 1$. The reaction rate ratio between H and D is dependent on the combination of the KIE of rds (<1) and the EIE of hydrogen adsorption (>1).

For PCET pathway, the rate equation of rate-determining step is

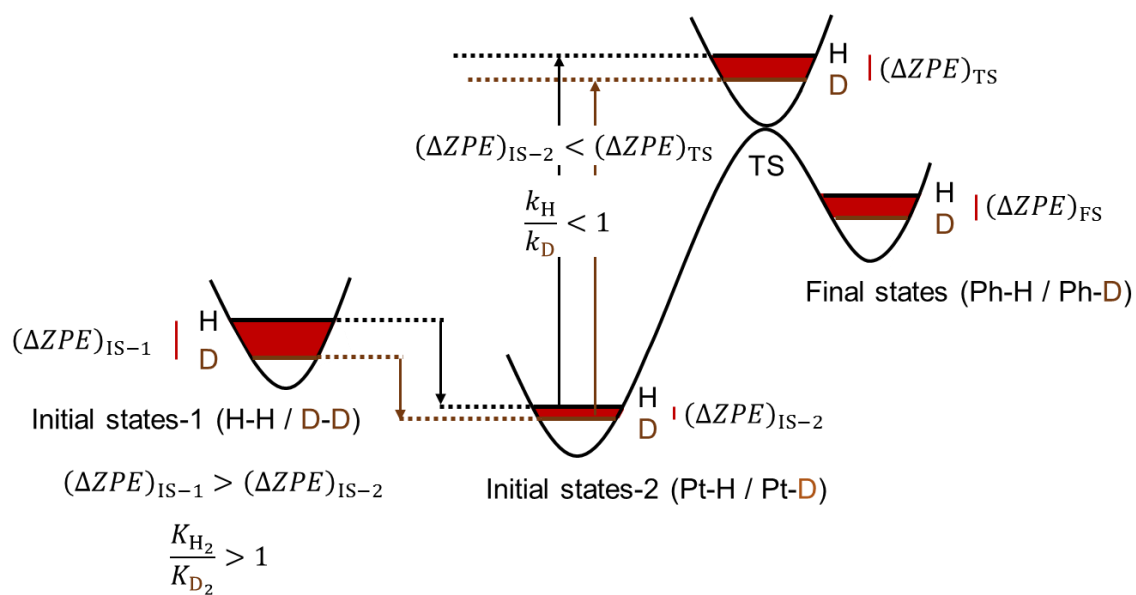
$$r_{\text{PCET}} = k_{\text{PCET}}\theta_{\text{ph}}[\text{H}^+] = k_{\text{PCET}}^{(\text{SHE})} \left(\frac{P_{\text{H}_2}^{0.5}}{[\text{H}^+]} \right)^\alpha [\text{H}^+]\theta_{\text{ph}}$$

$$\frac{r_{\text{H-PCET}}}{r_{\text{D-PCET}}} = \frac{k_{\text{H-PCET}}^{(\text{SHE})}}{k_{\text{D-PCET}}^{(\text{SHE})}}$$

Since the electrode reaction is in equilibrium, the initial state in PCET pathway is Pt-H or Pt-D. Then,

$$\frac{k_{\text{H-PCET}}^{(\text{SHE})}}{k_{\text{D-PCET}}^{(\text{SHE})}} < 1$$

$$\frac{r_{\text{H-PCET}}}{r_{\text{D-PCET}}} = \frac{k_{\text{H-PCET}}^{(\text{SHE})}}{k_{\text{D-PCET}}^{(\text{SHE})}} < 1$$



Scheme A4.1. The diagram of normal and inverse kinetic isotope effect for the rate-determining step of phenol hydrogenation on 1% Pt/CNT.

4.6 References

- [1] C. Zhao, S. Kasakov, J. He, J. A. Lercher, *Journal of Catalysis* **2012**, 296, 12-23.
- [2] S. Kasakov, C. Zhao, E. Baráth, Z. A. Chase, J. L. Fulton, D. M. Camaioni, A. Vjunov, H. Shi, J. A. Lercher, *Chemistry—A European Journal* **2015**, 21, 1567-1577.
- [3] W. Song, Y. Liu, E. Baráth, C. Zhao, J. A. Lercher, *Green Chemistry* **2015**, 17, 1204-1218.
- [4] C. A. Teles, R. C. Rabelo-Neto, J. R. de Lima, L. V. Mattos, D. E. Resasco, F. B. Noronha, *Catalysis Letters* **2016**, 146, 1848-1857.
- [5] R. C. Nelson, B. Baek, P. Ruiz, B. Goundie, A. Brooks, M. C. Wheeler, B. G. Frederick, L. C. Grabow, R. N. Austin, *ACS catalysis* **2015**, 5, 6509-6523.
- [6] P. M. de Souza, R. C. Rabelo-Neto, L. E. Borges, G. Jacobs, B. H. Davis, U. M. Graham, D. E. Resasco, F. B. Noronha, *ACS Catalysis* **2015**, 5, 7385-7398.
- [7] C. Zhao, Y. Kou, A. A. Lemonidou, X. Li, J. A. Lercher, *Angewandte Chemie International Edition* **2009**, 48, 3987-3990.
- [8] Q. Han, M. U. Rehman, J. Wang, A. Rykov, O. Y. Gutiérrez, Y. Zhao, S. Wang, X. Ma, J. A. Lercher, *Applied Catalysis B: Environmental* **2019**, 253, 348-358.
- [9] J. Chen, J. Huang, L. Chen, L. Ma, T. Wang, U. I. Zakai, *ChemCatChem* **2013**, 5, 1598-1605.
- [10] C. Zhao, J. A. Lercher, *ChemCatChem* **2012**, 4, 64-68.
- [11] N. Singh, M.-T. Nguyen, D. C. Cantu, B. L. Mehdi, N. D. Browning, J. L. Fulton, J. Zheng, M. Balasubramanian, O. Y. Gutiérrez, V.-A. Glezakou, *Journal of Catalysis* **2018**, 368, 8-19.
- [12] Y. Song, S. H. Chia, U. Sanyal, O. Y. Gutiérrez, J. A. Lercher, *Journal of Catalysis* **2016**, 344, 263-272.
- [13] Y. Song, U. Sanyal, D. Pangotra, J. D. Holladay, D. M. Camaioni, O. Y. Gutiérrez, J. A. Lercher, *Journal of Catalysis* **2018**, 359, 68-75.
- [14] N. Singh, Y. Song, O. Y. Gutiérrez, D. M. Camaioni, C. T. Campbell, J. A. Lercher, *ACS Catalysis* **2016**, 6, 7466-7470.
- [15] S. Trasatti, *Journal of Electroanalytical Chemistry and Interfacial Electrochemistry* **1972**, 39, 163-184.

- [16] N. Singh, M.-S. Lee, S. A. Akhade, G. Cheng, D. M. Camaioni, O. Y. Gutiérrez, V.-A. Glezakou, R. Rousseau, J. A. Lercher, C. T. Campbell, *ACS Catalysis* **2018**, *9*, 1120-1128.
- [17] H. Yang, J. L. Whitten, *The Journal of chemical physics* **1993**, *98*, 5039-5049.
- [18] G. Mills, H. Jónsson, G. K. Schenter, *Surface Science* **1995**, *324*, 305-337.
- [19] S. Sakong, A. Groß, *Surface science* **2003**, *525*, 107-118.
- [20] G. Henkelman, H. Jónsson, *Physical review letters* **2001**, *86*, 664.
- [21] N. B. Arboleda Jr, H. Kasai, W. A. Dino, H. Nakanishi, *Japanese Journal of Applied Physics* **2007**, *46*, 4233.
- [22] S. Dag, Y. Ozturk, S. Ciraci, T. Yildirim, *Physical Review B* **2005**, *72*, 155404.
- [23] D. A. McCormack, R. A. Olsen, E. J. Baerends, *The Journal of chemical physics* **2005**, *122*, 194708.
- [24] A. Luntz, J. Brown, M. Williams, *The Journal of chemical physics* **1990**, *93*, 5240-5246.
- [25] P. Kraus, I. Frank, *International Journal of Quantum Chemistry* **2017**, *117*, e25407.
- [26] J. A. Lopez-Ruiz, U. Sanyal, J. Egbert, O. Y. Gutiérrez, J. Holladay, *ACS Sustainable Chemistry & Engineering* **2018**, *6*, 16073-16085.
- [27] D. C. Cantu, A. B. Padmaperuma, M.-T. Nguyen, S. A. Akhade, Y. Yoon, Y.-G. Wang, M.-S. Lee, V.-A. Glezakou, R. Rousseau, M. A. Lilga, *ACS Catalysis* **2018**, *8*, 7645-7658.
- [28] C. J. Bondue, F. Calle-Vallejo, M. C. Figueiredo, M. T. Koper, *Nature Catalysis* **2019**, *2*, 243-250.
- [29] C. Bondue, M. Koper, *Journal of Catalysis* **2019**, *369*, 302-311.
- [30] K. Koh, U. Sanyal, M. S. Lee, G. Cheng, M. Song, V. A. Glezakou, Y. Liu, D. Li, R. Rousseau, O. Y. Gutiérrez, *Angewandte Chemie* **2020**, *132*, 1517-1521.
- [31] Y. Song, O. Y. Gutiérrez, J. Herranz, J. A. Lercher, *Applied Catalysis B: Environmental* **2016**, *182*, 236-246.
- [32] E. Buncl, C. C. Lee, **1977**.
- [33] J. Greeley, M. Mavrikakis, *The Journal of Physical Chemistry B* **2005**, *109*, 3460-3471.
- [34] J. Evans, *Spectrochimica Acta* **1960**, *16*, 1382-1392.
- [35] K. K. Irikura, *Journal of Physical and Chemical Reference Data* **2009**, *38*, 749-749.

Chapter 5

Summary and conclusions

The aim of this thesis is to get a deep insight of the impact of pH on hydrogenation reactions on Pt catalyst in the aqueous phase. A carbon nanotube (CNT) supported Pt catalyst was employed in the whole work due to the clean surface of CNT with very small amount of carboxylic and phenolic functional groups. Hydrogenation of organic molecules requires sequential addition of two H atoms to the substrate. So far, two pathways have been identified for this reaction on transition metal particles in water: conventional hydrogenation (CH) and proton coupled electron transfer (PCET). In water, a metal particle itself is a hydrogen electrode in presence of H₂ and at a certain pH, having a so-called open circuit potential (OCP). We use the hydrogenation reaction of phenol on Pt to explore whether the OCP on a transition metal can induce a PCET pathway, in particular at which conditions PCET overtakes CH pathway at OCP. There are three parts (1) the impact of water on adsorption of H₂ over Pt/CNT from the perspective of electronic structure of metal surface; (2) the impact of pH on adsorption of H₂ in the aqueous phase and (3) the impact of pH on hydrogenation of phenol in the aqueous phase.

First, the adsorption heat of H₂ in the aqueous phase was determined by using a kinetic method based on the reaction of D₂O with H₂ on Pt/CNT, and compared with that in the gas phase. According to Van't Hoff and Arrhenius equations, the equilibrium and rate adsorption constants, heat of adsorption for H₂ can be determined by measuring the formation rate of HD and D₂ with variation of H₂ pressure and reaction temperatures. In contrast to the gas phase, the adsorption heat of H₂ in the aqueous phase is smaller due to the change of electronic structure on Pt surface. When Pt catalyst is immersed into water, the Fermi level of Pt would be in line with that of water at a certain H₂ pressure with redox couple (hydronium ions and H₂), which alters the Fermi level in the antibonding state of Pt-H bond to a lower level, leading to a strong H binding on Pt surface with a high H₂ adsorption heat.

Then, the adsorption of H₂ under different pH in the aqueous phase was evaluated by using the same kinetic method. As pH decreasing from 7 to 2, the adsorption heat of H₂ decreases from 45 to 38 kJ·mol⁻¹. In addition, the activation energy of adsorption increases from 1 to 8 kJ·mol⁻¹, whereas the activation energy of desorption remains constant with the variation of pH. Due to the decrease of pH, an increase of work is required to shift the electric double layer away from the surface of Pt. This resulted in a decrease of the adsorption heat of H₂ on Pt surface and a weaker strength of Pt-H bond as pH decreasing from 7 to 2 in the aqueous phase.

Furthermore, the impact of pH on hydrogenation of phenol in water was investigated over Pt/CNT catalyst. The turnover frequency shows a clear increasing trend, growing by an order

of magnitude as pH decreasing from 5.3 to 2. In order to determine the reaction pathway, kinetic experiments were designed based on the difference between two pathways. The H atom for addition into phenol molecule in CH pathway is from dissociative adsorption of gaseous H₂, whereas that in PCET pathway is from hydronium ions in water. It was demonstrated that CH and PCET pathways are both participated in phenol hydrogenation, with the dominated route transforming from CH to PCET as pH decreasing. It should be noted that all the reactions were carried out in absence of over potential, that only OCP drove the PCET pathway. When pH decreases, the reaction rate of CH is enhanced by the decrease of activation barrier that is caused by decrease of HBE on Pt. The reaction rate of PCET is promoted by decrease of pH because of the largely increased hydronium ion concentration even though the activation Gibbs free energy is increased in parallel. These results demonstrate that an electrocatalytic hydrogenation reaction can still occur under OCP.

In conclusion, understanding of the impact of pH on OCP, reaction pathways and kinetic parameters provides the mechanistic basis to promote hydrogenation reactions via modulating the concentration of hydronium ions. This is also applicable to other reactions involving hydrogen addition, e.g. hydrogenolysis for the targeted conversion of biomass into chemicals and fuels.

Curriculum Vitae

Xi Chen was born on November 25th, 1987 in Heilongjiang, China. He entered college of Chemistry, Chemical Engineering and Biotechnology in Donghua University (Shanghai, China) in September 2007, majoring in the Textile Chemistry, and received the bachelor's degree of Engineering in July 2011. In September 2013, he continued his education at department of Chemistry, Fudan University as a master student in the research on hydrogenation of ethylene carbonate into methanol and obtained his master's degree of Science in Physical Chemistry in June 2016 under the supervision of Prof. Weilin Dai. During the period of master, he received the ExxonMobil Award, Kwang-Hua Award and graduated as Excellent Graduates of Shanghai General Colleges and Universities by Shanghai Municipal Education Commission. In the same year, he started his doctoral study as a PhD student in the group of Prof. Dr. Johannes A. Lercher at the Institute of Chemical Technology, Technische Universität München with scholarship by China Scholarship Council. His research is focused on the fundamental understanding of impact of pH on hydrogenation reactions over Pt catalysts.

List of publications

Journals

1. Guoju Yang, Sneha A. Akhade, Xi Chen, Yue Liu*, Mal-Soon Lee*, Vassiliki-Alexandra Glezakou, Roger Rousseau, and Johannes A. Lercher*. **“The Nature of Hydrogen Adsorption on Platinum in the Aqueous Phase”**. Angewandte Chemie-International Edition. 2019, 58(11), 3527-3532.
2. Xi Chen, Yue Liu* and Johannes A. Lercher*. **“Electrocatalytic hydrogenation of phenol on Pt under pH-dependent open circuit potential”**, to be submitted.
3. Philipp Fischer[§], Xi Chen[§], Yue Liu* and Johannes A. Lercher*. **“Impact of external electric potential on electrocatalytic adsorption of hydrogen on Pt nanoparticles in the aqueous phase”**, to be submitted.

Poster presentations

1. **Impact of pH on adsorption of hydrogen on Pt in the aqueous phase.**

Xi Chen, Yue Liu and Johannes A. Lercher

The 6th edition of the Nanotech France 2021 International Conference, Paris, France, June 2021.

2. **Electrocatalytic hydrogenation of phenol on Pt under pH-dependent open circuit potential.**

Xi Chen, Yue Liu and Johannes A. Lercher.

The 240th Electrochemical Society (ECS) meeting, Orlando, Florida, USA, October 2021.